ABSTRACT

Gravitational Waves in Einstein-aether Theory

Xiang Zhao, Ph.D.

Advisor: Anzhong Wang, Ph.D.

We study gravitational waves produced by N-body systems in Einstein-aether theory. In particular, we calculate the gravitational waveforms, polarizations, response functions of the detectors and the radiation power by using the post-Newtonian approximations to the lowest order. Applying the general formulas to three different triple systems with periodic orbits, we find that the scalar mode and the longitudinal mode (h_b and h_L) are all suppressed by a factor of $c_{14} < \mathcal{O}(10^{-5})$ with respect to the transverse-traceless modes (h_+ and $h_\times$), while the vector modes (h_X and h_Y) are suppressed by a factor of $c_{13} < \mathcal{O}(10^{-15})$. We also find that gravitational waves depend sensitively on the configurations of the triple systems, their orientations with respect to the detectors, and the binding energies of the three compact bodies. The result for the first relativistic triple system, PSR J0337+1715, shows that the quadrupole emissions in different theories of gravity have almost the same amplitude, but the dipole emission can be as big as the quadrupole emission in Einstein-aether theory. This provides a very promising window to obtain severe constraints on Einstein-aether theory by multi-band gravitational wave astronomy.

Gravitational Waves in Einstein-aether Theory

by

Xiang Zhao, B.S., M.A.,

A Dissertation

Approved by the Department of Physics

Dwight P. Russell, Ph.D., Interim Chairperson

Submitted to the Graduate Faculty of
Baylor University in Partial Fulfillment of the
Requirements for the Degree
of
Doctor of Philosophy

Approved by the Dissertation Committee

Anzhong Wang, Ph.D., Chairperson

Dwight P. Russell, Ph.D.

Gerald B. Cleaver, Ph.D.

Lorin S. Matthews, Ph.D.

Klaus Kirsten, Ph.D.

Accepted by the Graduate School
August 2021

J. Larry Lyon, Ph.D., Dean

Page bearing signatures is kept on file in the Graduate School.

TABLE OF CONTENTS

LIST OF FIGURES

LIST OF TABLES

ACKNOWLEDGMENTS

I would like to thank Dr. Anzhong Wang for teaching me the physics of the Universe and supporting my research interests. His attitude towards science always sets an example for me. I am really grateful for everything he has done for me.

I would like to acknowledge my committee members, Dr. Dwight P. Russell, Dr. Gerald B. Cleaver, Dr. Lorin S. Matthews and Dr. Klaus Kirsten for their advice and guidance.

Special thanks to Chao Zhang for his enlightening discussions and collaboration, and to Bowen Li for his company.

I would also like to thank the Physics Department of Baylor University and our staff members Mrs. Chava Baker and Mrs. Marian Nunn-Graves for the support during my graduate studies at Baylor.

To my parents Jinzhu Zhao and Yonghua Cao

CHAPTER ONE

Introduction to Einstein-aether Theory

1.1 Beyond General Relativity

Theoretical physicists are not satisfied by their current theoretical toolbox. In fact, the Standard Model of Particle Interactions (SM) and Classical General Relativity (GR) are extremely powerful tools and are correctly listed among the most impressive achievements of mankind. But these theories are insufficient to answer many pressing questions. Our cosmology makes sense in our current theoretical framework, at the cost of a very absurd choice of matter-energy content. We actually understand only 4% of it. What is worse is that GR has failed to give predictions in many interesting and relevant situations. Indeed, many solutions of Einstein's equations are singular in some regions, such as the very beginning of the Universe and the interior of black holes. Last but not least, when applying the well-understood quantum field theories to GR to obtain a theory of quantum gravity (QG), we have been facing a tremendous resistance: GR is not perturbatively renormalizable [1].

In order to address some of the unsolved physics problems that GR has brought to the forefront, physicists are trying to modify Einstein's beautiful theory of gravity (GR). These problems will eventually be solved, because a modified gravity theory can better describe nature. In some well-studied scenarios (such as the Solar System or binary pulsars), a modified gravity theory can be simplified to Einstein's theory, but in other scenarios (for example, on a large scale, in the early Universe or near black holes) we can make important modifications to Einstein's theory. For example, the late-time acceleration of the Universe, instead of being described by a cosmological constant, may perhaps be explained by an additional tensor field that interacts with the gravitational field, as in bi-gravity theories [2, 3]. Another example is the Hořava–Lifshitz (HL) gravity [4] , which achieves power-counting renormalizability by modifying the graviton propagator in the ultraviolet. The action includes terms containing only higher order spatial derivatives of the metric, but not higher order time derivatives, so as to preserve unitarity. This procedure naturally leads to a space-time foliation into spacelike surfaces, labeled by the T coordinate.

The third example is the Einstein-aether theory (ae-theory) [5, 6], which violates Lorentz invariance in the gravitational sector without abandoning the framework of GR. Lorentz invariance is considered to be a fundamental symmetry of modern physical theories. Indeed, there are severe observational constraints on Lorentz-violating effects in the matter sector [7]. However constraints of such violations in the gravitational sector are much weaker than those in the matter sector.

One possible reason is that some mechanism suppresses the percolation of Lorentz-violating effects from the gravitational sector to the matter sector [8]. Of course, this is done at the price of large Lorentz-violating effects in the gravitational sector. Therefore, it is interesting to test Lorentz symmetry in the gravitational sector further.

Apart from providing a test bed for constraining Lorentz violations in the gravitational sector, ae-theory is an interesting theoretical laboratory to explore preferred frame effects. Ae-theory breaks the Lorentz symmetry by introducing a preferred time direction at each point in spacetime via a timelike unit vector u^{α}. Like the metric, the unit vector cannot vanish anywhere, so it breaks local Lorentz symmetry down to a rotation subgroup. It defines a congruence of timelike curves filling all of spacetime, like an omnipresent fluid, and so has been dubbed the "aether".

In fact, it was shown in [9] that the ae-theory is equivalent to the the infrared limit of HL gravity if the aether is assumed to be hypersurface orthogonal. More precisely, hypersurface orthogonality can be imposed through the local condition

$$u_\mu = \frac{\partial_\mu T}{\sqrt{g^{\alpha\beta}\partial_\alpha T \partial_\beta T}}, \tag{1.1}$$

where T is a scalar field that defines a foliation. It should be obvious that given the relation in the infrared between hypersuface orthogonal ae-theory and HL gravity, the experimental constraints on ae-theory can in principle be related to constraints for the latter theory.

Recently, the well-posedness of the initial value (Cauchy) problem of vacuum ae-theory has been confirmed [10]. In GR, the Cauchy problem can be put in a "well-posed" form, i.e. such that for given initial data there exists a unique time evolution which depends continuously on the initial data [11] . Very few results for the well-posedness of the Cauchy problem exist beyond GR, with the exception of scalar tensor theories of the Fierz-Jordan-Brans-Dicke type [12–14].

Experiments and observations are the foolproof method to test the modified gravity alternatives that have been postulated to address these unsolved problems. Many of these modified theories can be straightforwardly ruled out with current Solar System [15], binary pulsar [16] and cosmological observations. But even after imposing the requirement that modified theories must pass all current experimental tests, there still remains a large group that is only weakly constrained today. One must then rely on new observations coming from spacetime that is strongly curved and highly dynamical. For instance, gravitational wave (GW) observations of the coalescence of binary compact objects, like black holes and neutron stars. A binary system experiences three phases during its lifetime: inspiral, merger, and ringdown. Hence there are usually three parts in a GW signal corresponding to the three phases, and each part exhibits different characteristics. GW tests are quite different from other tests of gravity that have been carried out to date. GWs are unique probes of the extreme gravity regime, being sensitive both to the propagation and the generation of these waves. Moreover, GWs are weakly interacting. They travel to detectors on Earth without being affected by intervening matter.

The era of GW physics has begun, beginning with the observation of gravitational waves by Laser Interferometer Gravitational-Wave Observatory (LIGO) and Virgo collaborations [17–22]. These observations have already confirmed that indeed GWs exist, but the era of precision experimental relativity with GWs is only beginning. In the next few years, the LIGO/Virgo collaboration will continue to make detections at an increasing rate with larger and larger signal-to-noise ratios. In the near future new detectors (such as The Kamioka Gravitational Wave Detector (KAGRA) in Japan and LIGO-India in India) will join the network, which will allow for precise probes of the polarization content of GWs. And in the early 2030s, Laser Interferometer Space Antenna (LISA) will be launched [23]. The LIGO/Virgo detectors are sensitive to GWs with frequencies between 20 and 2000 Hz, since at frequencies lower than 20 Hz they are limited by the Newtonian ground noise. The LISA detector will be sensitive to GWs with frequencies between 10^{-5} and 1 Hz. As a consequence, the early inspiral phase of binaries for several years prior to their coalescence may also be detectable by space-based LISA. This extended frequency band will enable the discovery of different evolutionary stages of the same system. Massive systems will be observed by ground-based detectors with high signal-to-noise ratios, after being tracked for years by space-based detectors in their early inspiral phase. In particular, joint observations from LIGO/Virgo and space-based detectors can potentially improve current constraints by more than six orders of magnitude, which will impose severe constraints on various theories of gravity [24].

Besides the coalescence of binary compact objects, the triple system also emits strong gravitational waves. Gravitationally bound hierarchies containing three or more components are very common in our Universe [25]. Roughly speaking, about 13% of low-mass stellar systems contains three or more stars [26], and 96% of low-mass binaries with periods shorter than three days are part of a larger hierarchy [27]. The simplest example is the triple system of our Sun, Earth and Moon. In fact, any star in the vicinity of a supermassive black hole binary naturally forms a triple system.

A triple system is an ideal place to test strong gravity effects. For example, after the 6-year observation of a relativistic triple system, PRS J0337 + 1715, it has been found that the accelerations of the pulsar and its nearby white-dwarf companion differ fractionally by no more than 2.6×10^{-6} [28], which provides the most severe constraint on the violation of the strong equivalence principle.

During my Ph.D., my collaborators and I did a lot of work on modified gravity theories. We obtained gravitational waveforms and angular momentum loss for eccentric compact binary systems in screened modified gravity [29,30]. We also found new constraints of general screened modified gravity from comprehensive analysis of binary pulsars [31]. We proved that there are no static regular black holes in Einstein-complex-scalar-Gauss-Bonnet gravity [32]. However in this dissertation, I will focus on the topic of the gravitational waves in ae-theory, which is based on a series of my recent publications [33–36].

1.2 Einstein-aether Theory's Action

Greek letters α, β, μ... are reserved for tensor indices, which run from 0 to 3. English letters $i, j, k, ...$ run from 1 to 3. The metric convention used is $(-,+,+,+)$. Repeated indices $i, j, k, ...$ are summed over 1 to 3 regardless of their vertical positions. The speed of light in vacuum is set to 1.

In ae-theory, the fundamental fields of the gravitational sector are $g_{\alpha\beta}$, u^α and λ. The general action of the theory is given by [37–39]

$$S = S_{æ} + S_m, \tag{1.2}$$

where S_m denotes the matter action, and $S_{æ}$ is the gravitational action of the theory,

$$S_{æ} = \int d^4x \frac{1}{16\pi G}\sqrt{-g}\left[R - K^{\alpha\beta}{}_{\mu\nu}\nabla_\alpha u^\mu \nabla_\beta u^\nu + \lambda(u^\alpha u^\beta g_{\alpha\beta} + 1)\right], \tag{1.3}$$

$$K^{\alpha\beta}{}_{\mu\nu} = c_1 g^{\alpha\beta} g_{\mu\nu} + c_2 \delta^\alpha_\mu \delta^\beta_\nu + c_3 \delta^\alpha_\nu \delta^\beta_\mu - c_4 u^\alpha u^\beta g_{\mu\nu}. \tag{1.4}$$

It is convenient to define the following combinations of of coupling constants,

$$\begin{aligned} c_{14} &= c_1 + c_4, \\ c_\pm &= c_1 \pm c_3, \\ c_{123} &= c_1 + c_2 + c_3. \end{aligned} \tag{1.5}$$

The combination of the GW event GW170817 [40], observed by the LIGO/Virgo collaboration, and the event of the gamma-ray burst GRB 170817A [41] provides a remarkably stringent constraint on the speed of the spin-2 gravitational wave,

$-3 \times 10^{-15} < c_T - 1 < 7 \times 10^{-16}$, which implies that

$$|c_{13}| < 10^{-15}. \tag{1.6}$$

Requiring that the theory: (a) be self-consistent, such as free of ghosts and instability; and (b) satisfy all the observational constraints obtained so far, it was found that the parameter space of the theory is considerably restricted [42]. In particular, c_{14} and c_2 are restricted to

$$0 \lesssim c_{14} \lesssim 2.5 \times 10^{-5}, \tag{1.7}$$

$$c_{14} \lesssim c_2 \lesssim 0.095. \tag{1.8}$$

The constraints on other parameters depend on the values of c_{14}. By dividing the above range (1.7) into three intervals: (i) $0 \lesssim c_{14} \leq 2 \times 10^{-7}$; (ii) $2 \times 10^{-7} < c_{14} \lesssim 2 \times 10^{-6}$; and (iii) $2 \times 10^{-6} \lesssim c_{14} \lesssim 2.5 \times 10^{-5}$, in the first and last intervals, one finds

$$\begin{aligned} \text{(i)} \quad & 0 \lesssim c_{14} \leq 2 \times 10^{-7}, \\ & c_{14} \lesssim c_2 \lesssim 0.095, \end{aligned} \tag{1.9}$$

$$\begin{aligned} \text{(iii)} \quad & 2 \times 10^{-6} \lesssim c_{14} \lesssim 2.5 \times 10^{-5}, \\ & 0 \lesssim c_2 - c_{14} \lesssim 2 \times 10^{-7}. \end{aligned} \tag{1.10}$$

In the intermediate regime (ii) $2 \times 10^{-7} < c_{14} \lesssim 2 \times 10^{-6}$, in addition to the constraints given by equations (1.7) and (1.8), the following constraints must be also satisfied,

$$-10^{-7} \leq \frac{c_{14}\left(c_{14} + 2c_2c_{14} - c_2\right)}{c_2\left(2 - c_{14}\right)} \leq 10^{-7}. \tag{1.11}$$

Note that in writing equation(1.11), c_{13} is set to 0, for which the errors are of the order $\mathcal{O}\left(c_{13}\right) \simeq 10^{-15}$, which can be safely neglected for the current and forthcoming experiments.

When it comes to strong fields in the vicinity of the compact bodies, such as neutron stars and black holes, the strong field effects will be handled via an effective approach in which the compact bodies are treated as point particles whose action contains nonstandard couplings that depend on the velocity of the particles in the preferred frame where aether is at rest. Hence the matter action is given by the action of N-particle sources with a modification that the compact body's gravitational mass will be a function of γ_A. γ_A describes the compact body's motion relative to the aether.

$$S_m = -\sum_A \int d\tau_A \tilde{m}_A(\gamma_A), \tag{1.12}$$

$$\gamma_A = -u_\alpha v_A^\alpha, \tag{1.13}$$

where v_A^β is the four velocity of a source particle relative to the aether [1]

$$v_A^\beta = \frac{dx_A^\beta}{d\tau_A}. \tag{1.14}$$

In general, because of the effective coupling between the aether field and matter in the strong field regime, a compact object's structure, its binding energy and its gravitational mass will be a function of the motion relative to the aether, γ_A.

This matter action can be thought of as a Taylor expansion of the standard world line action, but with a mass that is a function of γ_A. If the particle is comoving with the local aether, $\gamma_A = 1$, so $\tilde{m}_A(\gamma_A)$ is expanded about 1,

$$\tilde{m}_A(\gamma_A) = \tilde{m}_A \left(1 + \sigma_A (u_\alpha v_A^\alpha + 1) + \frac{\sigma'_A}{2} (u_\alpha v_A^\alpha + 1)^2 + \dots \right), \tag{1.15}$$

$$\sigma_A = -\frac{1}{\tilde{m}_A} \frac{d\tilde{m}_A}{d\gamma_A}\bigg|_{\gamma_A = 1}, \tag{1.16}$$

[1] $x_A^0(t) = t$, $v_A^0 = dt/d\tau_A$

$$\sigma'_A = \frac{1}{\tilde{m}_A}\frac{d^2\tilde{m}_A}{d\gamma_A^2}\bigg|_{\gamma_A=1}, \tag{1.17}$$

where σ_A and σ'_A are called sensitivities. Sensitivities can be determined by matching this approach to the perfect fluid approach [39]. It will be convenient to introduce the parameter

$$s_A = \frac{\sigma_A}{1+\sigma_A}.$$

It is found in [37, 39] that the form of the sensitivity at lowest order in the compact body's field strength is given by

$$s_A = (\alpha_1 - \frac{2}{3}\alpha_2)\frac{\Omega_A}{m_A} + \mathcal{O}\left(\frac{G_N m_A}{d_A}\right). \tag{1.18}$$

where Ω_A is the gravitational binding energy $(\Omega_A/m_A \sim G_N m_A/d_A)$, $m_A = \tilde{m}_A(1+\sigma_A)$ is the active gravitational mass and d_A is the characteristic size of the body A. These quantities measure how much the binding energy of an isolated star changes with its motion relative to the preferred frame (i.e. relative to the aether).

In order to couple the matter source to the field, it is useful to re-express S_m as an integral over all of spacetime using a δ function representation of the form [43]

$$S_m = -\int d^4x \sum_A \int d\tau_A \delta^4(x - x_A(\tau_A))\tilde{m}_A\left(g_{\mu\nu}(x), u^\mu(x), x_A^\mu(\tau_A)\right). \tag{1.19}$$

Introducing an arbitrary parameter p to describe the particle's path, after changing the integration variable $\tau_A \to p$

$$\begin{aligned} S_m &= -\int d^4x \sum_A \int dp \frac{d\tau_A}{dp}\delta^4(x - x_A(p))\tilde{m}_A\left(g_{\mu\nu}(x), u^\mu(x), x_A^\mu(p)\right) \\ &= -\int d^4x \sum_A \int dp \left(-g_{\mu\nu}(x)\frac{dx_A^\mu(p)}{dp}\frac{dx_A^\nu(p)}{dp}\right)^{1/2} \\ &\times \delta^4(x - x_A(p))\tilde{m}_A\left(g_{\mu\nu}(x), u^\mu(x), x_A^\mu(p)\right), \end{aligned} \tag{1.20}$$

We define two Lagrangian densities

$$S_{æ} = \int d^4x \mathcal{L}_{æ}, \tag{1.21}$$

$$S_m = \int d^4x \mathcal{L}_m. \tag{1.22}$$

1.3 Einstein Equations

Let us first consider a variation of $g_{\alpha\beta}$, the least action principle states

$$\delta S = \int d^4x \left(\delta\mathcal{L}_{æ} + \delta\mathcal{L}_m\right) = \int d^4x \left(\frac{\delta\mathcal{L}_{æ}}{\delta g_{\alpha\beta}} + \frac{\delta\mathcal{L}_m}{\delta g_{\alpha\beta}}\right)\delta g_{\alpha\beta} = 0. \tag{1.23}$$

That is

$$\left(\frac{\delta\mathcal{L}_{æ}}{\delta g_{\alpha\beta}} + \frac{\delta\mathcal{L}_m}{\delta g_{\alpha\beta}}\right) = 0. \tag{1.24}$$

We calculate the variational derivative using Mathematica and xAct [2]

$$\frac{\delta\mathcal{L}_{æ}}{\delta g_{\alpha\beta}} = \frac{-1}{16\pi G}\sqrt{-g}(G^{\alpha\beta} - S^{\alpha\beta}), \tag{1.25}$$

where $G^{\alpha\beta}$ is the Einstein tensor, $S^{\alpha\beta}$ is

$$\begin{aligned} S_{\alpha\beta} =& \nabla_\mu (J^\mu{}_{(\alpha} u_{\beta)} + J_{(\alpha\beta)} u^\mu - J_{(\alpha}{}^\mu u_{\beta)}) \\ &+ c_1(\nabla_\alpha u_\mu \nabla_\beta u^\mu - \nabla_\mu u_\alpha \nabla^\mu u_\beta) + c_4(u^\mu \nabla_\mu u_\alpha)(u^\nu \nabla_\nu u_\beta) \\ &+ \lambda u_\alpha u_\beta - \frac{1}{2} g_{\alpha\beta}(J^\mu{}_\nu \nabla_\mu u^\nu), \end{aligned} \tag{1.26}$$

$$J^\alpha{}_\mu = K^{\alpha\beta}{}_{\mu\nu} \nabla_\beta u^\nu. \tag{1.27}$$

On the other hand

$$\delta\mathcal{L}_m = \left.\frac{d\mathcal{L}_m\left(g_{\alpha\beta} + \epsilon\delta g_{\alpha\beta}\right)}{d\epsilon}\right|_{\epsilon=0}. \tag{1.28}$$

$$\frac{\delta\mathcal{L}_m}{\delta g_{\alpha\beta}} = \frac{\sqrt{-g}}{2} T^{\alpha\beta}, \tag{1.29}$$

[2] Variation.nb

where the energy-momentum tensor $T^{\alpha\beta}$ is

$$T^{\alpha\beta} = \sum_A \tilde{m}_A \frac{\delta^3(\vec{x} - \vec{x}_A(t))}{v_A^0 \sqrt{-g}} \left[A_1 v_A^\alpha v_A^\beta + 2A_2 u^{(\alpha} v_A^{\beta)} \right], \tag{1.30}$$

$$A_1 = 1 + \sigma_A (u_\mu v_A^\mu + 1) + \frac{\sigma'_A}{2} (u_\mu v_A^\mu + 1)^2, \tag{1.31}$$

$$A_2 = -\sigma_A - \sigma'_A (u_\mu v_A^\mu + 1). \tag{1.32}$$

Combining equation (1.24), (1.25) and (1.29), the modified Einstein equation in ae-theory is

$$G^{\alpha\beta} - S^{\alpha\beta} = 8\pi G T^{\alpha\beta}. \tag{1.33}$$

1.4 Aether Equations

Let us consider a variation of u^α, the least action principle states

$$\delta S = \int d^4x \, (\delta \mathcal{L}_{æ} + \delta \mathcal{L}_m) = \int d^4x \left(\frac{\delta \mathcal{L}_{æ}}{\delta u^\alpha} + \frac{\delta \mathcal{L}_m}{\delta u^\alpha} \right) \delta u^\alpha = 0. \tag{1.34}$$

That is

$$\left(\frac{\delta \mathcal{L}_{æ}}{\delta u^\alpha} + \frac{\delta \mathcal{L}_m}{\delta u^\alpha} \right) = 0. \tag{1.35}$$

We calculate the following variational derivatives

$$\frac{\delta \mathcal{L}_{æ}}{\delta u^\alpha} = \frac{\sqrt{-g}}{8\pi G} Æ_\alpha, \tag{1.36}$$

$$\frac{\delta \mathcal{L}_m}{\delta u^\alpha} = -\sqrt{-g} T_\alpha, \tag{1.37}$$

where

$$Æ_\alpha = \nabla_\beta J^\beta{}_\alpha + c_4 (u^\mu \nabla_\mu u_\beta) \nabla_\alpha u^\beta + \lambda u_\alpha, \tag{1.38}$$

$$T_\alpha = -\sum_A \tilde{m}_A \frac{\delta^3(\vec{x} - \vec{x}_A(t))}{v_A^0 \sqrt{-g}} A_2 (v_A)_\alpha. \tag{1.39}$$

In a word, we have aether equation

$$\text{Æ}_\alpha = 8\pi G T_\alpha. \tag{1.40}$$

In addition, a variation of λ leads to

$$u_\alpha u^\alpha + 1 = 0. \tag{1.41}$$

This equation actually constraints or eliminates λ if we make use of equation (1.40)

$$\lambda = u^\alpha \nabla_\beta J^\beta{}_\alpha + c_4 (u^\mu \nabla_\mu u_\beta)(u^\alpha \nabla_\alpha u^\beta) - 8\pi G u^\alpha T_\alpha. \tag{1.42}$$

1.5 Covariant Equations of Motion for a Single Particle

Let us consider a variation of x_A^α, the least action principle gives

$$\nabla_\beta T_A^{\alpha\beta} - \nabla_\beta (T_A^\alpha u^\beta) - T_A^\beta \nabla^\alpha u_\beta = 0, \tag{1.43}$$

where $T_A^{\alpha\beta}$ and T_A^α are the one-particle summands in equation (1.30) and (1.39). This is the exact equation of motion for compact particles in ae-theory. By inserting post-Newtonian expansions of fields to it, the post-Newtonian orbit of the compact bodies can be obtained.

CHAPTER TWO

Gravitational Waves in the Inspiral Phase

2.1 Linearized Field Equations

Now let us expand the exact field equations about a Minkowski spacetime and a purely timelike aether field,

$$h_{\alpha\beta} = g_{\alpha\beta} - \eta_{\alpha\beta}, \quad \omega^\alpha = u^\alpha - \delta^\alpha_0, \tag{2.1}$$

where we assume $h_{\alpha\beta}$ and ω^α are small quantities of the same order, $h_{\alpha\beta} \sim \omega^\alpha \sim \epsilon$, and we have implicitly chosen the reference frame in which this separation holds. Because the action allows $SO(3)$ symmetry, we can further decompose $h_{\alpha\beta}$ and ω^α into irreducible transverse (divergence-free) and longitudinal (curl-free) pieces [44],

$$\begin{aligned} &h_{00}, \quad h_{0i} = \gamma_i + \gamma_{,i}, \quad h_{ij} = \phi_{ij} + \frac{1}{2}P_{ij}[f] + 2\phi_{(i.j)} + \phi_{,ij}, \\ &P_{ij}[f] = \delta_{ij} f_{,kk} - f_{,ij}, \end{aligned} \tag{2.2}$$

$$\omega^0, \quad \omega^i = \nu^i + \nu^{,i}. \tag{2.3}$$

We will refer ϕ_{ij} as tensor filed, ϕ_i, γ_i and ν_i as vector filed, h_{00}, γ, f, ϕ, ω^0 and ν as scalar field under a 3D rotation. With the following constraints, the same number of degrees of freedom is ensured,

$$\phi_{ij,j} = 0, \quad \phi_{ii} = 0, \quad \gamma_{i,i} = 0, \quad \phi_{i,i} = 0, \quad \nu^{i,i} = 0. \tag{2.4}$$

Inserting equations (2.1)-(2.3) into equations (1.33), (1.40) and (1.41), and keeping terms to the first order in $h_{\alpha\beta}$ and ω^α, we get

$$\bar{G}_{\alpha\beta} - \bar{S}_{\alpha\beta} = 8\pi G(T_{\alpha\beta} + t_{\alpha\beta}), \tag{2.5}$$

the aether equation reduces to

$$\bar{Æ}_\alpha = 8\pi G(T_\alpha + t_\alpha), \tag{2.6}$$

$$\omega^0 = \frac{1}{2}h_{00}, \tag{2.7}$$

where the overbar denotes the portion of the tensor linear in $h_{\alpha\beta}$ and ω^α, while $t_{\alpha\beta}$ and t_α are the nonlinear portion of the equation. $T_{\alpha\beta}$ and T_α start from the first order, $T_{\alpha\beta} \sim T_\alpha \sim \epsilon$. Using Mathematica and xAct [1], it is not difficult to obtain the linearized field equations. They are given by

$$\bar{G}_{00} = -\frac{1}{2}\Delta F, \tag{2.8}$$

where $F = f_{,ii} = \Delta f$,

$$\bar{G}_{0i} = -\frac{1}{2}\Delta(\gamma_i - \dot{\phi}_i) - \frac{1}{2}\dot{F}_{,i}, \tag{2.9}$$

$$\begin{aligned}\bar{G}_{ij} &= -\frac{1}{2}[\Delta\phi_{ij} - \ddot{\phi}_{ij}] + [\ddot{\phi}_{(i,j)} - \dot{\gamma}_{(i,j)}] \\ &+ \frac{1}{4}P_{ij}[\Delta f - \ddot{f} - 2h_{00} - 2\ddot{\phi} + 4\dot{\gamma}] - \frac{1}{2}\ddot{f}_{,ij},\end{aligned} \tag{2.10}$$

$$\bar{S}_{00} = c_{14}\Delta(\dot{\nu} + \dot{\gamma} - \frac{1}{2}h_{00}) - 8\pi G T_0, \tag{2.11}$$

and the $(0, i)$ component is

$$\bar{S}_{0i} = c_{14}(\ddot{\nu}_i + \ddot{\gamma}_i) - \frac{c_-}{2}\Delta(\nu_i + \gamma_i) + c_{14}(\ddot{\nu} + \ddot{\gamma} - \frac{1}{2}\dot{h}_{00})_{,i}, \tag{2.12}$$

$$\bar{S}_{ij} = \frac{c_+}{2}\ddot{\phi}_{ij} + c_+(\dot{\nu}_{(i,j)} + \ddot{\phi}_{(i,j)}) + \frac{1}{2}P_{ij}\left[c_2(2\dot{\nu} + \ddot{\phi} + \ddot{f}) + \frac{c_+}{2}\ddot{f}\right] \tag{2.13}$$

$$+ \frac{1}{2}\left[c_{123}(\ddot{\phi} + 2\dot{\nu}) + c_2\ddot{f}\right]_{,ij}, \tag{2.14}$$

$$\bar{Æ}_0 = 8\pi G T_0, \tag{2.15}$$

[1] Linearized.nb

the i component of aether equation is

$$\begin{aligned}\bar{Æ}_i = \frac{1}{2}\Big[& c_{14}\dot{h}_{00,i} + c_+\Delta\dot{\phi}_i + c_2\Delta\dot{f}_{,i} + c_{123}\Delta\dot{\phi}_{,i} \\ & -2c_{14}(\ddot{\gamma}_i + \ddot{\nu}_i) - 2c_{14}(\ddot{\gamma} + \ddot{\nu})_{,i} + c_-\Delta\gamma_i + 2c_1\Delta\nu_i + 2c_{123}\Delta\nu_{,i}\big],\end{aligned} \tag{2.16}$$

where the T_0 term representing matter sector comes from λ in equation (1.42).

It is convenient to combine equation (2.5) and (2.6),

$$\bar{G}_{\alpha\beta} - \bar{S}_{\alpha\beta} - \bar{Æ}_\alpha\delta^0_\beta = 8\pi G\tau_{\alpha\beta}, \tag{2.17}$$

where we define the new source as

$$\tau_{\alpha\beta} = T_{\alpha\beta} - T_\alpha\delta^0_\beta + t_{\alpha\beta} - t_\alpha\delta^0_\beta, \tag{2.18}$$

where the precise form of nolinear temrs t_{ab} and t_a will not be needed [38]. Now we decompose the new source $\tau_{\alpha\beta}$ as before,

$$\tau_{00}, \quad \tau_{0i} = \tau^T_{0i} + \tau^L_{0i}, \quad \tau_{i0} = \tau^T_{i0} + \tau^L_{i0}, \quad \tau_{ij} = \tau^{TT}_{ij} + \tau^T_{ij} + \tau^L_{ij}, \tag{2.19}$$

where T indicates the transverse part of a field, L indicates the logitudinal part of a field and TT indicates transverse-traceless part of a field.

It can be verified that the linear portions of equation (2.17) satisfy a conservation law,

$$\left(\bar{G}_{\alpha\beta} - \bar{S}_{\alpha\beta} - \bar{Æ}_\alpha\delta^0_\beta\right)^{,\beta} = 0, \tag{2.20}$$

hence the right side of equation (2.17)

$$\tau_{\alpha\beta}{}^{,\beta} = -\tau_{\alpha 0,0} + \tau_{\alpha i,i} = 0. \tag{2.21}$$

Note that the non-symmetric $\tau_{\alpha\beta}$ satisfies the conservation law with respect to the right-index only.

Equivalently, using $\eta^{\alpha\beta}$ to raise the indices, we get

$$\tau^{\alpha\beta} = T^{\alpha\beta} - T^{\alpha}\eta^{\beta 0}, \tag{2.22}$$

$$\tau^{\alpha\beta}{}_{,\beta} = \tau^{\alpha 0}{}_{,0} + \tau^{\alpha i}{}_{,i} = 0. \tag{2.23}$$

Integrating this equation

$$0 = \int d^3x \left(\tau^{\alpha 0}{}_{,0} + \tau^{\alpha i}{}_{,i}\right) = \int d^3x \tau^{\alpha 0}{}_{,0} + \int dS_i \tau^{\alpha i},$$

where the surface term is dropped, hence

$$0 = \frac{\partial}{\partial t} \int d^3x \tau^{\alpha 0}. \tag{2.24}$$

The corresponding conserved total energy E is defined as

$$E = \int d^3x \tau^{00} = \int d^3x (T^{00} + T^0). \tag{2.25}$$

To lowest post-Newtonian (PN) order,

$$v_A^0 = \frac{dt}{d\tau_A} = 1, \quad \sqrt{-g} = 1, \quad A_1 = 1, \quad A_2 = 0, \tag{2.26}$$

$$T^{00} = \sum_A \tilde{m}_A \delta^3(\vec{x} - \vec{x}_A), \quad T^0 = 0. \tag{2.27}$$

Therefore

$$E = \sum_A \tilde{m}_A = \sum_A (1 - s_A) m_A, \tag{2.28}$$

where m_A is the active gravitational mass of body A, which is defined through the Newtonian order equations of motion [38].

The corresponding conserved momentum P^i is defined as

$$P^i = \int d^3x \tau^{i0} = \int d^3x (T^{i0} + T^i), \tag{2.29}$$

and to lowest PN order,

$$T^{i0} = \sum_A \tilde{m}_A \delta^3(\vec{x} - \vec{x}_A) v_A^i, \quad T^i = 0, \tag{2.30}$$

after the integration of δ function

$$P^i = \sum_A \tilde{m}_A v_A^i = \sum_A m_A v_A^i, \tag{2.31}$$

where the high order term $s_A m_A v_A^i$ is dropped.

2.2 Wave Equations

Now we impose coordinate gauge conditions to simplify the linearized field equations,

$$\nu = \gamma = \phi_i = 0. \tag{2.32}$$

This gauge condition can be chosen because under the infinitesimal coordinate transformations

$$t' = t + \xi^0(x), \quad x'^i = x^i + \xi^i(x) + \partial^i \xi(x), \tag{2.33}$$

where $\partial_i \xi^i(x) = 0$. Following the derivations shown in Appendix A, the decomposed $h_{\alpha\beta}$ and ω^α transform as

$$\begin{aligned}
&h'_{00} = h_{00} + 2\dot{\xi}^0, \\
&\gamma'_i = \gamma_i - \dot{\xi}_i, \quad \gamma' = \gamma + \xi^0 - \dot{\xi}, \\
&\phi'_{ij} = \phi_{ij}, \quad \phi'_i = \phi_i - \xi_i, \quad f' = f, \quad \phi' = \phi - 2\xi, \\
&\omega'^0 = \omega^0 + \dot{\xi}^0, \\
&\nu'^i = \nu^i + \dot{\xi}^i, \quad \nu' = \nu + \dot{\xi}.
\end{aligned} \tag{2.34}$$

From above results, we can see that the coordinate gauge condition, equation (2.32), can be satisfied by choosing

$$\xi^0 = -\gamma - \nu, \quad \dot{\xi} = -\nu, \quad \xi^i = \phi^i. \tag{2.35}$$

Thanks to the decomposition we use in equation (2.2) and (2.3), we can deal with the tensor field, vector field, and scalar field separately.

2.2.1 Tensor Field

The transverse-traceless part of the i, j component of equation (2.17) gives the wave equation of a tensor field, (L.H.S retains ϕ_{ij} terms, R.H.S. retains τ_{ij}^{TT})

$$-\frac{1}{c_T^2}\ddot{\phi}_{ij} + \Delta\phi_{ij} = -16\pi G\tau_{ij}^{TT}, \tag{2.36}$$

$$c_T^2 = \frac{1}{1-c_+}, \tag{2.37}$$

where ϕ_{ij} is already a transverse-traceless field by definition.

2.2.2 Vector Field

The transverse part of the $i, 0$ component of equation (2.17) gives (L.H.S. retains ν_i, γ_i terms, R.H.S. retains τ_{i0}^T)

$$-\frac{1}{2}\Delta(c_+\nu^i + \gamma_i) = 8\pi G\tau_{i0}^T. \tag{2.38}$$

The transverse part of the $0, i$ component of equation (2.17) gives (L.H.S. retains ν_i, γ_i terms, R.H.S. retains τ_{0i}^T)

$$-c_{14}(\ddot{\nu}_i + \ddot{\gamma}_i) + \frac{1}{2}\Delta(c_-\nu_i + (c_- - 1)\gamma_i) = 8\pi G\tau_{0i}^T. \tag{2.39}$$

Ignoring the nonlinear terms, we have

$$\tau_{0i} = \tau_{i0} + T_i. \tag{2.40}$$

Equation (2.39) can be written as

$$-c_{14}(\ddot{\nu}_i + \ddot{\gamma}_i) + \frac{1}{2}\Delta(c_-\nu_i + (c_- - 1)\gamma_i) = 8\pi G(\tau_{i0} + T_i)^T. \tag{2.41}$$

[equation (2.38) + $(c_+ - 1) \times$ equation (2.41)] gives the wave equation of vector field,

$$-\frac{1}{c_V^2}(\ddot{\nu}_i + \ddot{\gamma}_i) + \Delta(\nu_i + \gamma_i) = -\frac{16\pi G}{2c_1 - c_+c_-}(c_+\tau_{i0} + (c_+ - 1)T_i)^T, \tag{2.42}$$

$$c_V^2 = \frac{2c_1 - c_+c_-}{2(1-c_+)c_{14}}. \tag{2.43}$$

2.2.3 Scalar Field

The trace of the i, j component of equation (2.17) gives

$$(2+3c_2+c_+)\Delta(\ddot{f}+\ddot{\phi})+2\Delta h_{00}-\Delta F=-16\pi G\tau_{ii}. \tag{2.44}$$

The transverse part of the i, j component of equation (2.17) gives (L.H.S. retains the terms with $P_{ij}[*]$, R.H.S. retains τ^T_{ij})

$$-\frac{1}{4}P_{ij}[(1+2c_2+c_+)\ddot{f}+(2+2c_2)\ddot{\phi}+2h_{00}-F]=8\pi G\tau^T_{ij}. \tag{2.45}$$

The trace of the above is

$$(1+2c_2+c_+)\ddot{F}-\Delta(F-2h_{00}-2(1+c_2)\ddot{\phi})=-16\pi G\tau^T_{ii}, \tag{2.46}$$

where $\tau^T_{ii}\equiv tr(\tau^T_{ij})$. The longitudinal part of the i, j component of equation (2.17) gives (L.H.S. retains the all terms except $P_{ij}[*]$, R.H.S. retains τ^L_{ij})

$$-\frac{1}{2}\left((1+c_2)\ddot{f}_{,ij}+(c_++c_2)\ddot{\phi}_{,ij}\right)=8\pi G\tau^L_{ij}. \tag{2.47}$$

The trace of the above is

$$(1+c_2)\ddot{F}+c_{123}\Delta\ddot{\phi}=-16\pi G\tau^L_{ii}, \tag{2.48}$$

where $\tau^L_{ii}\equiv tr(\tau^L_{ij})$. The $0,0$ component of equation (2.17) gives

$$\Delta F-c_{14}\Delta h_{00}=-16\pi G\tau_{00}. \tag{2.49}$$

The longitudinal part of the $i, 0$ component of equation (2.17) gives (L.H.S. retains all terms except ν_i, γ_i terms, R.H.S. retains τ^L_{i0})

$$\Delta((1+c_2)\dot{f}+c_{123}\dot{\phi})_{,i}=-16\pi G\tau^L_{i0}. \tag{2.50}$$

$\Big[$equation (2.44) $-\ \frac{2+3c_2+c_+}{c_{123}}\times$ equation (2.48) $+\ \frac{2}{c_{14}}\times$ equation (2.49)$\Big]$ gives the wave equation of scalar field,

$$-\frac{1}{c_S^2}\ddot{F}+\Delta F=-\frac{16\pi Gc_{14}}{2-c_{14}}(\tau_{ii}-\frac{2+3c_2+c_+}{c_{123}}\tau^L_{ii}+\frac{2}{c_{14}}\tau_{00}), \tag{2.51}$$

$$c_S^2 = \frac{(2-c_{14})c_{123}}{(2+c_+ + 3c_2)(1-c_+)c_{14}}. \tag{2.52}$$

There is another important wave equation of scalar fields. However it is not independent of equation (2.51), (the derivation is given in Appendix B)

$$-\frac{1}{c_S^2}\ddot{f}_{,ij} + \Delta f_{,ij} = \tau'_{ij}. \tag{2.53}$$

2.3 Waves

We use Green's function to the solve wave equations and the Poissonnian equations above. Then we simplify the solution with a standard approxiamtion [45]. We denote field point as $x^i = x\hat{x}^i$ and the typical length scale of source as d. In the region far away from the source (far zone), $x \gg d$, we only need the the portion of the field $\sim\ O(1/x)$.

Wave equations of the form

$$-\frac{1}{s^2}\ddot{\psi} + \Delta\psi = -16\pi\tau, \tag{2.54}$$

can be solved via retarded Green's function (no incoming wave boundary condition)

$$\begin{aligned}\psi(t,\vec{x}) &= 4\int d^3x' \frac{\tau(t-|\vec{x}-\vec{x}'|/s, \vec{x}')}{|\vec{x}-\vec{x}'|} \\ &\approx \frac{4}{x}\sum_{m=0}^{\infty}\frac{1}{m!s^m}\frac{\partial^m}{\partial t^m}\int d^3x'\tau(t-x/s,\vec{x}')(x'^i\hat{x}^i)^m,\end{aligned} \tag{2.55}$$

where we only keep to $O(1/x)$.

Poissonnian equations of the form

$$\Delta\psi = -16\pi\tau \tag{2.56}$$

can be solved via Green's function $(1/|\vec{x}-\vec{x}'|)$,

$$\begin{aligned}\psi(t,\vec{x}) &= 4\int d^3x' \frac{\tau(t,\vec{x}')}{|\vec{x}-\vec{x}'|} \\ &\approx \frac{4}{x}\int d^3x'\tau(t,\vec{x}'),\end{aligned} \tag{2.57}$$

where we only keep to $O(1/x)$. In addition, when using the equations (2.55) and (2.57), we can first using the full τ to do integration $\int d^3x'(*)$ and then take the projection TT, T or L of the integral [37], e.g.

$$\int d^3x' \frac{\tau_{ij}^{TT}}{|\vec{x}-\vec{x}'|} = \left(\int d^3x' \frac{\tau_{ij}}{|\vec{x}-\vec{x}'|}\right)^{TT}. \tag{2.58}$$

Also, in the far zone, equation (4.2) to $O(1/x)$ gives (Appendix C)

$$s\psi_{,i} = -\dot{\psi}\hat{x}^i. \tag{2.59}$$

Hence differentially transverse becomes equivalent to geometrically transverse to direction of propagation, $\hat{x}^i$. For instance,

$$c_T\phi_{ij,i} = -\dot{\phi}_{ij}\hat{x}^i = 0.$$

Thus, we construct a transverse operator by only using $\hat{x}^i$ [46]. The transverse operator is defined as

$$\tilde{P}_{ij} = \delta_{ij} - \hat{x}^i\hat{x}^j, \tag{2.60}$$

the transverse-traceless operator is defined as

$$\Lambda_{ijkl} = \tilde{P}_{ik}\tilde{P}_{jl} - \frac{1}{2}\tilde{P}_{ij}\tilde{P}_{kl}. \tag{2.61}$$

For any vector ψ_i or tensor ψ_{ij}, we use T to denote the transverse portion and TT to denote the transeverse-traceless portion, mathematically $(\psi_i)^T = \tilde{P}_{ik}\psi_k$ and $\psi_{ij}^{TT} = \Lambda_{ijkl}\psi_{kl}$.

First, we solve the Poissonnian equation (3.7),

$$c_+\nu_i + \gamma_i = \left(\frac{4G}{x}\int d^3x'\tau_{i0}(t,\vec{x}')\right)^T = \frac{4G}{x}\theta_i^T, \tag{2.62}$$

where we define

$$\int d^3x'\tau_{i0}(t,\vec{x}') \equiv \theta_i. \tag{2.63}$$

From conservation law equation (2.21), we know θ_i is a constant vector. Equation (2.62) gives

$$\gamma_i = -c_+\nu_i + \frac{4G}{x}\theta_i^T. \tag{2.64}$$

Similarly, equation (2.50) gives

$$((1+c_2)\dot{f} + c_{123}\dot{\phi})_{,i} = \left(\frac{4G}{x}\int d^3x'\tau_{i0}(t,\vec{x}')\right)^L = \frac{4G}{x}\theta_i^L, \tag{2.65}$$

hence

$$\dot{\phi}_{,i} = -\frac{1+c_2}{c_{123}}\dot{f}_{,i} + \frac{4G}{x}\frac{\theta_i^L}{c_{123}}. \tag{2.66}$$

Equation (2.49) gives

$$F - c_{14}h_{00} = \frac{4G}{x}\int d^3x'\tau_{00}(t,\vec{x}') = \frac{4G}{x}\theta, \tag{2.67}$$

where

$$\int d^3x'\tau_{00}(t,\vec{x}') \equiv \theta. \tag{2.68}$$

From conservation law equation (2.21), we know θ is a constant. Equation (2.67) gives

$$h_{00} = \frac{F}{c_{14}} - \frac{4G}{x}\frac{\theta}{c_{14}}. \tag{2.69}$$

Second, we solve wave equation (2.36),

$$\begin{aligned}\phi_{ij}(t,\vec{x}) &= \left(\frac{4G}{x}\int d^3x'\tau_{ij}(t-x/c_T,\vec{x}')\right)^{TT} \\ &= \left(\frac{2G}{x}\ddot{I}_{ij}(t-x/c_T)\right)^{TT}.\end{aligned} \tag{2.70}$$

We refer to Appendix D for details. We have defined the following in Appendix D

$$I_{ij}(t) \equiv \sum_A m_A x_A^i(t)x_A^j(t), \quad Q_{ij} \equiv I_{ij} - \frac{1}{3}\delta_{ij}I_{kk}. \tag{2.71}$$

It is not difficult to verify that $I_{ij}^{TT} = Q_{ij}^{TT}$, the interested reader may refer to page 110 Note 15 in [46]. Thus, the tensor wave ϕ_{ij} can be written as

$$\phi_{ij} = \frac{2G}{x}\ddot{Q}_{ij}^{TT}, \tag{2.72}$$

where the R.H.S. is evaluated at $t - x/c_T$.

Third, we solve wave equation (2.42), (refer to Appendix E for the details)

$$\begin{aligned} \nu_i = &-\frac{2G}{x}\frac{1}{2c_1 - c_+ c_-}\left(\frac{\hat{x}^k}{c_V}\left(\frac{c_+}{1-c_+}\ddot{Q}_{ik} + \ddot{\mathcal{Q}}_{ik} + \mathcal{V}_{ik}\right) - 2\Sigma^i\right)^T \\ &+ \frac{4G}{x}\frac{c_+ - 2c_1 + c_+ c_-}{(1-c_+)(2c_1 - c_+ c_-)}\theta_i^T, \end{aligned} \tag{2.73}$$

where the R.H.S. is evaluated at $t - x/c_V$, and

$$\begin{aligned} &\mathcal{I}_{ik} \equiv \sum_A \tilde{m}_A \sigma_A (x_A^i x_A^k), \quad \mathcal{Q}_{ik} \equiv \mathcal{I}_{ik} - \frac{1}{3}\delta_{ik}\mathcal{I}_{jj}, \\ &\mathcal{V}_{ik} \equiv 2\sum_A \tilde{m}_A \sigma_A \dot{v}_A^{[i} x_A^{k]}, \quad \Sigma^i \equiv -\sum_A \tilde{m}_A \sigma_A v_A^i. \end{aligned} \tag{2.74}$$

Fourth, we solve wave equation (2.51), (refer to Appendix E for the details)

$$\begin{aligned} F = &\frac{4G}{x}\frac{c_{14}}{(2-c_{14})}\left[\frac{3}{2}(Z-1)\hat{x}^i\hat{x}^j\ddot{Q}_{ij} + \frac{1}{2}Z\ddot{I}_{kk} - \frac{\hat{x}^i\hat{x}^j}{c_{14}c_S^2}\ddot{\mathcal{I}}_{ij} + \frac{2}{c_{14}c_S}\hat{x}^i\Sigma_i\right] \\ &+ \frac{4G}{x}\frac{c_{14}}{(2-c_{14})}\frac{2}{c_{14}}\left(\theta - \frac{\hat{x}^i}{c_S}\theta_i\right), \end{aligned} \tag{2.75}$$

where the R.H.S. is evaluated at $t - x/c_S$, and

$$\begin{aligned} &Z \equiv \frac{(\alpha_1 - 2\alpha_2)(1-c_+)}{3(2c_+ - c_{14})}, \quad \alpha_1 = -\frac{8(c_3^2 + c_1 c_4)}{2c_1 - c_+ c_-}, \\ &\alpha_2 = \frac{\alpha_1}{2} - \frac{(c_1 + 2c_3 - c_4)(2c_1 + 3c_2 + c_3 + c_4)}{(2-c_{14})c_{123}}. \end{aligned} \tag{2.76}$$

Fifth, we look at equation (2.53): it will give a useful relation in the far zone (of course, outside the source too). From Appendix B the following equations are used

$$\tau'_{ij} = \frac{c_{14}}{2-c_{14}}\left[-\frac{2+2c_2}{c_{123}}\dot{\Theta}_{i,j} + \frac{2}{c_{14}}\Theta_{,ij}\right], \tag{2.77}$$

$$\Theta_i(t,\vec{x}) = 4G\int d^3x'\frac{\tau_{i0}^L(t,\vec{x}')}{|\vec{x}-\vec{x}'|} \approx \left(\frac{4G}{x}\int d^3x'\tau_{i0}(t,\vec{x}')\right)^L = \frac{4G}{x}\theta_i^L, \tag{2.78}$$

$$\Theta(t,\vec{x}) = 4G\int d^3x' \frac{\tau_{00}(t,\vec{x}')}{|\vec{x}-\vec{x}'|} \approx \frac{4G}{x}\int d^3x' \tau_{00}(t,\vec{x}') = \frac{4G}{x}\theta. \tag{2.79}$$

Since

$$\frac{\partial}{\partial x^i}\left(\frac{1}{x}\right) = -\frac{\hat{x}^i}{x^2}, \tag{2.80}$$

to $O(1/x)$,

$$\tau'_{ij} = 0, \tag{2.81}$$

hence

$$-\frac{1}{c_S^2}\ddot{f}_{,ij} + \Delta f_{,ij} = 0, \tag{2.82}$$

or

$$\ddot{f}_{,ij} = c_S^2 F_{,ij}. \tag{2.83}$$

2.4 Polarizations

In proper detector frame, the geodesic deviation equation is [46]

$$\ddot{\zeta}_i = -R_{0i0j}\zeta^j = \frac{1}{2}\ddot{\mathcal{P}}_{ij}\zeta^j, \tag{2.84}$$

where ζ_i is the spatial part of the deviation vector between two nearby trajectories of test particles. Therefore we should compute Riemann tensor R_{0i0j} in the proper detector frame. However in linearized theory the Riemann tensor is invariant under the coordinate transformations equation (2.33). Hence we can compute it in the frame we have chosen such that $\nu = \gamma = \phi_i = 0$. In linearized theory,

$$
\begin{aligned}
R_{0i0j} &= \frac{1}{2}\left(h_{0j,0i} + h_{0i,0j} + h_{ij,00} - h_{00,ij}\right) \\
&= \dot{\gamma}_{(i,j)} - \frac{1}{2}\ddot{\phi}_{,ij} - \frac{1}{4}\delta_{ij}\Delta\ddot{f} + \frac{1}{4}\ddot{f}_{,ij} - \frac{1}{2}\ddot{\phi}_{ij} - \omega^0_{,ij} \\
&= -c_+\dot{\nu}_{(i,j)} + \frac{1+c_2}{2c_{123}}c_S^2 F_{,ij} - \frac{1}{4}\delta_{ij}\ddot{F} + \frac{1}{4}c_S^2 F_{,ij} - \frac{1}{2}\ddot{\phi}_{ij} - \frac{1}{2c_{14}}F_{,ij} \\
&= -\frac{1}{2}\ddot{\phi}_{ij} - c_+\dot{\nu}_{(i,j)} + \left(\frac{1+c_2}{2c_{123}}c_S^2 + \frac{1}{4}c_S^2 - \frac{1}{2c_{14}}\right)F_{,ij} - \frac{1}{4}\delta_{ij}\ddot{F},
\end{aligned}
\tag{2.85}
$$

where, to obtain the third equality, we used the previous results in equations (2.64), (2.66), (2.69), (2.83), (2.7) and only keep terms up to $O(1/x)$.

In our case, from equation (2.59),

$$
c_T\phi_{ij,k} = -\dot{\phi}_{ij}\hat{x}^k, \quad c_V\nu_{i,k} = -\dot{\nu}_i\hat{x}^k, \quad c_S F_{,k} = -\dot{F}\hat{x}^k. \tag{2.86}
$$

Then R_{0i0j} can be written as

$$
R_{0i0j} = -\frac{1}{2}\ddot{\phi}_{ij} + \frac{c_+}{c_V}\ddot{\nu}_{(i}\hat{x}_{j)} + \left(\frac{1+c_2}{2c_{123}} + \frac{1}{4} - \frac{1}{2c_{14}c_S^2}\right)\ddot{F}\hat{x}^i\hat{x}^j - \frac{1}{4}\delta_{ij}\ddot{F}. \tag{2.87}
$$

Therefore,

$$
\mathcal{P}_{ij} = \phi_{ij} + a_1\nu_{(i}\hat{x}_{j)} + a_2 F\hat{x}^i\hat{x}^j + \frac{1}{2}\delta_{ij}F, \tag{2.88}
$$

where we define

$$
a_1 = -\frac{2c_+}{c_V}, \quad a_2 = \frac{(2+3c_2+c_+)(c_1+2c_3-c_4)}{2c_{123}(c_{14}-2)}. \tag{2.89}
$$

Note that the constant terms θ_i and θ in $\mathcal{P}$ will not affect R_{0i0j} due to second derivative with respect to time, so we will drop them from now on. Equation (2.88) agrees with equation (4.51) in [47].

In order to calculate polarizations, we need to have a basis to decompose $\mathcal{P}_{ij}$ [48]. Given that $\hat{x}^i$ is the direction of propagation(equivalently the direction of the field point vector), we can construct a plane perpendicular to $\hat{x}^i$. Introducing a new symbol $e^i_Z = \hat{x}^i$, the plane is determined by the unit vectors e^i_X and e^i_Y, which satisfy $\vec{e}_X \times \vec{e}_Y = \vec{e}_Z$. The unit vector $\vec{e}_Z$ points from the source to the detector (The wave is traveling in the z-direction). Now it is time to set up the reference frame explicitly. Since linearized theory has the Poincare symmetry [46], we can further change to a frame in which it is easy to compute the source integral (summation for discrete matter). We will use Cartesian coordinate system (t, x, y, z) to denote it. A reference frame has two properties: motion of the origin and orientation of the axes. We choose the reference frame so it is rest relative to the aether and the (x, y)-plane coincides with the orbital plane of the source system, we call this aether frame. In aether frame (t, x, y, z), the basis $(e^i_Z,\, e^i_X,\, e^i_Y)$ can be parameterized by two angles ι and φ as follows

$$\begin{aligned}
e^i_Z &= (\, \sin\vartheta\, \cos\varphi,\, \sin\vartheta\, \sin\varphi,\, \cos\vartheta\,)\,, \\
e^i_X &= (\, \cos\vartheta\, \cos\varphi,\, \cos\vartheta\, \sin\varphi,\, -\sin\vartheta\,)\,, \\
e^i_Y &= (\, -\sin\varphi,\, \cos\varphi, 0\,)\,.
\end{aligned} \tag{2.90}$$

There is a useful property

$$\delta^{ij} = e^i_X e^j_X + e^i_Y e^j_Y + e^i_Z e^j_Z. \tag{2.91}$$

Then, with the basis $(e^i_Z,\, e^i_X,\, e^i_Y)$, we can define six polarizations as

$$\begin{aligned}
h_+ &\equiv \frac{1}{2}\left(\mathcal{P}_{XX} - \mathcal{P}_{YY}\right), \quad h_\times \equiv \frac{1}{2}\left(\mathcal{P}_{XY} + \mathcal{P}_{YX}\right), \\
h_b &\equiv \frac{1}{2}\left(\mathcal{P}_{XX} + \mathcal{P}_{YY}\right), \quad h_L \equiv \mathcal{P}_{ZZ}, \\
h_X &\equiv \frac{1}{2}\left(\mathcal{P}_{XZ} + \mathcal{P}_{ZX}\right), \quad h_Y \equiv \frac{1}{2}\left(\mathcal{P}_{YZ} + \mathcal{P}_{ZY}\right),
\end{aligned} \tag{2.92}$$

where $\mathcal{P}_{XY} \equiv \mathcal{P}_{ij} e^i_X e^j_Y$, and so on. Inserting equation (2.88) into equation (2.92),

$$\begin{aligned}
h_+ &= \frac{1}{2}\phi_{ij} e^{ij}_+, \quad h_\times = \frac{1}{2}\phi_{ij} e^{ij}_\times, \\
h_b &= \frac{1}{2}\phi_{ij} e^i_X e^j_X + \frac{1}{2}\phi_{ij} e^i_Y e^j_Y + \frac{1}{2}F, \\
h_L &= \phi_{ij} e^i_Z e^j_Z + a_1 \nu_i e^i_Z + (a_2 + \frac{1}{2})F, \\
h_X &= \phi_{ij} e^i_X e^j_Z + \frac{1}{2} a_1 \nu_i e^i_X, \\
h_Y &= \phi_{ij} e^i_Y e^j_Z + \frac{1}{2} a_1 \nu_i e^i_Y,
\end{aligned} \tag{2.93}$$

where $e^{ij}_+ \equiv e^i_X e^j_X - e^i_Y e^j_Y$, $e^{ij}_\times \equiv e^i_X e^j_Y + e^i_Y e^j_X$. The polarizations can be simplified by using the transverse-traceless property of ϕ_{ij} and transverse property of ν_i, (refer to equations (2.4) and (2.91))

$$\begin{aligned}
h_+ &= \frac{1}{2}\phi_{ij} e^{ij}_+, \quad h_\times = \frac{1}{2}\phi_{ij} e^{ij}_\times, \\
h_b &= \frac{1}{2}F, \qquad h_L = \left[1 - \frac{c_{14} - 2c_+}{c_{14}(c_+ - 1)c_S^2}\right] h_b, \\
h_X &= -\frac{c_+}{c_V}\nu_i e^i_X, \quad h_Y = -\frac{c_+}{c_V}\nu_i e^i_Y.
\end{aligned}$$

In Einstein-aether theory, there are three fields, ϕ_{ij}, ν_i, and F, which have five degrees of fredom. Hence only five polarizations are independent in Einstein-aether theory, as you can see from the above equation. From the previous section (the θ and θ_i can be dropped if only the derivatives of ν_i, and F will be used), we have to $O(1/x)$

$$\phi_{ij} = \frac{2G}{x}\ddot{Q}^{TT}_{ij}\bigg|_{t-x/c_T}, \tag{2.94}$$

$$\nu^i = -\frac{2G}{x}\frac{1}{2c_1 - c_+ c_-}\left(\frac{e^j_Z}{c_V}\left(\frac{c_+}{1-c_+}\ddot{Q}_{ij} - \ddot{\mathcal{Q}}_{ij} - \mathcal{V}_{ij}\right) + 2\Sigma^i\right)^T\Bigg|_{t-x/c_V}, \tag{2.95}$$

$$\begin{aligned}
F &= \frac{4G}{x}\frac{c_{14}}{(2-c_{14})} \\
&\times \left[\frac{3}{2}(Z-1)e^i_Z e^j_Z \ddot{Q}_{ij} + \frac{1}{2}Z\ddot{I}_{kk} - \frac{e^i_Z e^j_Z}{c_{14}c_S^2}\ddot{\mathcal{I}}_{ij} - \frac{2}{c_{14}c_S}e^i_Z \Sigma_i\right]\Bigg|_{t-x/c_S}.
\end{aligned} \tag{2.96}$$

With equation (2.91), transverse operator can be rewritten as

$$\tilde{P}_{ij} = e^i_X e^j_X + e^i_Y e^j_Y, \tag{2.97}$$

It is not difficult to verify that the transverse-traceless operator satisfies

$$\begin{aligned} \Lambda_{ijkl} e^{ij}_{+} &= e^{kl}_{+}, \\ \Lambda_{ijkl} e^{ij}_{\times} &= e^{kl}_{\times}. \end{aligned} \tag{2.98}$$

Finally, we express the GW polarizations for N-body (particle-like) system in terms of source integrals (summations)

$$\begin{aligned} h_{+} &= \frac{G}{x} \ddot{Q}_{ij} e^{ij}_{+} \Big|_{t-x/c_T}, \quad h_{\times} = \frac{G}{x} \ddot{Q}_{ij} e^{ij}_{\times} \Big|_{t-x/c_T}, \\ h_b &= \frac{G}{x} \frac{2c_{14}}{2-c_{14}} \left[\frac{3}{2}(Z-1) \ddot{Q}_{ij} e^i_Z e^j_Z + \frac{1}{2} Z \ddot{I}_{kk} - \frac{e^i_Z e^j_Z}{c_{14} c_S^2} \ddot{\mathcal{I}}_{ij} - \frac{2}{c_{14} c_S} \Sigma_i e^i_Z \right] \Bigg|_{t-x/c_S}, \\ h_L &= \left[1 - \frac{c_{14} - 2c_{+}}{c_{14}(c_{+} - 1) c_S^2} \right] h_b, \\ h_X &= \frac{G}{x} \frac{2c_{+}}{c_V (2c_1 - c_{+} c_{-})} \left[\frac{e^j_Z}{c_V} \left(\frac{c_{+}}{1 - c_{+}} \ddot{Q}_{ij} - \ddot{\mathcal{Q}}_{ij} - \mathcal{V}_{ij} \right) + 2\Sigma_i \right] e^i_X \Bigg|_{t-x/c_V}, \\ h_Y &= \frac{G}{x} \frac{2c_{+}}{c_V (2c_1 - c_{+} c_{-})} \left[\frac{e^j_Z}{c_V} \left(\frac{c_{+}}{1 - c_{+}} \ddot{Q}_{ij} - \ddot{\mathcal{Q}}_{ij} - \mathcal{V}_{ij} \right) + 2\Sigma_i \right] e^i_Y \Bigg|_{t-x/c_V}, \end{aligned} \tag{2.99}$$

where $G = G_N \left(1 - \frac{c_{14}}{2}\right)$. The above expressions generalize the results in [47] to the case where sensitivities of neutron stars are not zero. In order to calculate polarizations, we need to know Σ_i, $\mathcal{V}_{ij}$, the second time derivatives of I_{ij}, Q_{ij}, $\mathcal{I}_{ij}$ and $\mathcal{Q}_{ij}$ for a given orbit of the system. And we shall focus on triple systems.

2.5 Response Function

To study the GWs, an important quantity is the response function $h(t)$, with respect to a specific detector, which, for the sake of simplicity, is assumed to have two orthogonal arms, such as aLIGO, aVIRGO or KAGRA.

These detectors are laser interferometers, which detect phase difference between two arms. It can be shown that the phase difference $\Delta\Phi$ is proportional to response function $h(t)$. Assume that the two arms of a detector are along the $\mathbf{e}_1$- and $\mathbf{e}_2$-directions respectively. Then, we can construct another unit vector $\mathbf{e}_3$ that forms an orthogonal basis together with $(\mathbf{e_1},\ \mathbf{e_2})$, that is, $\mathbf{e}_i \cdot \mathbf{e}_j = \delta_{ij}$. The choice of this frame is independent of the one $(\mathbf{e}_X, \mathbf{e}_Y, \mathbf{e}_Z)$, just introduced in the last subsection. But, we can always rotate properly from one frame to get the other with three independent angles, θ, ϕ and ψ [2], given by,

$$\begin{aligned}
\mathbf{e}_1 &= (\cos\theta\cos\phi\cos\psi - \sin\phi\sin\psi)\,\mathbf{e}_X \\
&\quad + (\cos\theta\cos\phi\sin\psi + \sin\phi\cos\psi)\,\mathbf{e}_Y \\
&\quad - \sin\theta\cos\phi\ \mathbf{e}_Z, \\
\mathbf{e}_2 &= (\cos\theta\sin\phi\cos\psi + \cos\phi\sin\psi)\,\mathbf{e}_X \\
&\quad + (\cos\theta\sin\phi\sin\psi - \cos\phi\cos\psi)\,\mathbf{e}_Y \\
&\quad - \sin\theta\sin\phi\ \mathbf{e}_Z, \\
\mathbf{e}_3 &= -\sin\theta\cos\psi\ \mathbf{e}_X - \sin\theta\sin\psi\ \mathbf{e}_Y \\
&\quad - \cos\theta\ \mathbf{e}_Z. \qquad (2.100)
\end{aligned}$$

Then, the response function $h(t)$ is defined as

$$\begin{aligned}
h(t) &\equiv \frac{1}{2}\left(e_1^i e_1^j - e_2^i e_2^j\right)\mathcal{P}^{ij} \\
&= F_+ h_+ + F_\times h_\times + F_b h_b + F_L h_L + F_X h_X + F_Y h_Y. \qquad (2.101)
\end{aligned}$$

[2] cf. Fig. 11.5 and equations (11.319a)-(11.319c) of [48]

The coefficients F_* only depend on the angular position of detectors, they are

$$\begin{aligned}
F_+ &\equiv \frac{1}{2}\left(1+\cos^2\theta\right)\cos 2\phi\cos 2\psi - \cos\theta\sin 2\phi\sin 2\psi, \\
F_\times &\equiv \frac{1}{2}\left(1+\cos^2\theta\right)\cos 2\phi\sin 2\psi + \cos\theta\sin 2\phi\cos 2\psi, \\
F_b &\equiv -\frac{1}{2}\sin^2\theta\cos 2\phi, \\
F_L &\equiv \frac{1}{2}\sin^2\theta\cos 2\phi, \\
F_X &\equiv -\sin\theta\left(\cos\theta\cos 2\phi\cos\psi - \sin 2\phi\sin\psi\right), \\
F_Y &\equiv -\sin\theta\left(\cos\theta\cos 2\phi\sin\psi + \sin 2\phi\cos\psi\right).
\end{aligned} \tag{2.102}$$

Hence, its Fourier transformation takes the form

$$\tilde{h}(f) = \frac{1}{2\pi}\int h(t)e^{-i2\pi ft}dt. \tag{2.103}$$

We also adopt the discrete Fourier transform (DFT) for non-analytical waveforms. First, the time interval of signal $h(t)$ is divided into $N-1$ subintervals, $t = \{t_0, t_1, ..., t_{N-1}\}$, $t_m = m\Delta t$, Δt is the length of a subinterval. Then we have a list of discrete values $h^m \equiv h(t_m)$, and we get the DFT according to the following formula

$$\tilde{h}^n = \frac{1}{N}\sum_{m=0}^{N-1} h^m e^{-i2\pi nm/N}, \tag{2.104}$$

where $\tilde{h}^n \approx \tilde{h}(f)$, $f = \{f_0, f_1, ..., f_{N-1}\}$, $f_n = n/(N\Delta t)$. In this paper, we shall use the built-in function of software **Mathematica** to calculate DFT of waves.

2.6 Radiation Power

Ultimately, one is interested in calculating physical, observable quantities from the GWs that can be measured at spatial infinity. One example is the rate of energy transported by GWs away from any system per unit time, the so called energy loss rate.

Using the Noether current method described in [49], we find that the energy loss rate is

$$\dot{\mathcal{E}} = -\frac{1}{16\pi G}\left\langle \int d\Omega\, x^2 \left[\frac{1}{2c_T}\dot{\phi}_{ij}\dot{\phi}_{ij} + \frac{(2c_1 - c_+c_-)(1-c_+)}{c_V}\dot{\nu}^i\dot{\nu}^i + \frac{2-c_{14}}{4c_{14}c_S}\dot{F}\dot{F}\right]\right\rangle, \tag{2.105}$$

where the dot over the function stands for a time derivative, Ω is the solid angle, and the angle brackets stand for an average over several periods of the GW, defined by

$$\langle f(t)\rangle \equiv \frac{1}{3T}\int_0^T f(t)dt, \tag{2.106}$$

with T is the period of the GW.

The power radiated by GWs is the negative energy loss rate

$$P = -\dot{\mathcal{E}}. \tag{2.107}$$

The power can be further evaluated by substituting in the expressions for the fields given by equations (2.94-2.96), and performing the angular integral [37],

$$\begin{aligned} P \;=\;& G\left\langle \frac{\mathcal{A}_1}{5}\dddot{Q}_{ij}\dddot{Q}_{ij} + \frac{\mathcal{A}_2}{5}\dddot{Q}_{ij}\dddot{\mathcal{Q}}_{ij} + \frac{\mathcal{A}_3}{5}\dddot{\mathcal{Q}}_{ij}\dddot{\mathcal{Q}}_{ij}\right. \\ & \left. +\mathcal{B}_1\dddot{I}\dddot{I} + \mathcal{B}_2\dddot{I}\dddot{\mathcal{I}} + \mathcal{B}_3\dddot{\mathcal{I}}\dddot{\mathcal{I}} + \mathcal{C}\dot{\Sigma}^i\dot{\Sigma}^i + \mathcal{D}\dot{\mathcal{V}}_{ij}\dot{\mathcal{V}}_{ij}\right\rangle, \end{aligned} \tag{2.108}$$

$$\begin{aligned} \mathcal{A}_1 &\equiv \frac{1}{c_T} + \frac{2c_{14}c_+^2}{(2c_1-c_+c_-)^2c_V} + \frac{3c_{14}(Z-1)^2}{2(2-c_{14})c_S}, \\ \mathcal{A}_2 &\equiv -\frac{2c_+}{(2c_1-c_+c_-)c_V^3} - \frac{2(Z-1)}{(2-c_{14})c_S^3}, \\ \mathcal{A}_3 &\equiv \frac{1}{2c_{14}c_V^5} + \frac{2}{3c_{14}(2-c_{14})c_S^5}, \\ \mathcal{B}_1 &\equiv \frac{c_{14}Z^2}{4(2-c_{14})c_S}, \quad \mathcal{B}_2 \equiv -\frac{Z}{3(2-c_{14})c_S^3}, \quad \mathcal{B}_3 \equiv \frac{1}{9c_{14}(2-c_{14})c_S^5}, \\ \mathcal{C} &\equiv \frac{4}{3c_{14}c_V^3} + \frac{4}{3c_{14}(2-c_{14})c_S^3}, \quad \mathcal{D} \equiv \frac{1}{6c_{14}c_V^5}. \end{aligned} \tag{2.109}$$

CHAPTER THREE

Gravitational Waves from Triple Systems

Consider a triple system with masses m_A and positions $\mathbf{x}_A(t)$, where A specifies the three bodies, $A = 1, 2, 3$. Then, from equation (2.99) we can see that all polarization modes are functions of the type $h_N(\mathbf{x}; \mathbf{x}_A(t))$, where $\mathbf{x}_A(t)$'s are the trajectories of the three bodies. So, once $\mathbf{x}_A(t)$'s are known, we can study the polarizations of GWs emitted by this triple system. Similarly, we could easily obtain the power radiated by GWs with equation (2.108) in Einstein-aether theory.

In the framework of Einstein-aether theory the analytical trajectories of a triple system have not been studied, yet. So we shall use the Newtonian trajectories of the triple systems [1], which have been intensively studied in the past three hundred years, for which various periodic solutions have been found, see for example, [50] and references therein. Some of these orbits have been used to study the GWs in the framework of GR. In particular, in [51] it was shown that the quadrupole GWs of a figure eight trajectory discovered by Moore in 1993 [52] is indistinguishable from that of a binary system. In addition, Dmitrasinovic, Suvakov and Hodomal calculated the quadrupole wave forms and the corresponding luminosity for the $13 + 11$ periodic orbits of three-body problems in Newtonian gravity [53], discovered, respectively, in [54] and [55]. Among other things, they found that all of these $13 + 11$ orbits

[1] Corrections due to the aether effects are expected to be small, and should be consistent with the lowest PN order approximations adopted in this paper.

produce different waveforms and their luminosity (power) vary by up to 13 orders of magnitude in the mean, and up to 20 orders for the peak values.

On the other hand, we could also use observational data to extract the orbit of a real astronomical triple system. In fact, there are about 13% of low-mass stellar systems containing three or more stars [57], and 96% of low-mass binaries with periods shorter than three days which are part of a larger hierarchy [58]. Recently, a relativistic triple system was observed, PSR J0337 + 1715 (J0337) [59], which consists of an inner binary and a third companion. The inner binary consists of a pulsar with mass $m_1 = 1.44 M_{\odot}$ and a white dwarf (WD) with mass $m_2 = 0.20 M_{\odot}$ in a 1.6 day orbit. The outer binary consists of the inner binary and a second dwarf with mass $m_3 = 0.41 M_{\odot}$ in a 327 day orbit. The two orbits are very circular with eccentricities $e_I \simeq 6.9 \times 10^{-4}$ for the inner binary and $e_O \simeq 3.5 \times 10^{-2}$ for the outer orbit. The two orbital planes are remarkably coplanar with an inclination $\lesssim 0.01^o$ [See Fig. 3.1].

In this chapter, we shall use weak field limit of sensitivities equation (1.18), since the gravitational field is relatively weak for the systems are considered here.

3.1 Triple Systems with Periodic Orbits

In this section, we shall consider some of the periodical trajectories provided in [56]. In the configurations provided in this site, the three bodies are assumed all to have equal masses, $m_1 = m_2 = m_3 = m$, and the units were chosen so that $G_N = 1,\ m = 1$. Also, we set $c_1 = 4 \times 10^{-5}, c_2 = 9 \times 10^{-5}, c_3 = -c_1$, and $c_4 = -2 \times 10^{-5}$, a condition that will be adopted for the rest of this section. For such choices, the coupling constants c_i's clearly satisfy the theoretical and observational constraints of the æ-theory [42]. In addition, with these choices, we have $c_+ = 0$, and then

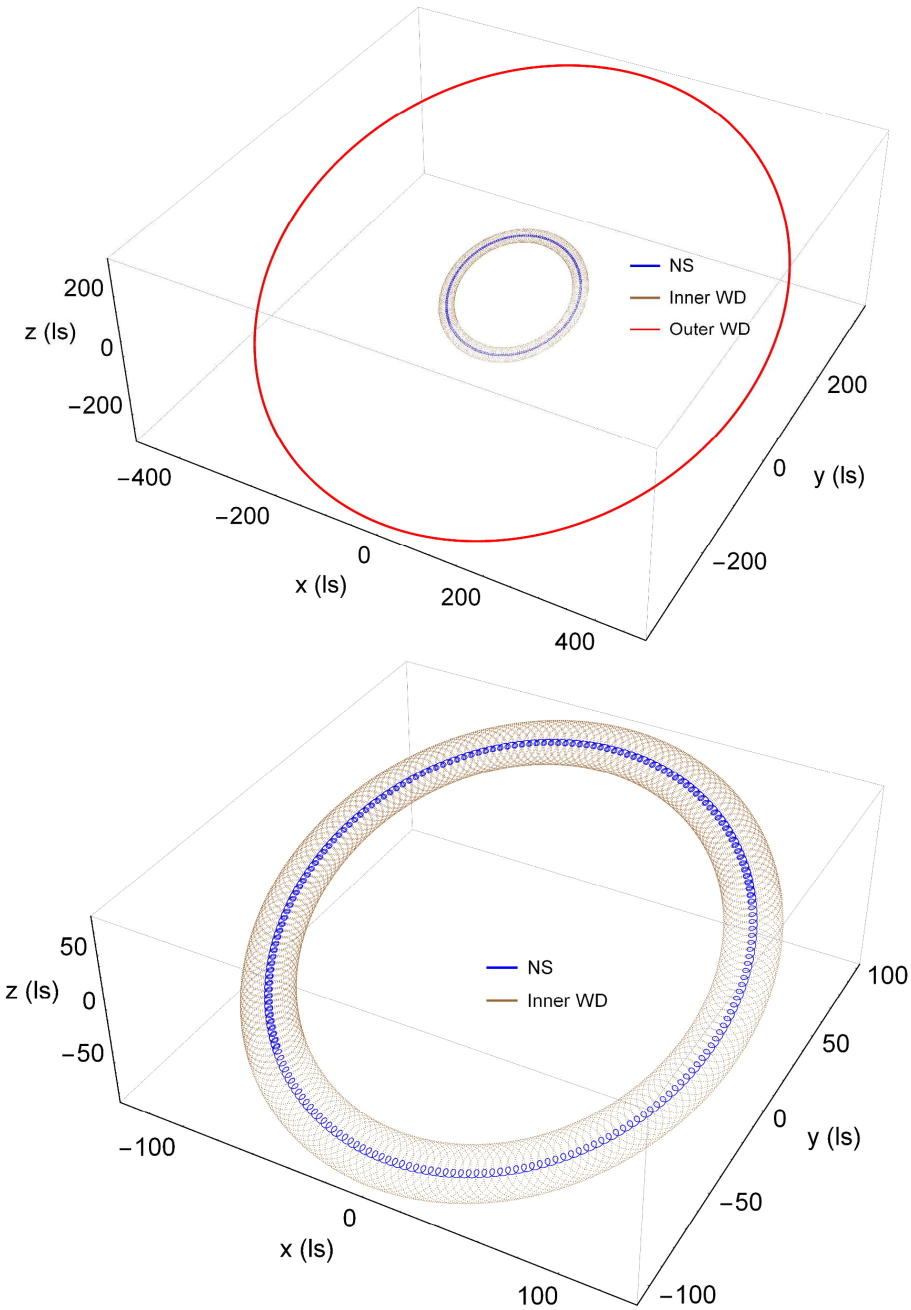

Figure 3.1: Orbit of the neutron star, inner white dwarf and the outer white dwarf where the units are in light second (ls). This shows the trajectories observed in the center-of-mass coordinate system for about 330 days starting from 01-04-2012 [65].

from equation (2.99) we find that the vector polarizations h_X and h_Y are identically zero, So, in the rest of this section we only need to consider the $h_+,\ h_\times,\ h_b$ and h_L polarizations.

Let us first consider the GWs of the Simo's figure-eight trajectory [61], the GWs in GR have been studied in [53]. In figure 3.2, the trajectory of the 3-body problem is plotted out in the (x, y)-plane for many periods, in order to make sure that our numerical codes converge well after a sufficiently long run.

Assuming that the detector is along the z-axis, we plot the polarization polarizations h_+ and $h_\times$ in figure 3.3. In this figure, we plot these polarizations given in GR as well as in Einstein-aether theory. Precisely, the difference between waves of ae-theory and those of GR is of the order of $\mathcal{O}\left(10^{-5}\right)$. This can be seen clearly from this figure, in which the lines are almost identical in both theories.

In Fig. 3.4 we plot the polarization polarizations h_b and h_L in æ-theory, which all vanish in GR. Comparing results with those shown in figure 3.3 it can be seen that the amplitudes of these polarizations are about five orders lower than h_+ and $h_\times$.

In Figs. 3.5, 3.6 and 3.7, we plot the corresponding response function $h(t)$, its Fourier transform $\tilde{h}(f)$ and the radiation power $P(\equiv -\dot{\mathcal{E}})$ for the Simo's figure-eight 3-body system. From Fig. 3.7 we can see that both of the dipole and monopole contributions are suppressed.

While plotting figures 3.2-3.7, we assumed that the binding energies of the three bodies are $\Omega_1 = -0.1,\ \Omega_2 = -2.76 \times 10^{-6}$ and $\Omega_3 = -2.9 \times 10^{-5}$ respectively. In addition, the locations and orientations of the source and the detector are all independent, which are parameterized by the five angles $(\vartheta, \varphi; \theta, \phi, \psi)$, defined in equations (2.90) and (2.100). We chose $(\vartheta, \varphi; \theta, \phi, \psi) = (0, 0; 0, 0, 0)$.

Next, we explore the effects of changes in these parameters. First, we will fix binding energies and vary angles.

In Figs. 3.8-3.12 we plot the polarization functions h_N, response function $h(t)$, its Fourier transform $\tilde{h}(f)$ and the radiation power $P_{\mathcal{A}}$, $P_{\mathcal{B}}$ and $P_{\mathcal{C}}$, respectively, for $(\vartheta, \varphi; \theta, \phi, \psi) = (0.6, 5.2; 1.3, 1.2, 1.8)$, while still choosing $(\Omega_1,\ \Omega_2,\ \Omega_3) = (-0.1,\ -2.76 \times 10^{-6},\ -2.9 \times 10^{-5})$. Clearly, the corresponding mode functions, response function and its Fourier transform are all different from the previous case. However, the radiation power is the same and is independent of the choice of these five angular parameters, as can be seen by comparing figures 3.7 and 3.12.

To study the effects of the binding energies of the three bodies on the wave forms and energy losses, we consider the same case shown by Figs. 3.8 - 3.12 but now with all three bodies having the same binding energy, $\Omega_1 = \Omega_1 = \Omega_1 = -10^{-2}$. With this choice, the dipole contribution to the radiated power is identically zero.

In Figs. 3.13 - 3.17 we plot the polarization functions h_N, response function $h(t)$, its Fourier transform $\tilde{h}(f)$ and the radiation power $P_{\mathcal{A}}$ and $P_{\mathcal{B}}$, respectively, for $(\vartheta, \varphi; \theta, \phi, \psi) = (0.6, 5.2; 1.3, 1.2, 1.8)$, and $(\Omega_1,\ \Omega_2,\ \Omega_3) = (-10^{-2}, -10^{-2}, -10^{-2})$. Clearly, the corresponding mode functions, response function, its Fourier transform and radiation power are all different from the previous case. In particular, the dipole contributions vanish now.

In Figs. 3.18-3.22, we plot, respectively, the trajectory of the Broucke R7 3-body system provided in [56], the polarization polarizations h_N, the response function $h(t)$, its Fourier transform $\tilde{h}(f)$ and the radiation power P, for $(\Omega_1,\ \Omega_2,\ \Omega_3) = (-0.1,\ -2.76 \times 10^{-6},\ -2.9 \times 10^{-5})$ and $(\vartheta, \varphi; \theta, \phi, \psi) = (0.6, 5.2; 1.3, 1.2, 1.8)$.

In Fig. 3.23 we plot the trajectory of the Broucke A16 3-body system provided in [56], while in Fig. 3.24-3.27 we plot the corresponding physical quantities for the same choice of the five angular parameters as selected in the case for the Broucke R7 3-body system in both GR and æ-theory with $(\Omega_1,\ \Omega_2,\ \Omega_3) = (-0.1,\ -2.76 \times 10^{-6},\ -2.9 \times 10^{-5})$ and $(\vartheta, \varphi; \theta, \phi, \psi) = (0.6, 5.2; 1.3, 1.2, 1.8)$.

From these figures we can clearly see that the GWs and radiation power not only depend on the relative positions, orientations between the source and detector, but also depend on the configurations of the orbits of the 3-body system. In addition, they also depend on their binding energies of the three compact bodies.

3.2 The Relativistic Triple System (PSR J0337+1715)

In this section, we shall focus on the relativistic triple system PSR J0337+1715. Specifically, we investigate this triple system in three different theories of gravity, General Relativity (GR), Einstein-aether theory (æ-theory) and Brans-Dicke (BD) gravity, by using the post-Newtonian approximations to their lowest order. We shall pay particular attention to the differences predicted by these theories. Although neither the current generation of detectors nor the next one can detect the GWs emitted by this system [2], it serves well as a realistic example to show clearly the different predictions from each of these theories. In particular, we shall study gravitational waveforms, their polarizations, Discrete Fourier transform (DFT) of polarizations as well as the radiation power. Among the modified theories of gravity, æ-theory locally breaks the Lorentz symmetry by introducing a globally time-like unit vector field (the

[2] The frequency of the GWs emitted by this system is about 10^{-8} Hz. With this frequency, only the pulsar timing array (PTA), such as IPTA and SKA, can detect such GWs. The amplitudes of these GWs are far below the sensitivities of these detectors.

aether) [62], while in BD gravity the gravitational interaction is mediated by both scalar and tensor fields [63].

Before jumping into the details, we would like to note that, in the framework of æ-theory, Foster [38] and Yagi *et al.* [39] derived the metric and equations of motion to the 1PN order for a N-body system. Recently, Will applied these to study the 3-body problem and obtained the accelerations of a 2-body system in the presence of the third body at the quasi-Newtonian order [64]. For nearly circular coplanar orbits, Will also calculated the strong-field Nordtvedt parameter $\hat{\eta}_N$. For triple system J0337, ignoring the sensitivities of the two white-dwarf companions, Will found that $\hat{\eta}_N$ is given by $\hat{\eta}_N = s_1/(1-s_1)$, where s_1 denotes the sensitivity of the pulsar.

Since J0337 is a triple system, there exists no analytical orbit, the numerical orbit supplied by Dr. Lijing Shao based on the observational data [65] is used. In the case of J0337, ϑ and φ are 0° and 270°, respectively [59].

3.2.1 General Relativity

In GR, the equations of the geodesic deviation take the form [46]

$$\ddot{\zeta}_i = -R_{0i0j}\zeta^j = \frac{1}{2}\ddot{h}_{ij}^{TT}\zeta^j, \tag{3.1}$$

$$h_{ij}^{TT}(t,\mathbf{x}) = \frac{2G_N}{R}\ddot{Q}_{ij}^{TT}(t-R), \tag{3.2}$$

with $R \equiv |\mathbf{x}|$ denoting the distance from the observer to the source and G_N denoting the Newtonian constant. In GR, h_{ij}^{TT} has only two degrees of freedom corresponding to the plus (+) and cross (×) polarizations, which are given by

$$h_+^{GR} = \frac{G_N}{R}\ddot{Q}_{kl}e_+^{kl}, \quad h_\times^{GR} = \frac{G_N}{R}\ddot{Q}_{kl}e_\times^{kl}, \tag{3.3}$$

where $e_+^{kl} \equiv e_X^k e_X^l - e_Y^k e_Y^l$, $e_\times^{kl} \equiv e_X^k e_Y^l + e_Y^k e_X^l$. In Figs. 3.28 and 3.29, we plot these two polarizations; from these figures it can be seen that the amplitudes of both polarizations are about 10^{-22}, which is in the range of the designed sensitivity of the current generation of the ground-based detectors, such as LIGO, Virgo and KAGRA, but their frequencies do not lie within the detectors frequency bands [66]. This is because the orbital frequency of J0337 is out of the observational bands of the current detectors. You can find the frequencies of these two polarizations easily from Figs. 3.30 and 3.31.

In Figs. 3.30 and 3.31 we plot $\tilde{h}_+^{GR}(f)$ and $\tilde{h}_\times^{GR}(f)$, respectively. In these figures, there are two peaks and the corresponding frequencies are

$$\begin{aligned} f_1^{+,\times} &= \quad 0.068658\ \mu\text{Hz} \simeq 2.0 f_o, \\ f_2^{+,\times} &= \qquad 14.212\ \mu\text{Hz} \simeq 1.9 f_i, \end{aligned}$$

where f_o and f_i represent outer and inner orbital frequencies of the triple system J0337 [59],

$$f_o = 0.035\ \mu\text{Hz}, \quad f_i = 7.103\ \mu\text{Hz}. \tag{3.4}$$

Thus, $f_1^{+,\times}$ and $f_2^{+,\times}$ are about twice the outer and inner orbital frequencies of the triple system, but not exactly. In GR, for a binary system the GW frequency is exactly equal to two times their orbital frequency [46]. However, it must be noted that here the difference is due to the presence of the third component of the triple system.

3.2.2 Einstein-aether Theory

In æ-theory, the equation of the geodesic deviation reads

$$\ddot{\zeta}_i = -R_{0i0j}\zeta^j \equiv \frac{1}{2}\ddot{\mathcal{P}}_{ij}\zeta^j. \tag{3.5}$$

The Riemann tensor is expressed in terms of linear perturbations as

$$\mathcal{P}_{ij} = \phi_{ij} + a_1 \nu_{(i}\hat{x}_{j)} + a_2 F \hat{x}^i \hat{x}^j + \frac{1}{2}\delta_{ij} F. \tag{3.6}$$

For the polarizations in ae-theory h_+, $h_\times$, h_b, $\ldots$, please refer to (2.99). From those expressions, in addition to the usual plus and cross polarization modes, æ-theory predicts three extra independent modes, $h_b^{æ}$, $h_X^{æ}$ and $h_Y^{æ}$. Comparing to $h_+^{æ}$ and $h_\times^{æ}$, these extra modes are suppressed, respectively, by factors of $c_{14} \lesssim 10^{-5}$ and $c_+ \lesssim 10^{-15}$ [33]. The longitudinal mode $h_L^{æ}$ is proportional to the breathing mode $h_b^{æ}$.

In the following, we first consider the case

$$\begin{aligned} c_1 &= 4\times 10^{-5},\;\; c_2 = 9\times 10^{-5}, \\ c_3 &= -c_1,\;\; c_4 = -2\times 10^{-5}, \end{aligned} \tag{3.7}$$

which satisfy all the theoretical and observational constraints. Note that for this choice we have $c_+ = 0$, and then the two modes $h_X^{æ}$ and $h_Y^{æ}$ vanish identically,

$$h_X^{æ} = h_Y^{æ} = 0,\;(c_+ = 0). \tag{3.8}$$

In the rest of this paper, we shall not consider them any further.

In Figs. 3.28 and 3.29, we plot the two polarization modes $h_+^{æ}$ and $h_\times^{æ}$, while in Figs. 3.30 and 3.31, we plot their DFTs. From these figures, it can be seen clearly that these two modes are almost identical to the ones given in GR, after all the constraints of æ-theory are taken into account. In fact, we have

$$\frac{h_{+,\times}^{æ}}{h_{+,\times}^{GR}} = 1 - \frac{1}{2}c_{14}. \tag{3.9}$$

The differences between æ-theory and GR are determined by c_{14},

$$\Delta h_{+,\times}^{æ} \equiv \frac{h_{+,\times}^{æ} - h_{+,\times}^{GR}}{h_{+,\times}^{GR}} = -\frac{1}{2}c_{14}. \tag{3.10}$$

Recall that $c_{14} \lesssim 2.5 \times 10^{-5}$. Therefore, the signals of these two modes in æ-theory and GR are overlapping, their frequencies are precisely the same, as shown in Figs. 3.30 and 3.31. Similarly, the differences in frequency domain can be defined as

$$\Delta|\tilde{h}^{æ}_{+,\times}| \equiv \left(|\tilde{h}^{æ}_{+,\times}| - |\tilde{h}^{GR}_{+,\times}|\right)/|\tilde{h}^{GR}_{+,\times}|. \tag{3.11}$$

In Fig. 3.32, we plot $h^{æ}_b$ and $h^{æ}_L$, which are about three orders lower than $h^{æ}_+$ and $h^{æ}_\times$. In Fig. 3.33, we plot the DFT of the h_b and h_L. It is remarkable that now the two peak frequencies are approximately equal to the outer and inner orbital frequencies,

$$\begin{aligned} f^{b,L}_1 &= 0.045772\,\mu\text{Hz} \simeq 1.3 f_o, \\ f^{b,L}_2 &= 7.0947\,\mu\text{Hz} \simeq 1.0 f_i, \end{aligned} \tag{3.12}$$

where f_o and f_i are given by equation (3.4). The GW frequencies $f^{b,L}_1$ and $f^{b,L}_2$ are almost equal to the outer and inner orbital frequencies of the triple system.

Recently, we find that for binary systems in æ-theory, the polarization modes h_b and h_L all contain two frequencies: one is equal to the binary's orbital frequency and the other is twice the orbital frequency [35]. This confirms the above result since J0337 can be considered a hierarchical system consisting of two binaries. Again, the reason that $f^{b,L}_1$ and $f^{b,L}_2$ are not exactly equal to the outer and inner orbital frequencies of the triple system is due to the influence of the third component of the triple system, rather than the predictions of the æ-theory itself.

To see further the dependence of $h^{æ}_{b,L}$ on c_i's, given that $c_{14}/c_2 \lesssim 1$,

$$\begin{aligned} h^{æ}_b &\simeq \frac{c_S}{1+c_S} h^{æ}_L \\ &\simeq \frac{G_{æ}}{2R}\left\{3c_{14}\ddot{Q}_{ij}e^i_Z e^j_Z - \sqrt{\frac{c_{14}}{c_2}}\Sigma_i e^i_Z + 2c_{14}\ddot{I}\right\}. \end{aligned} \tag{3.13}$$

From the above equation, we see that $h^{æ}_{b,L}$ are dependent on c_2 and c_{14} mainly. To see the effects explicitly, in the following we consider two more cases.

In the first case, c_2 is chosen to be different from that given in the equation (3.7), now we have

$$\begin{aligned} c_1 &= 4 \times 10^{-5}, \;\; c_2 = 0.095, \\ c_3 &= -c_1, \;\; c_4 = -2 \times 10^{-5}. \end{aligned} \tag{3.14}$$

In Figs. 3.34 and 3.35 we plot the breathing ($h^{æ}_b$) and longitudinal ($h^{æ}_L$) polarization modes for this case. Comparing them, respectively, with Figs. 3.32 and 3.33, we find that the amplitudes of $h^{æ}_b$ and $h^{æ}_L$ decrease when c_2 increases, whereas their frequencies remain the same.

In the second case, c_{14} is chosen to be different from the values given in equation (3.7); the parameters are

$$\begin{aligned} c_1 &= 4 \times 10^{-8}, \;\; c_2 = 9 \times 10^{-5}, \\ c_3 &= -c_1, \;\; c_4 = -2 \times 10^{-8}. \end{aligned} \tag{3.15}$$

The corresponding $h^{æ}_b$ and $h^{æ}_L$ modes are shown in Figs. 3.36 and 3.37. Comparing them with Figs. 3.32 and Fig. 3.33, we find that the amplitudes of $h^{æ}_b$ and $h^{æ}_L$ decrease when c_{14} decreases, whereas their frequencies stay the same, as is expected from equation (3.13).

3.2.3 Brans–Dicke Gravity

Brans–Dicke gravity is an example of a scalar–tensor theory in which the gravitational interaction is mediated by a scalar field as well as the tensor field of general relativity. The gravitational constant G is not presumed to be constant but instead $1/G$ is replaced by a scalar field ϕ, which can depend on a spacetime point. The metric perturbation and scalar field perturbation are given by [67]

$$\begin{aligned}
\theta^{ij} &= \frac{2}{\phi_0}\frac{1}{R}\frac{d^2}{dt^2}\sum_{a=1}^{3} m_a x_a^i x_a^j, \\
\varphi^{BD} &= \frac{4}{R}(N_i \dot{M}_1^i + \frac{1}{2}N_i N_j \ddot{M}_2^{ij}),
\end{aligned} \tag{3.16}$$

where ϕ_0 is the value of the BD scalar field in the Minkowski background, which satisfies $\phi_0 = (4+2\omega_{BD})/[(3+2\omega_{BD})G_N]$ [68], and

$$\begin{aligned}
M_1^i &= \tfrac{1}{6+4\omega_{BD}} \sum_{a=1}^{3} m_a(1-2s_a)x_a^i, \\
M_2^{ij} &= \tfrac{1}{6+4\omega_{BD}} \sum_{a=1}^{3} m_a(1-2s_a)x_a^i x_a^j,
\end{aligned} \tag{3.17}$$

where ω_{BD} is the BD parameter of the theory. In this chapter, we choose sensitivities such that s_1 (for pulsar) = 0.2, s_2 (for inner WD) = 0, s_3 (for outer WD) = 0 and the coupling constant $\omega_{BD} = 10^5$ [69]. Note that in writing the above expressions, we have dropped the non-propagating terms in φ^{BD}. Then, the components R_{0i0j} of the Riemann tensor can be cast in the form

$$R_{0i0j} = -\frac{1}{2}\frac{d^2}{dt^2}\left[\theta_{ij}^{TT} - \frac{\varphi^{BD}}{\phi_0}(\delta_{ij} - N_i N_j)\right]. \tag{3.18}$$

It can then be shown that there are only three independent polarization modes given, respectively, by

$$\begin{aligned}
h_+^{BD} &= \frac{1}{2}e_+^{ij}\theta_{ij}, \quad h_\times^{BD} = \frac{1}{2}e_\times^{ij}\theta_{ij}, \\
h_b^{BD} &= -\frac{\varphi^{BD}}{\phi_0},
\end{aligned} \tag{3.19}$$

which are plotted in Figs. 3.28, 3.29 and 3.32 respectively, while their DFTs are shown in Figs. 3.30, 3.31 and 3.33.

From these figures, it can be seen that the two polarization modes h_+^{BD} and $h_\times^{BD}$ overlap with those in GR and æ-theory, due to the observational constraints on the ω_{BD}. In fact, we have

$$\frac{h^{BD}_{+,\times}}{h^{GR}_{+,\times}} = \frac{3+2\omega_{BD}}{4+2\omega_{BD}}. \tag{3.20}$$

The differences between BD gravity and GR are determined by ω_{BD},

$$\Delta h^{BD}_{+,\times} \equiv \frac{h^{BD}_{+,\times} - h^{GR}_{+,\times}}{h^{GR}_{+,\times}} = \frac{3+2\omega_{BD}}{4+2\omega_{BD}} - 1. \tag{3.21}$$

Recall that $\omega_{BD} \sim \mathcal{O}(10^5)$. Therefore, the signals of these two modes in BD gravity and GR are overlapping, their frequencies are precisely the same, as shown in Figs. 3.30 and 3.31. Similarly the differences in frequency domain can be defined as

$$\Delta|\tilde{h}^{BD}_{+,\times}| \equiv \left(|\tilde{h}^{BD}_{+,\times}| - |\tilde{h}^{GR}_{+,\times}|\right)/|\tilde{h}^{GR}_{+,\times}|. \tag{3.22}$$

As seen in Fig. 3.32, the breathing mode (h^{BD}_b) is different from æ-theory. From Fig. 3.33, its DFT has also two peak frequencies which are equal to those of æ-theory, i.e., the breathing mode in BD gravity only has first harmonics of orbital phase. In contrast the polarization modes h_+ and $h_\times$ have second harmonics of orbital phase.

3.2.4 Radiation Power

In GR, the total radiation power is given by [46, 70]

$$P^{GR} = \frac{G_N}{5}\left\langle \dddot{Q}_{ij}\dddot{Q}_{ij}\right\rangle, \tag{3.1}$$

where Q_{ij} is the mass quadrupole moment defined in equation (2.71) and the angular brackets denote the time average. [3]. Note that in this section we shall not distinguish the time t and its corresponding retarded time. Strictly speaking, all the quantities should be evaluated at the retarded time. However, it is not necessary for our current purpose. The reference frame is chosen such that the inclination is 39.25°, where

[3] However, since we are considering periodic GWs, we will not take this time average in the relevant plots. Otherwise, it will be zero for such periodic waves. The same will also apply to the cases of æ-theory and BD gravity.

the inclination is the angle of the orbital plane relative to the plane perpendicular to the line-of-sight from Earth to the pulsar. In Fig. 3.38, we plot the radiation power calculated by GR for about 500 days, where the insert shows the details from day 12 to day 26.

In æ-theory, and in the weak field limit, we find that [37, 47]

$$P^{æ} = G_N \left\langle \frac{\mathcal{A}}{5} \dddot{Q}_{ij} \dddot{Q}_{ij} + \mathcal{B} \dddot{I} \dddot{I} + \mathcal{C} \dot{\Sigma}_i \dot{\Sigma}_i \right\rangle, \tag{3.2}$$

where Σ_i is defined as

$$\Sigma_i = \left(\alpha_1 - \tfrac{2}{3}\alpha_2\right) \sum_A \left(v_A^i \Omega_A\right), \tag{3.3}$$

and

$$\begin{aligned}
\mathcal{A} &\equiv \left(1 - \frac{c_{14}}{2}\right) \left(\frac{1}{c_T} + \frac{2c_{14}c_+^2}{(2c_1 - c_+c_-)^2 c_V} \right. \\
&\qquad \left. + \frac{3(Z-1)^2 c_{14}}{2(2-c_{14})c_S}\right), \\
\mathcal{B} &= \frac{Z^2 c_{14}}{8c_S}, \\
\mathcal{C} &\equiv \frac{2}{3c_{14}} \left(\frac{2-c_{14}}{c_V^3} + \frac{1}{c_S^3}\right), \\
Z &\equiv \frac{(\alpha_1 - 2\alpha_2)(1-c_+)}{3(2c_+ - c_{14})},
\end{aligned} \tag{3.4}$$

with [37]

$$\begin{aligned}
\alpha_1 &= -\frac{8\left(c_1 c_{14} - c_- c_+\right)}{2c_1 - c_- c_+}, \\
\alpha_2 &= \frac{1}{2}\alpha_1 + \frac{\left(c_{14} - 2c_{13}\right)\left(3c_2 + c_+ + c_{14}\right)}{c_{123}(2 - c_{14})}.
\end{aligned} \tag{3.5}$$

Here $v_A^i \equiv \dot{x}_A^i$ is the velocity of A-th body along x^i-direction, Ω_A is the binding energy of A-th body. For J0337 [59], we have Ω_1 (for pulsar) $=-2.56955 \times 10^{46}$ J, Ω_2 (for inner WD)$=-9.75554 \times 10^{40}$ J, Ω_3 (for outer WD)$=-2.12650 \times 10^{42}$ J. c_T, c_V and

c_S are the speeds of the tensor, vector and scalar modes, given by equation (2.37), (2.43) and (2.52).

In Fig. 3.39, we plot the radiation power in æ-theory of the parts $\mathcal{A}$, $\mathcal{B}$ and $\mathcal{C}$ separately, for about 500 days. Again, the inserts are from day 12 to day 26. Note that at every moment during the 252 days in the plot, the $\mathcal{A}$ part of æ-theory is quite close to that of GR with the relative difference proportional to c_{14} [33],

$$\frac{P^{æ}_{\mathcal{A}}}{P^{GR}} - 1 \simeq \mathcal{O}(c_{14}) \lesssim \mathcal{O}(10^{-5}). \tag{3.6}$$

From this figure, it is also clear that the dipole part $\mathcal{C}$ has almost the same amplitude as that of the quadrupole part $\mathcal{A}$, while the monopole part $\mathcal{B}$ is suppressed by a factor c_{14} [33]. The large magnitude of the dipole contribution $\mathcal{C}$ seemingly contradicts to the analysis given in [33]. In particular, equation (3.13) in [33] shows that $\mathcal{W}_{\mathcal{C}}^{\text{NS}}/\mathcal{W}_{\mathcal{A}}^{\text{NS}} \simeq 10^{-2}$, with

$$\begin{aligned} \mathcal{W}_{\mathcal{A}} &\equiv \frac{8}{15}\mathcal{A}\left(12v^2 - 11\dot{r}^2\right), \\ \mathcal{W}_{\mathcal{C}} &\equiv \mathcal{C}\Sigma^2, \end{aligned} \tag{3.7}$$

where $\mathcal{A}$, $\mathcal{C}$ and Σ are all given explicitly in [33]. However, in deriving $\mathcal{W}_{\mathcal{C}}^{\text{NS}}/\mathcal{W}_{\mathcal{A}}^{\text{NS}} \simeq 10^{-2}$ we assumed that $\mathcal{O}\left(v^2\right) \simeq 10^{-5}$, while in the case of J0337 we find that the relative velocities of the inner binary system are of the order of $\mathcal{O}\left(v^2\right) \simeq 10^{-7}$. After this is taken into account, we find that $\mathcal{W}_{\mathcal{C}}/\mathcal{W}_{\mathcal{A}} \simeq \mathcal{O}(1)$ for the current triple system.

It is remarkable to note that with the multi-band gravitational wave astronomy [91], joint observations of GWs by LIGO/Virgo/KAGRA and LISA will improve bounds on dipole emission from black hole binaries by six orders of magnitude relative to current constraints [92]. Thus, it is very promising that the third generation of detectors, both space-borne and ground-based, could provide severe constraints on ae-theory.

In BD gravity, following [67] we obtain

$$P^{BD} = P_1^{BD} + P_2^{BD}, \tag{3.8}$$

$$\begin{aligned}
P_1^{BD} &= \frac{1}{\phi_0}\left\langle \frac{1}{5}\dddot{Q}_{ij}\dddot{Q}_{ij} \right\rangle, \\
P_2^{BD} &= \frac{1}{\phi_0}\left\langle \frac{2\omega+3}{\pi}\left[\frac{4\pi}{3}\ddot{M}_1^i\ddot{M}_1^i \right.\right. \\
&\quad \left.\left. + \frac{\pi}{12}\left(\dddot{M}_2^{ii}\dddot{M}_2^{jj} + 2\dddot{M}_2^{ij}\dddot{M}_2^{ij}\right)\right]\right\rangle,
\end{aligned} \tag{3.9}$$

where M_1^i and M_2^{ij} are defined by equation (3.17). Note that in writing down the above expressions, we had dropped the non-propagating terms.

In Fig. 3.40, we plot the radiation power in BD gravity for about 500 days, where the insert shows the details only from day 12 to day 26. Note that at every moment during the 500 days, the first part of BD is quite close to that given in GR. In fact, we find that

$$\frac{P_1^{BD}}{P^{GR}} - 1 \simeq \mathcal{O}\left(\omega_{BD}^{-1}\right) \lesssim \mathcal{O}(10^{-5}). \tag{3.10}$$

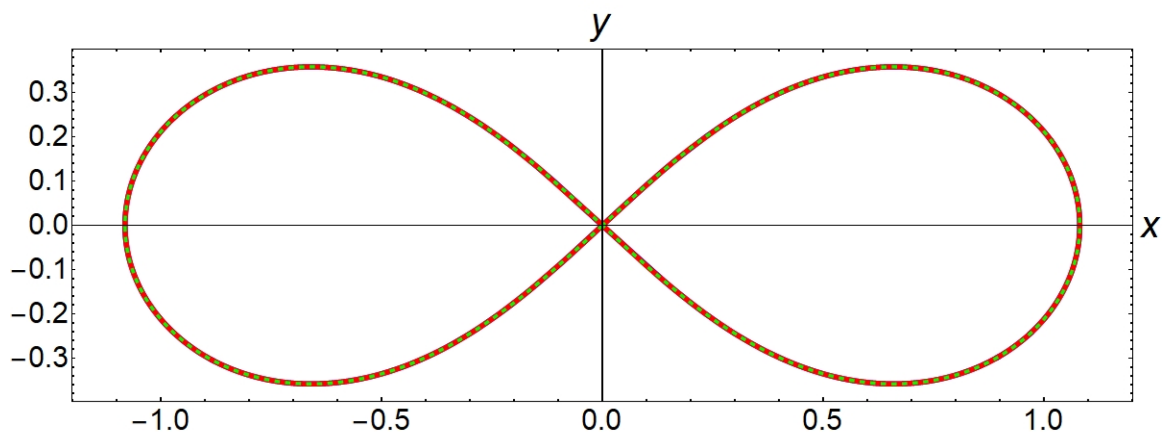

Figure 3.2: Trajectory of the Simo's figure-eight 3-body system. The bodies are moving in a 8-like orbit.

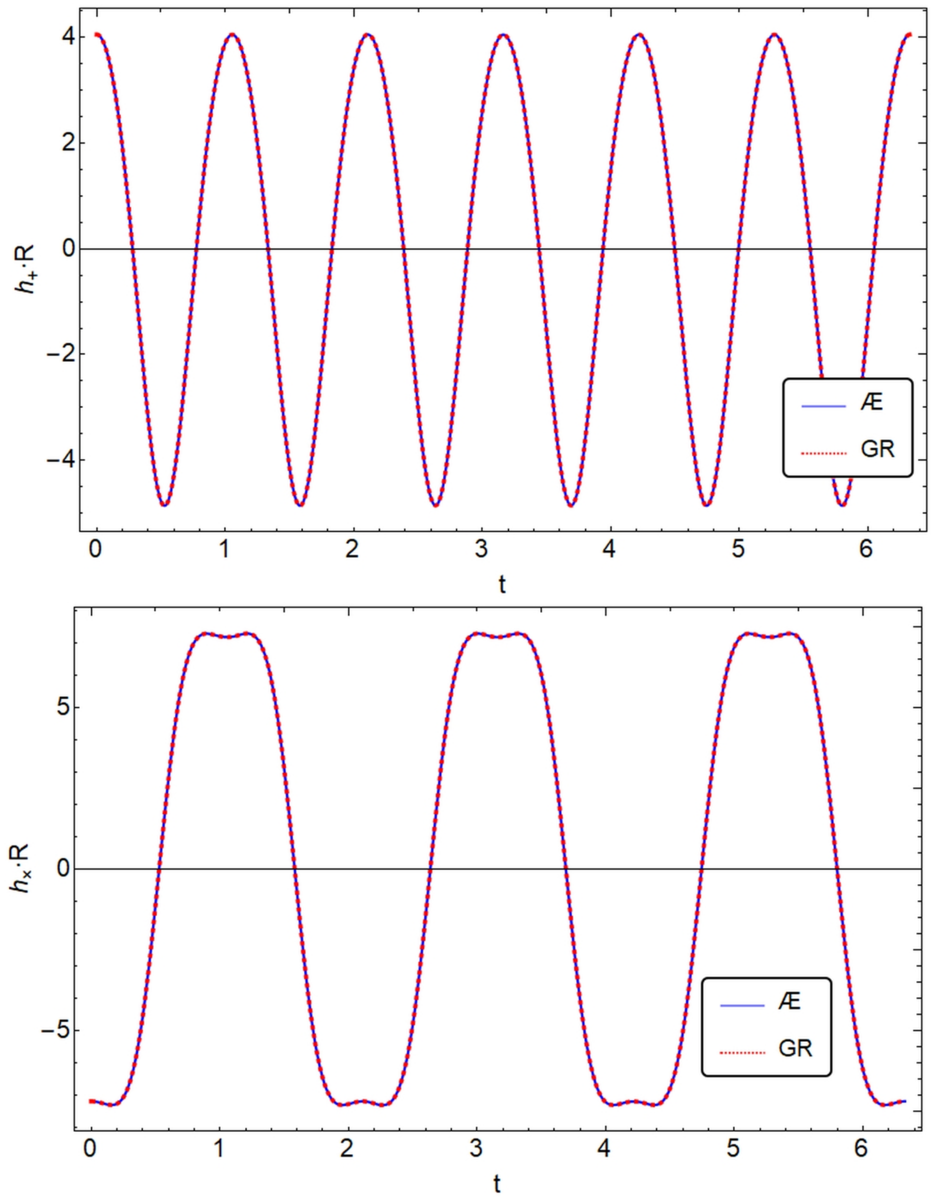

Figure 3.3: The polarization polarizations h_+ and $h_\times$ for the Simo's figure-eight 3-body system in both GR and Einstein-aether theory, where the polarizations are propagating along the positive z-direction. $R \equiv x$.

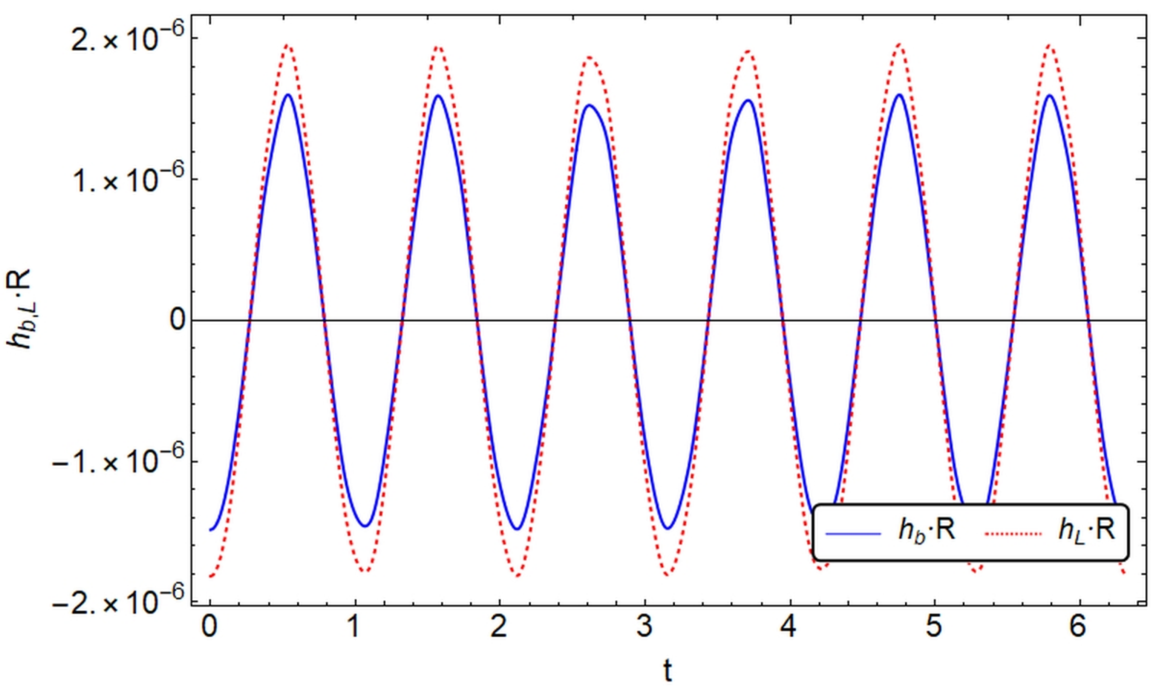

Figure 3.4: The polarization polarizations h_b and h_L for the Simo's figure-eight 3-body system in æ-theory.

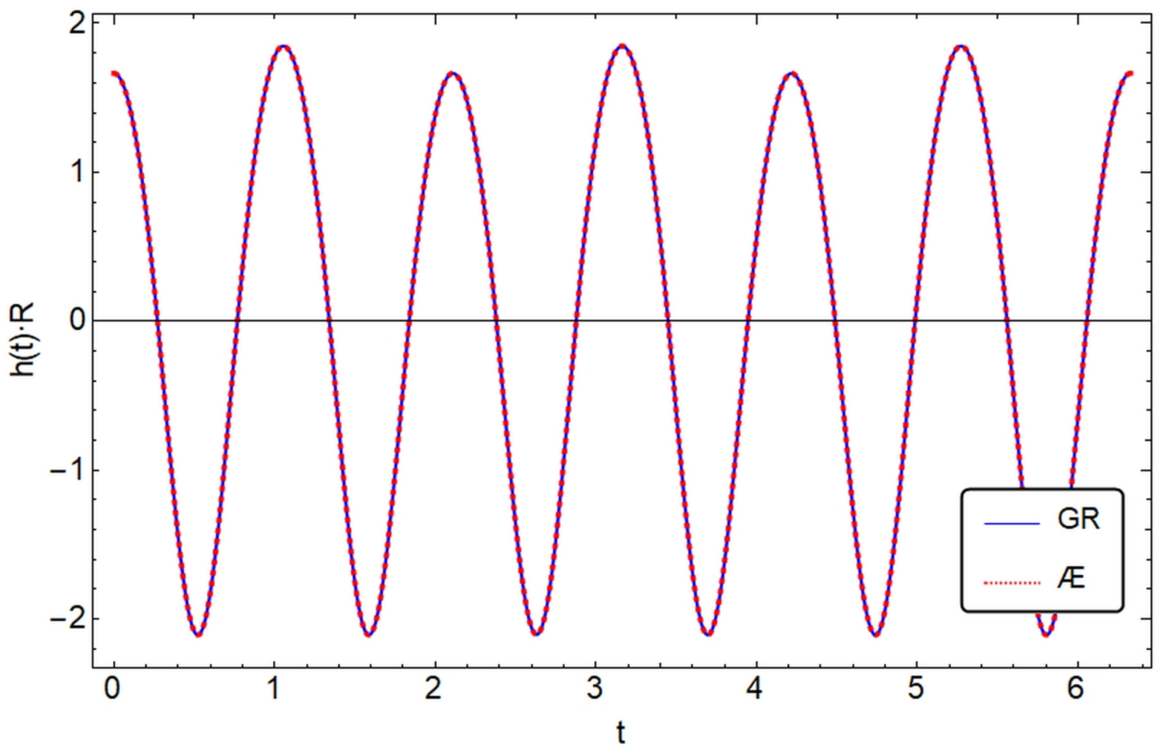

Figure 3.5: The response function $h(t)$ for the Simo's figure-eight 3-body system in GR and æ-theory.

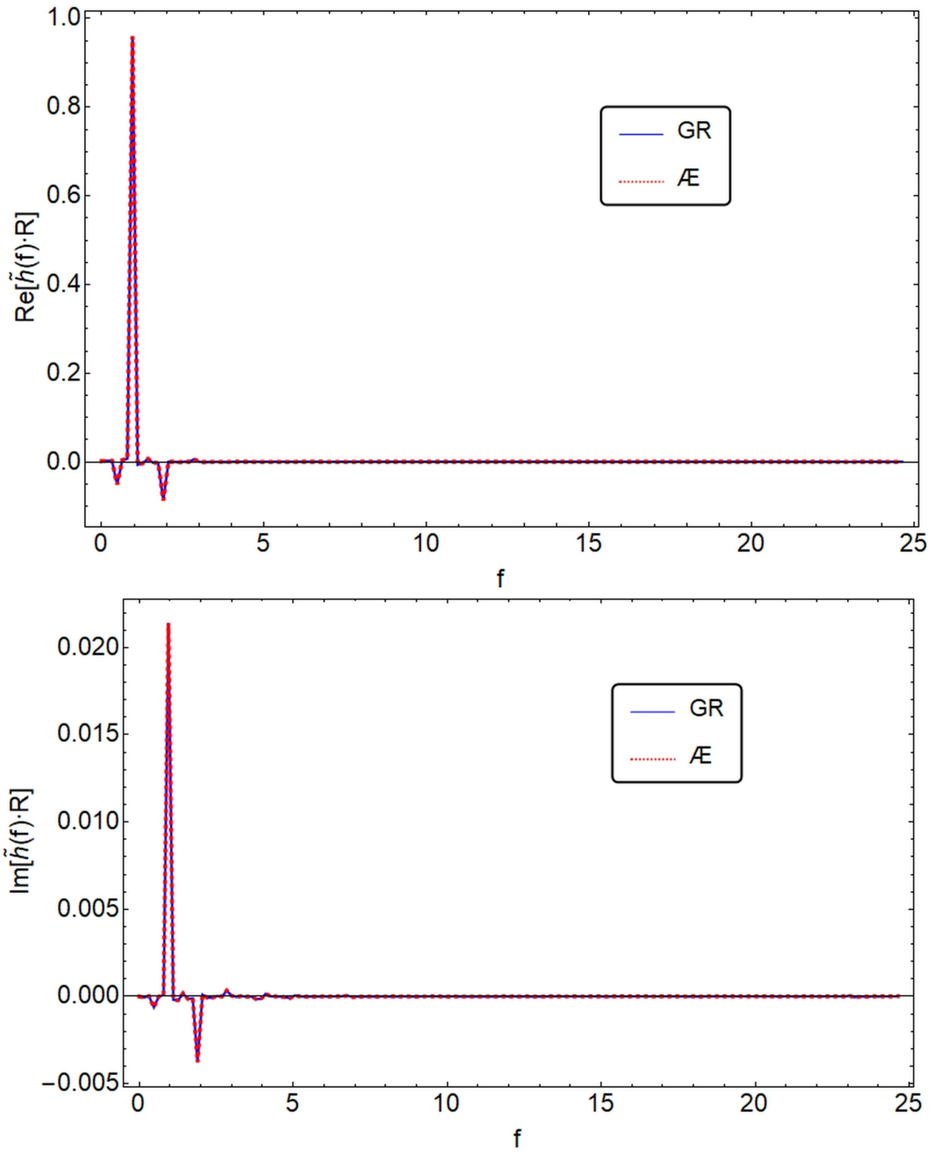

Figure 3.6: The Fourier transform $\tilde{h}(f)$ of the response function $h(t)$ for the Simo's figure-eight 3-body system in GR and æ-theory.

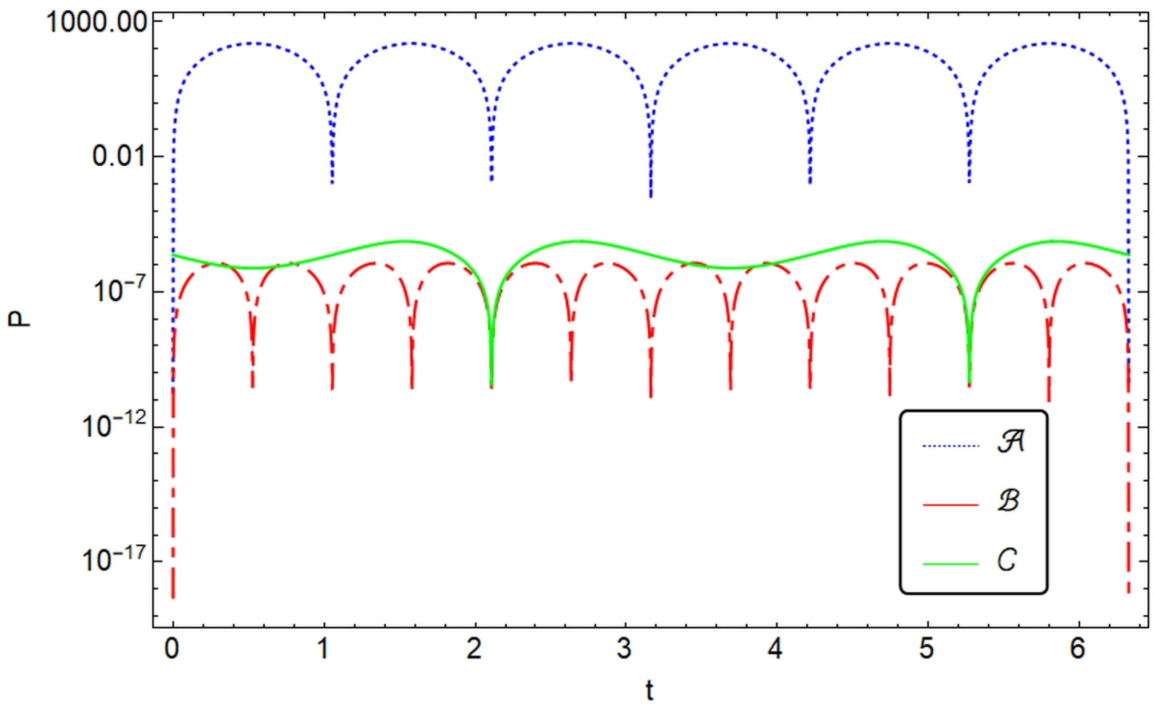

Figure 3.7: The radiation power $P(\equiv -\dot{\mathcal{E}})$ of the Simo's figure-eight 3-body system in æ-theory. The dotted (blue), dash-dotted (red) and solid (green) lines denote, respectively, the parts of quadrupole, monopole and dipole radiations given in (2.109).

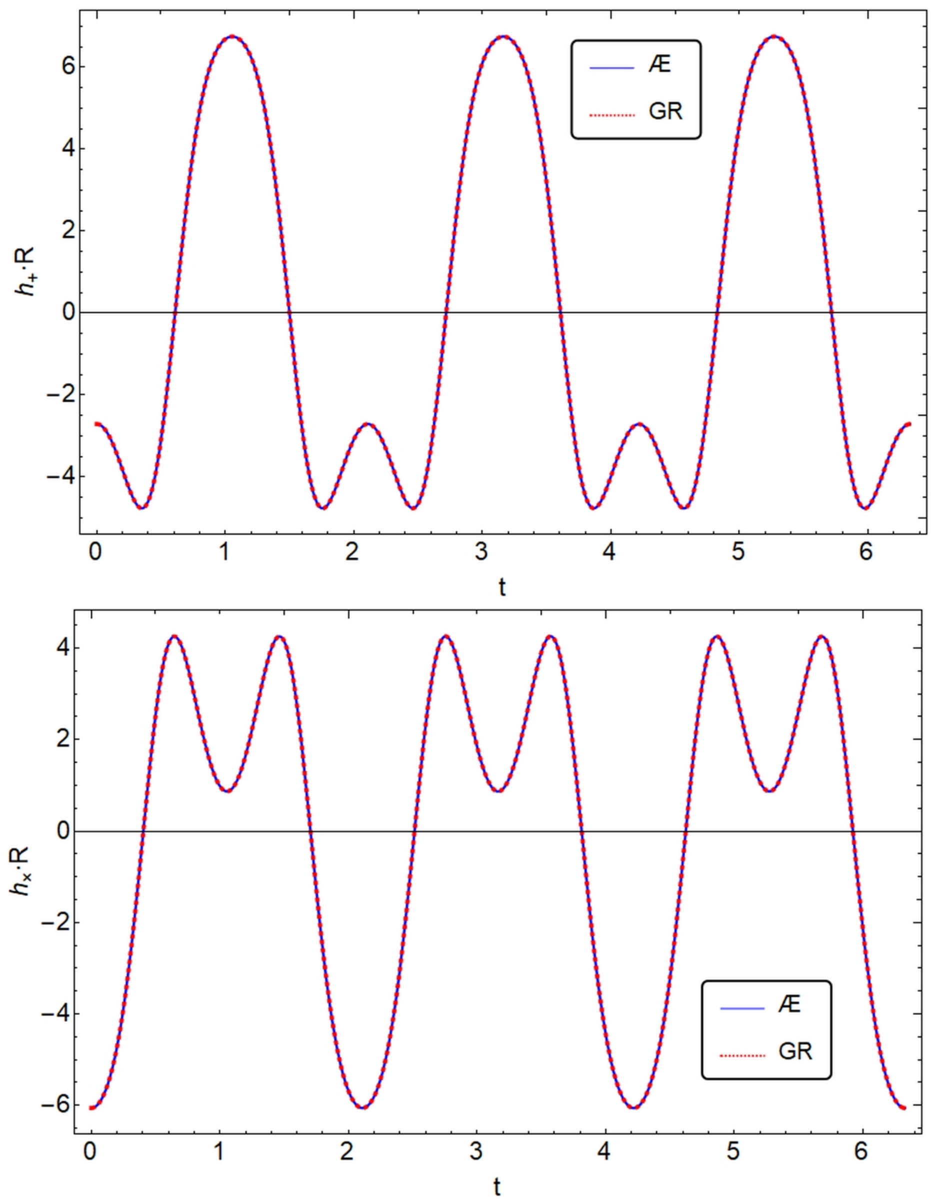

Figure 3.8: The polarization polarizations h_+ and $h_\times$ for the Simo's figure-eight 3-body system in both GR and æ-theory.

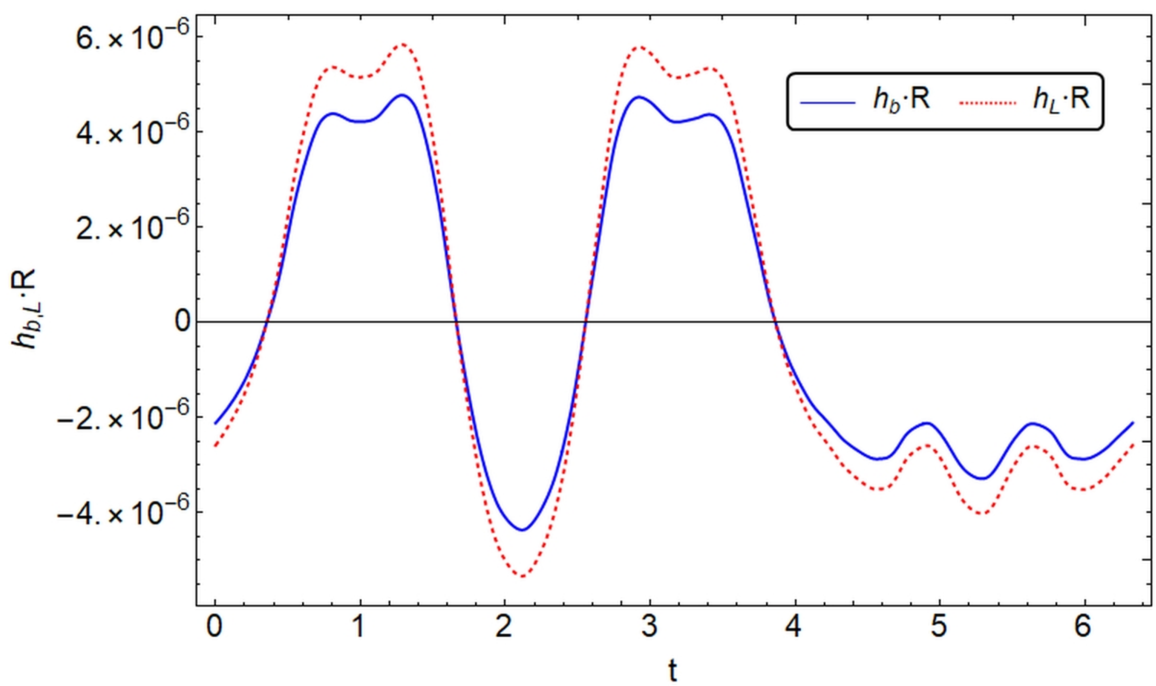

Figure 3.9: The polarization polarizations h_b and h_L for the Simo's figure-eight 3-body system in æ-theory.

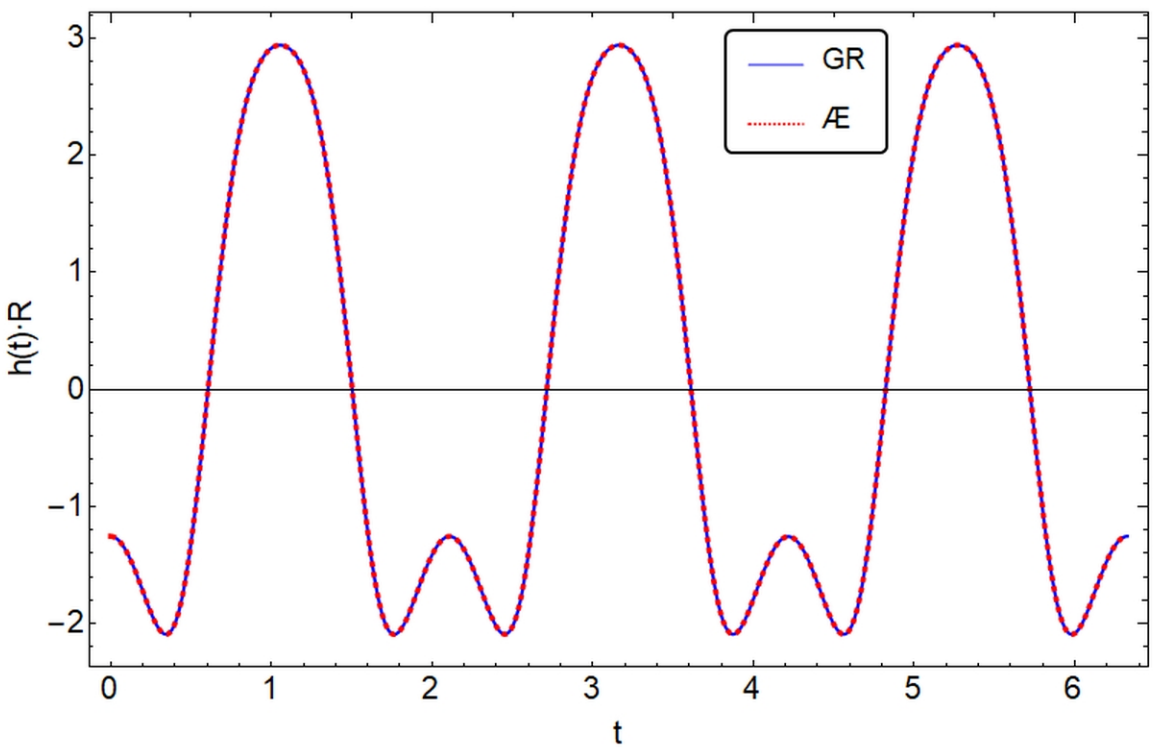

Figure 3.10: The response function $h(t)$ for the Simo's figure-eight 3-body system in GR and æ-theory.

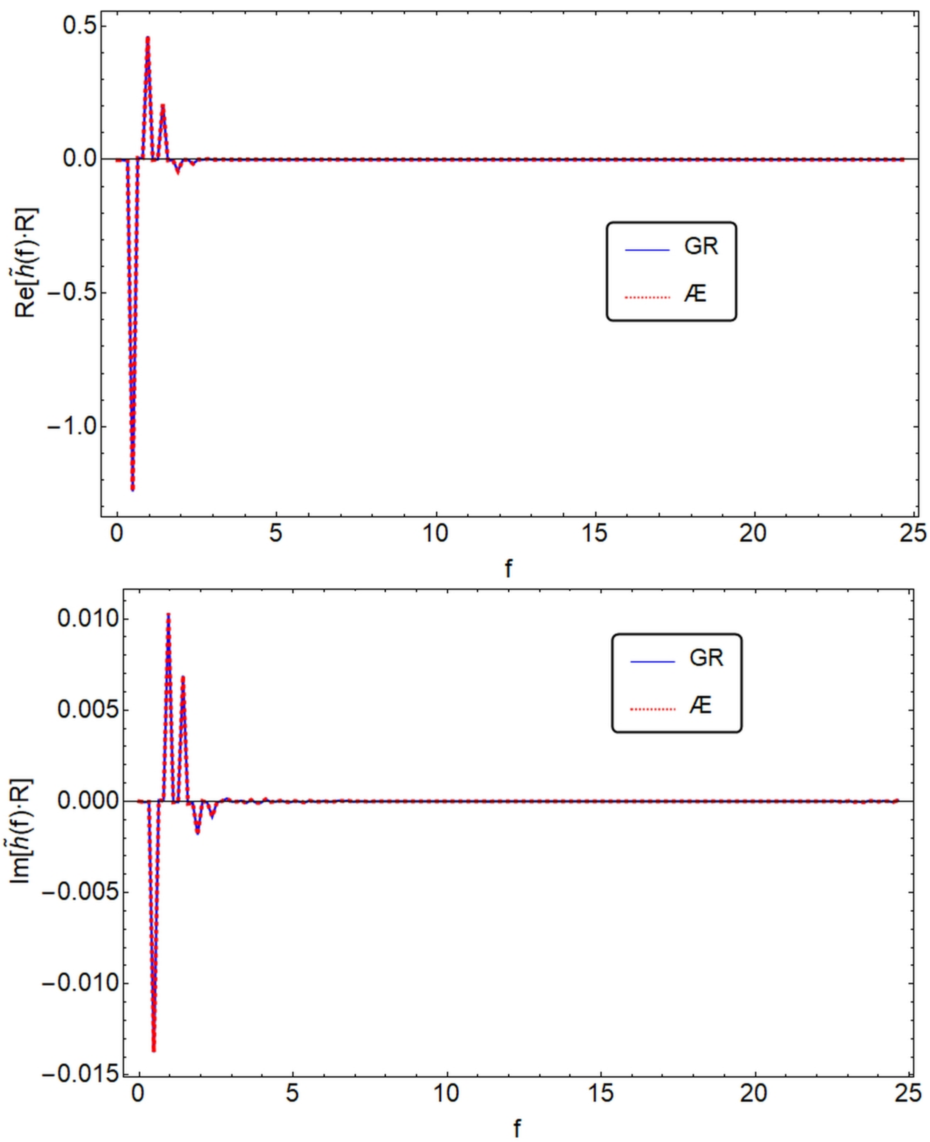

Figure 3.11: The Fourier transform $\tilde{h}(f)$ of the response function $h(t)$ for the Simo's figure-eight 3-body system in GR and æ-theory.

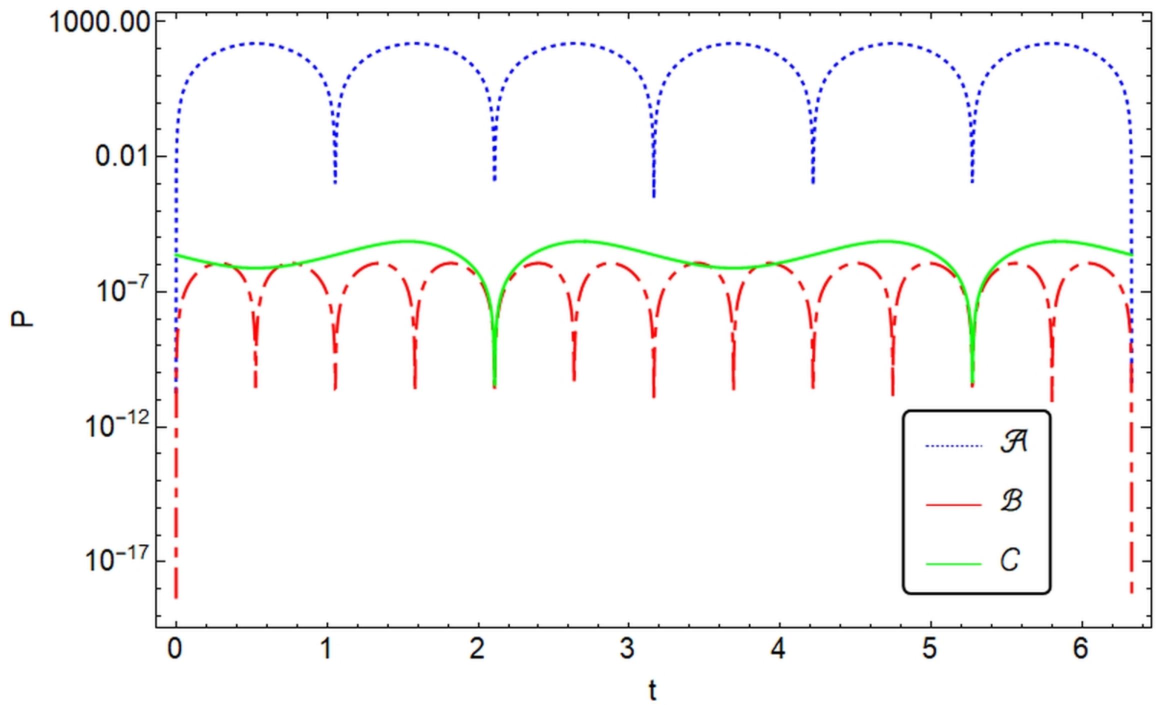

Figure 3.12: The radiation power $P(\equiv -\dot{\mathcal{E}})$ of the Simo's figure-eight 3-body system in æ-theory. The dotted (blue), dash-dotted (red) and solid (green) lines denote, respectively, the parts of quadrupole, monopole and dipole radiations.

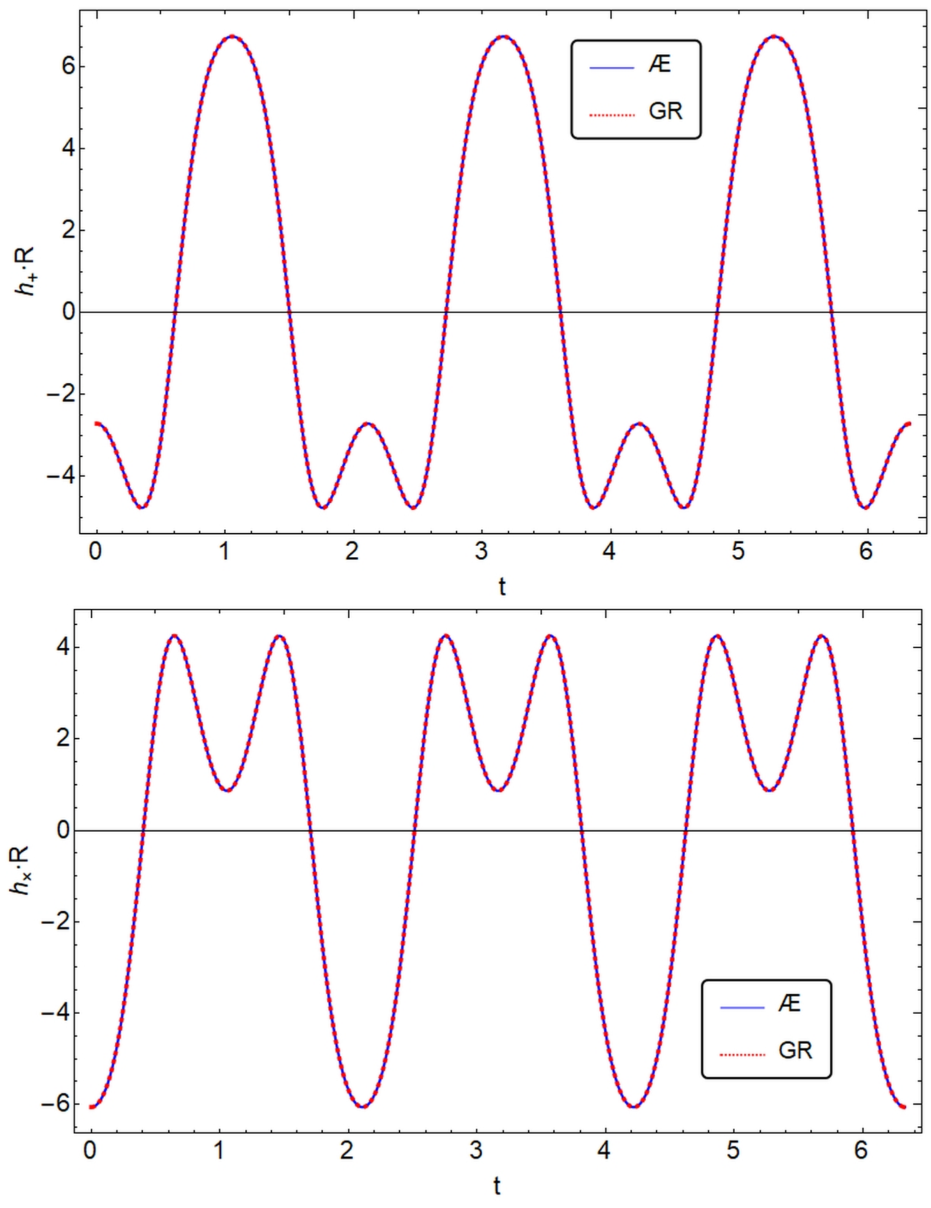

Figure 3.13: The polarization polarizations h_+ and $h_\times$ for the Simo's figure-eight 3-body system in both GR and æ-theory.

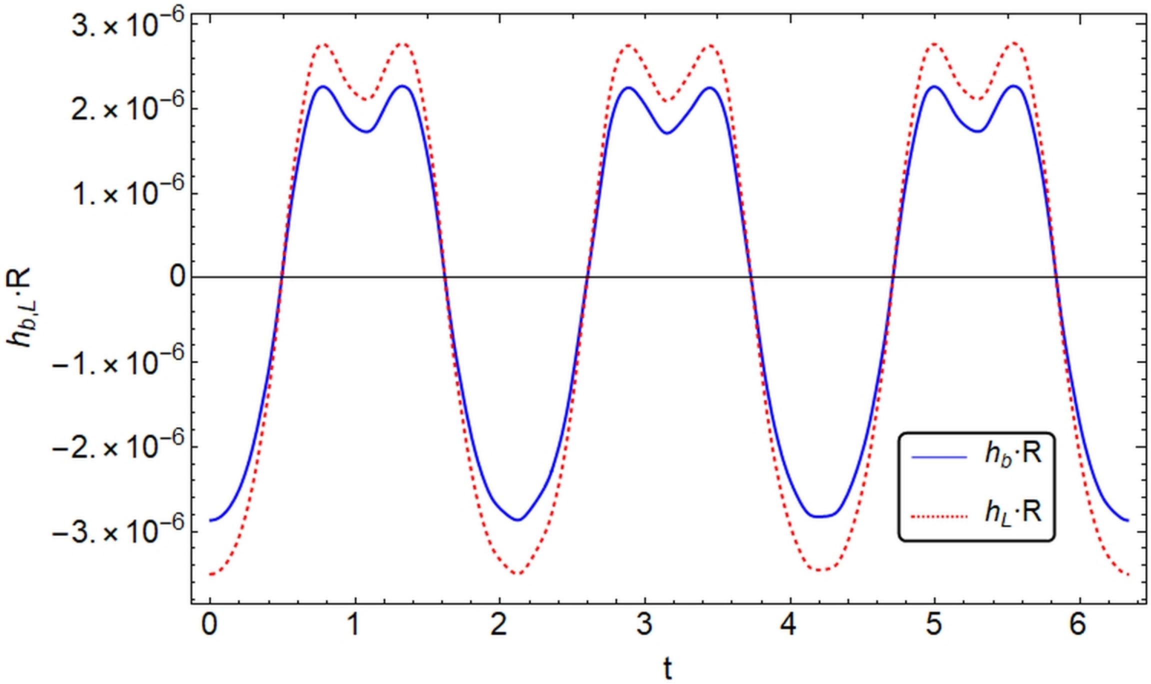

Figure 3.14: The polarization polarizations h_b and h_L for the Simo's figure-eight 3-body system in æ-theory.

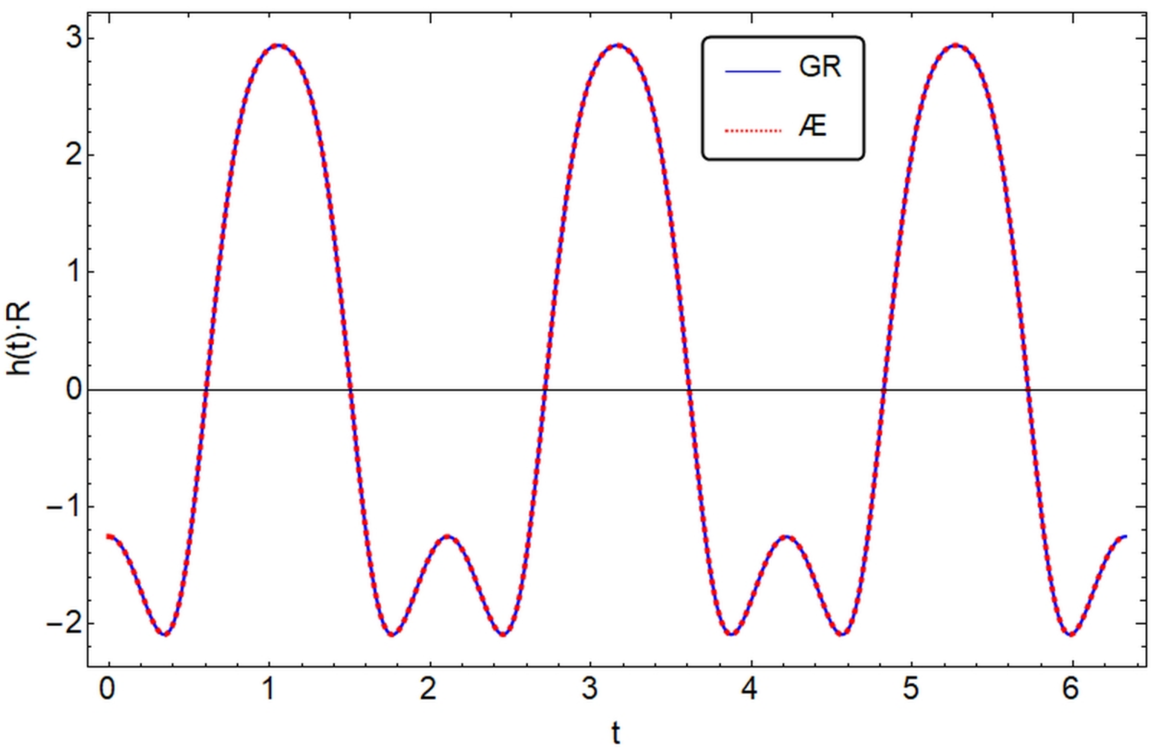

Figure 3.15: The response function $h(t)$ for the Simo's figure-eight 3-body system in GR and æ-theory.

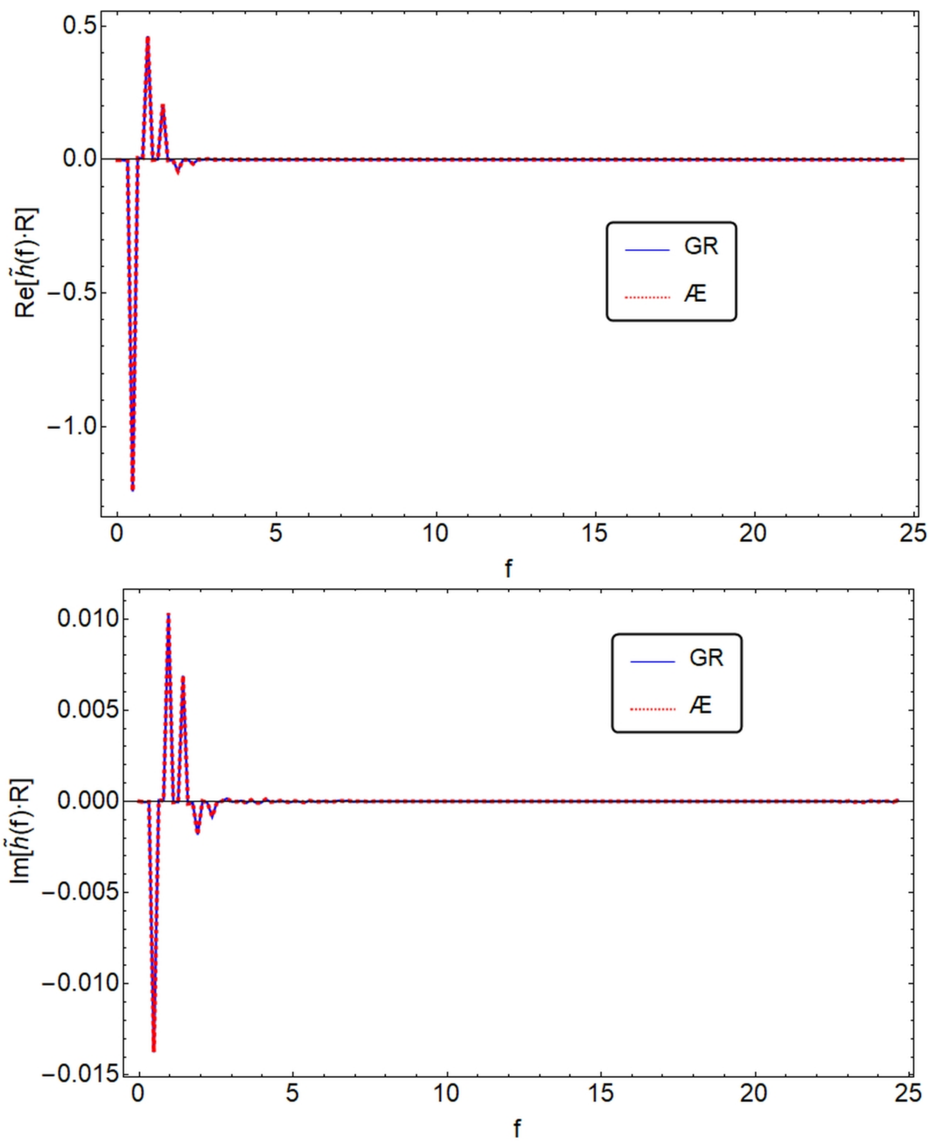

Figure 3.16: The Fourier transform $\tilde{h}(f)$ of the response function $h(t)$ for the Simo's figure-eight 3-body system in GR and æ-theory.

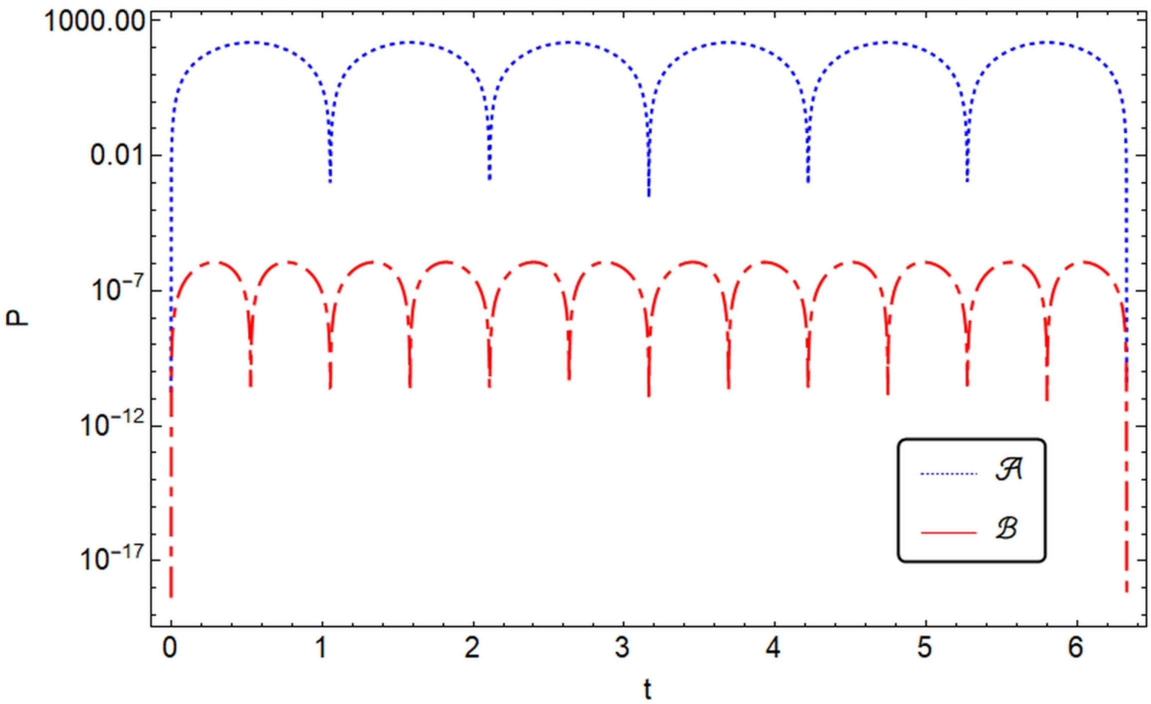

Figure 3.17: The radiation power P of the Simo's figure-eight trajectory of 3-body system in GR and æ-theory. The dotted (blue) and solid (red) lines denote, respectively, the parts of quadrupole and monopole radiations.

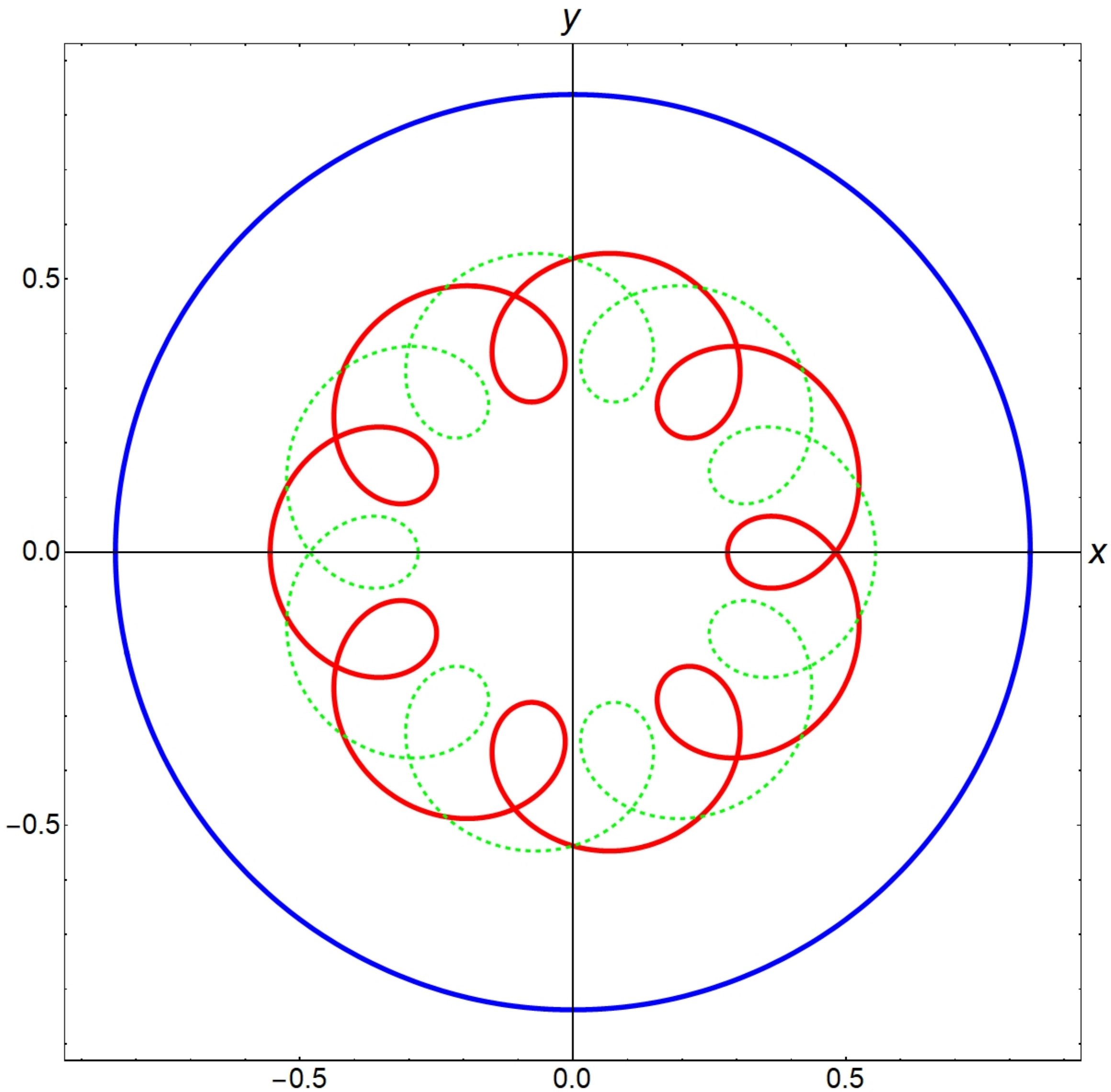

Figure 3.18: Trajectory of the 3-body system for the Broucke R7 figure provided in [56].

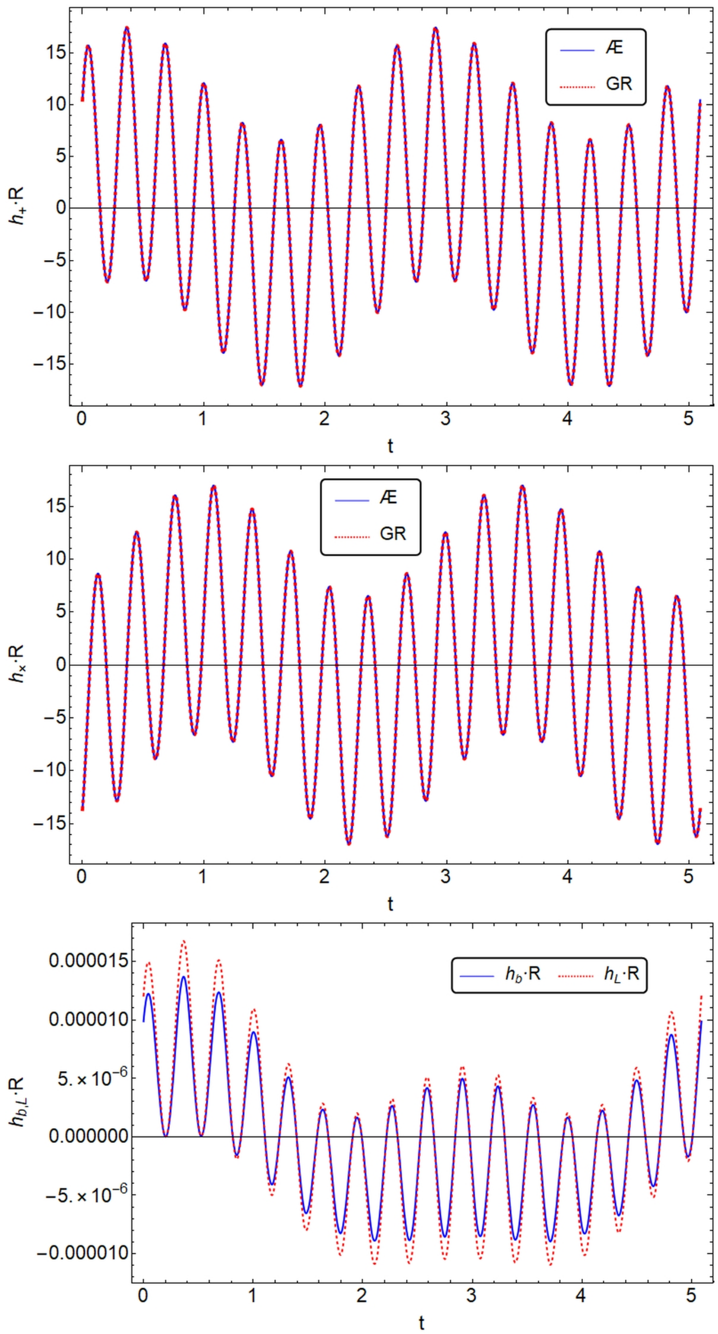

Figure 3.19: The polarizations h_N for the Broucke R7 3-body system with the choice.

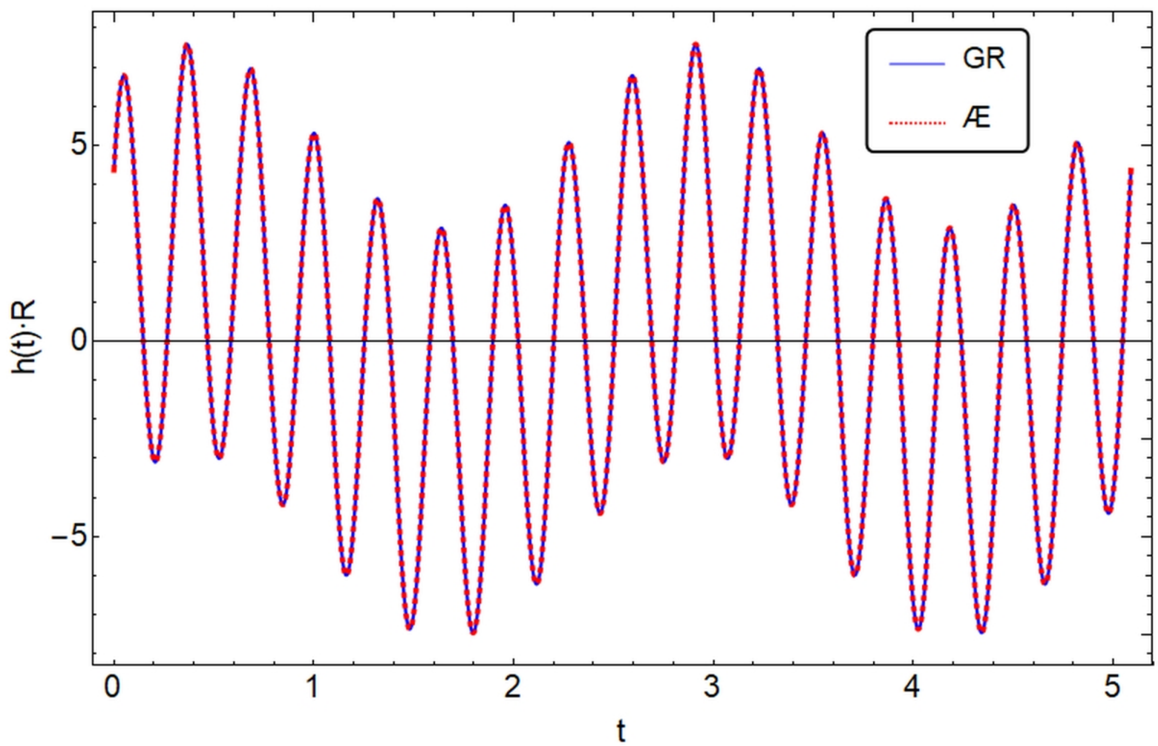

Figure 3.20: The response function $h(t)$ for the Broucke R7 3-body system with the choice.

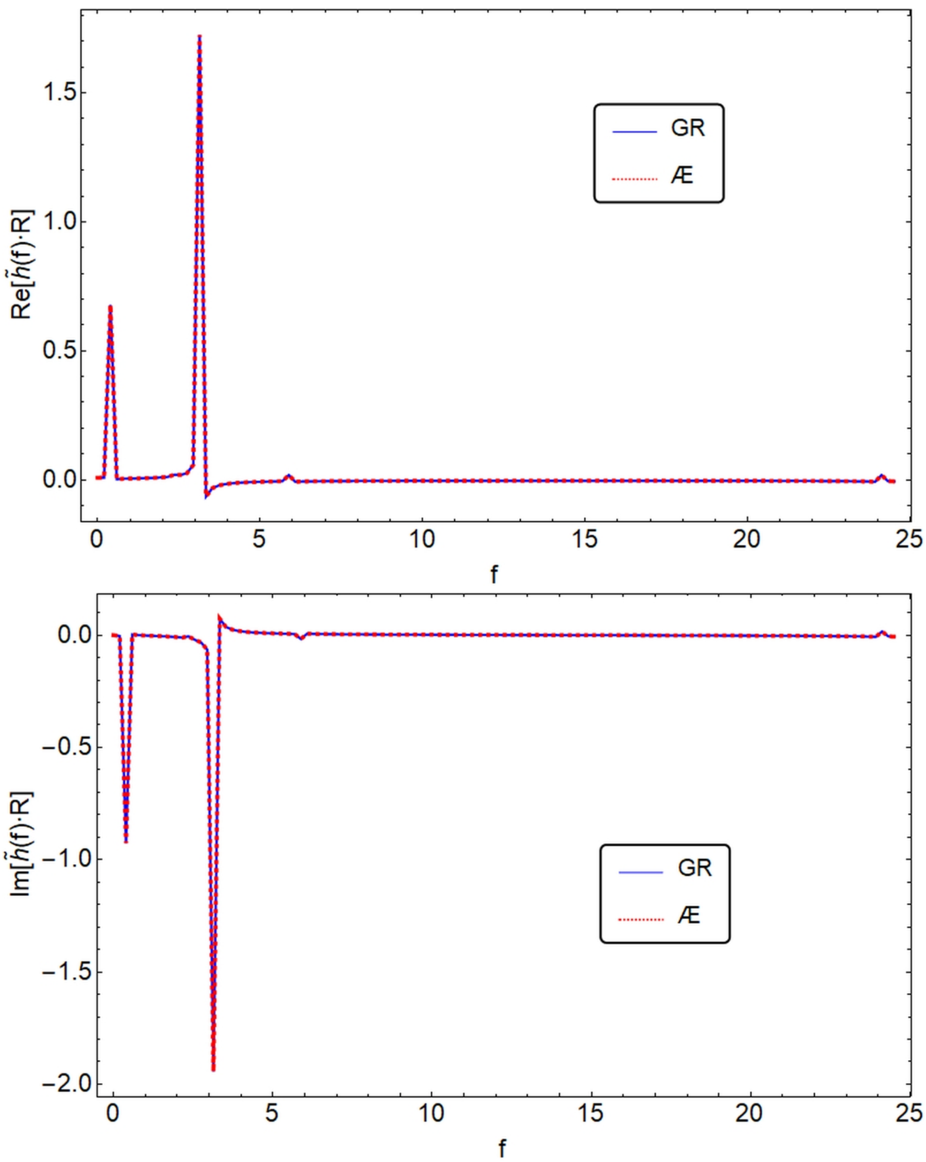

Figure 3.21: The Fourier transform $\tilde{h}(f)$ of the response function $h(t)$ for the Broucke R7 3-body system.

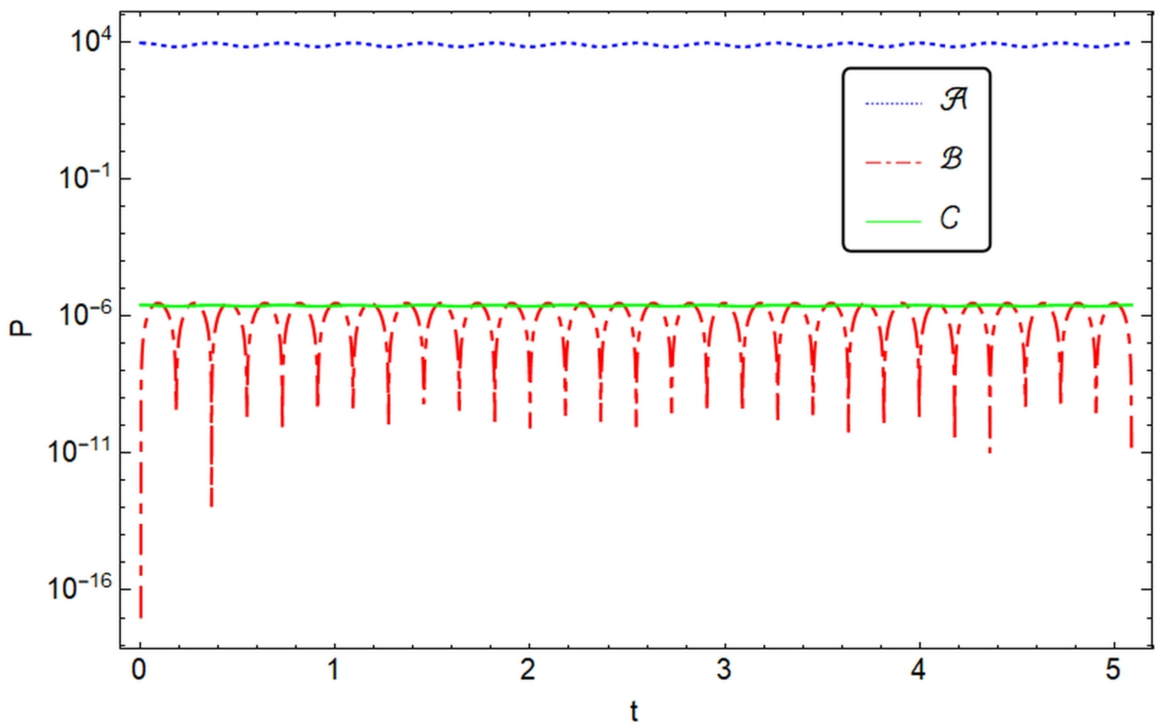

Figure 3.22: The radiation power P of the 3-body system of the Broucke R7 figure with the choice. The dotted (blue), dash-dotted (red) and solid (green) lines denote, respectively, the parts of quadrupole, monopole and dipole radiations.

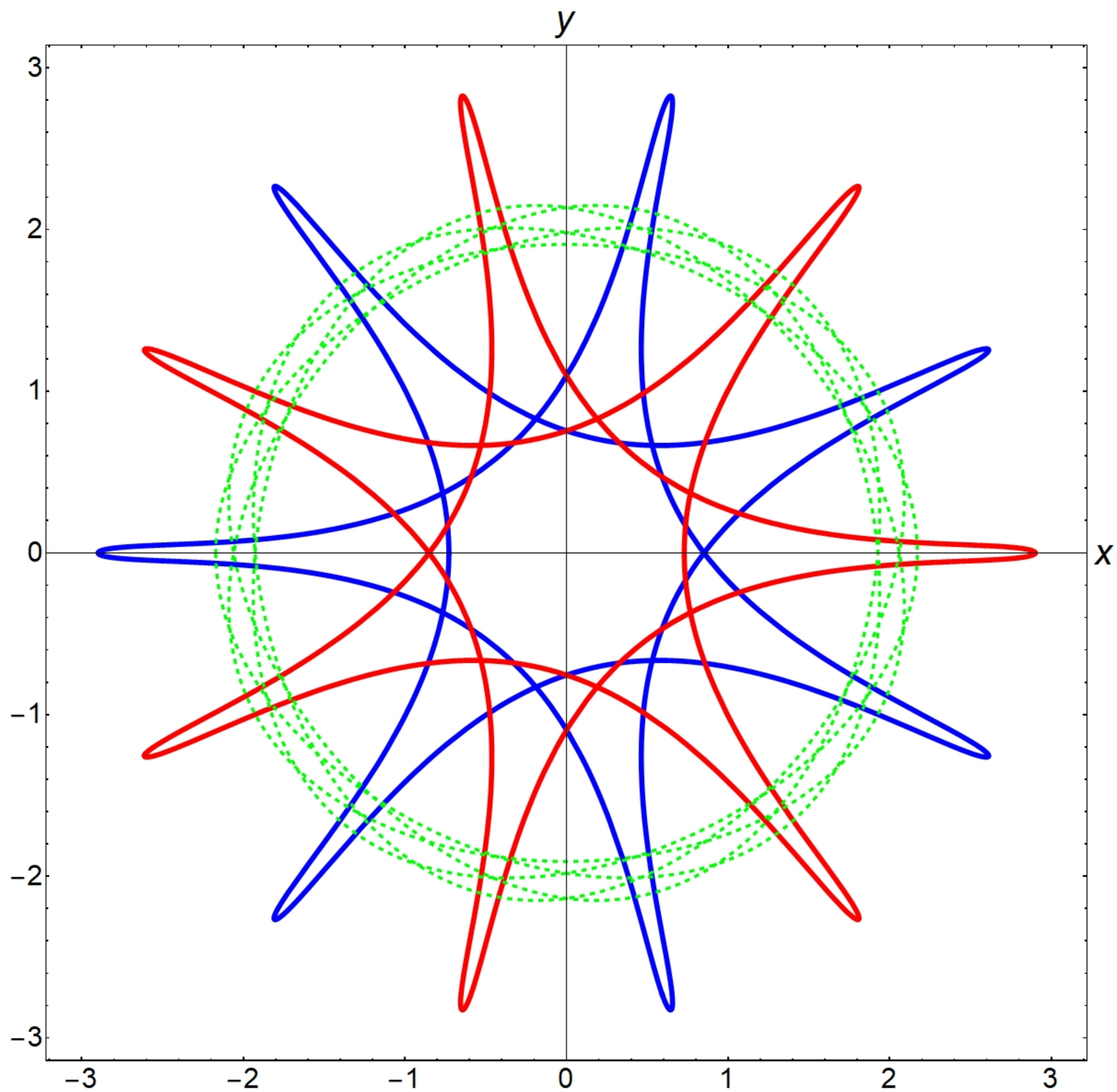

Figure 3.23: Trajectory of the 3-body system for the Broucke A16 figure provided in [56].

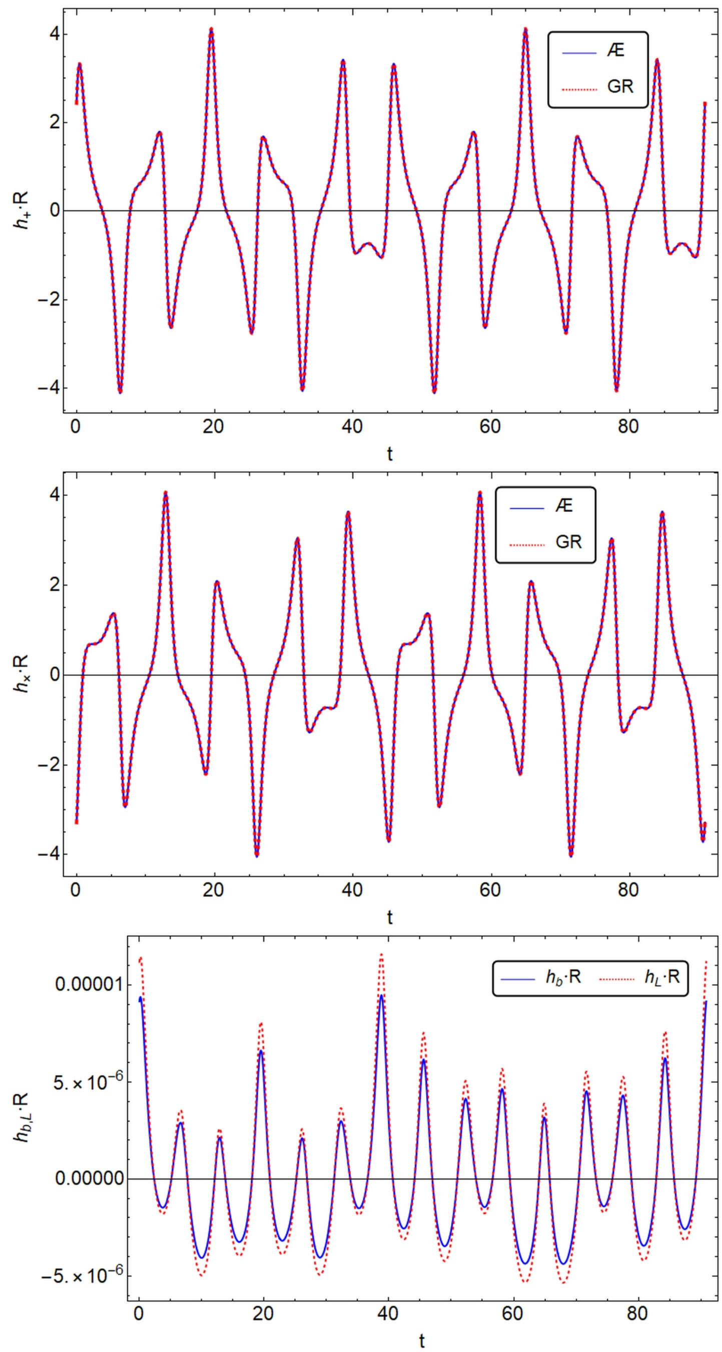

Figure 3.24: The polarization polarizations h_N for the Broucke A16 3-body system.

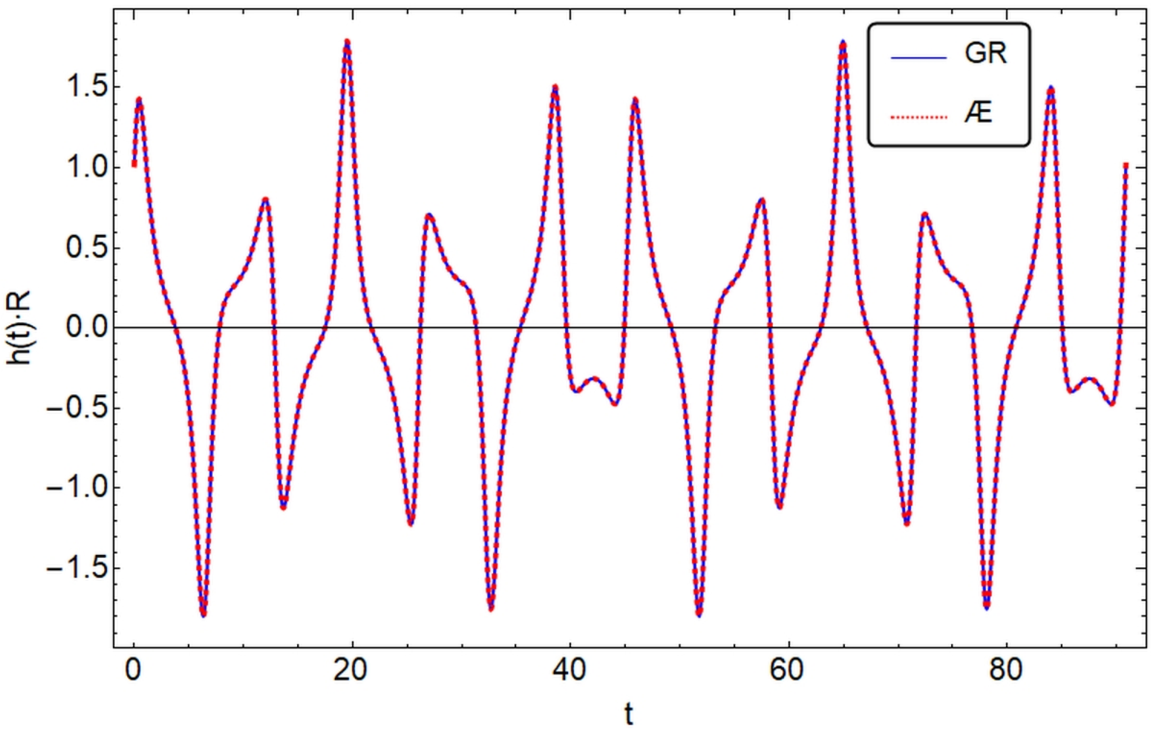

Figure 3.25: The response function $h(t)$ for the Broucke A16 3-body system.

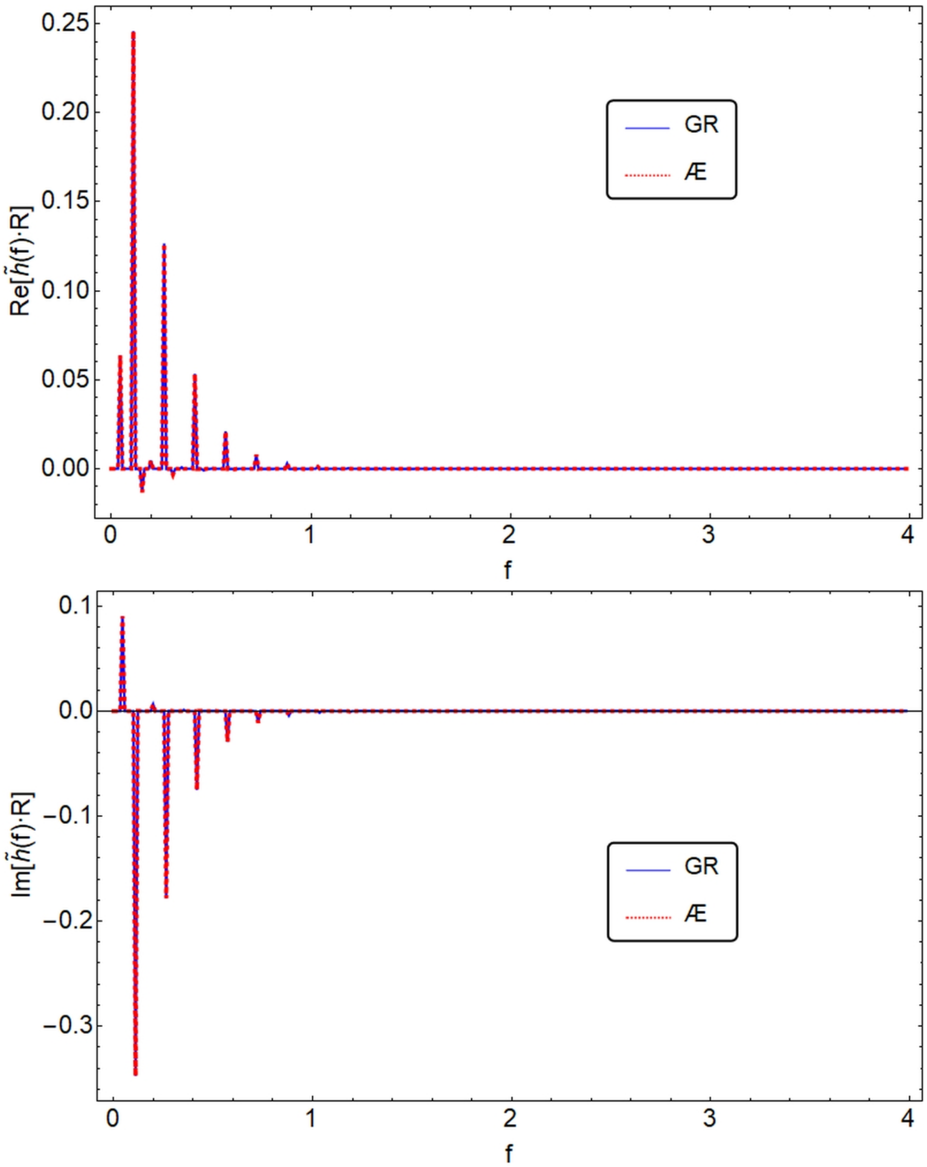

Figure 3.26: The Fourier transform $\tilde{h}(f)$ of the response function $h(t)$ for the Broucke A16 3-body system.

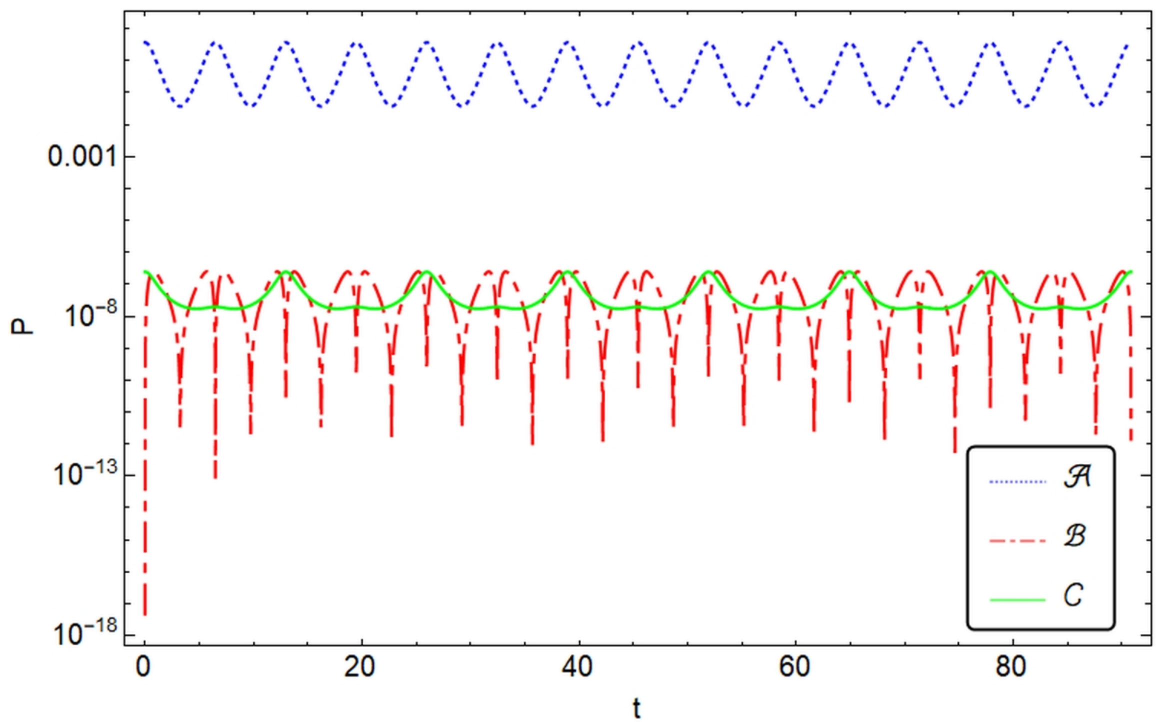

Figure 3.27: The radiation power $P(\equiv -\dot{\mathcal{E}})$ of the 3-body system of the Broucke A16. The dotted (blue), dash-dotted (red) and solid (green) lines denote, respectively, the parts of quadrupole, monopole and dipole radiations.

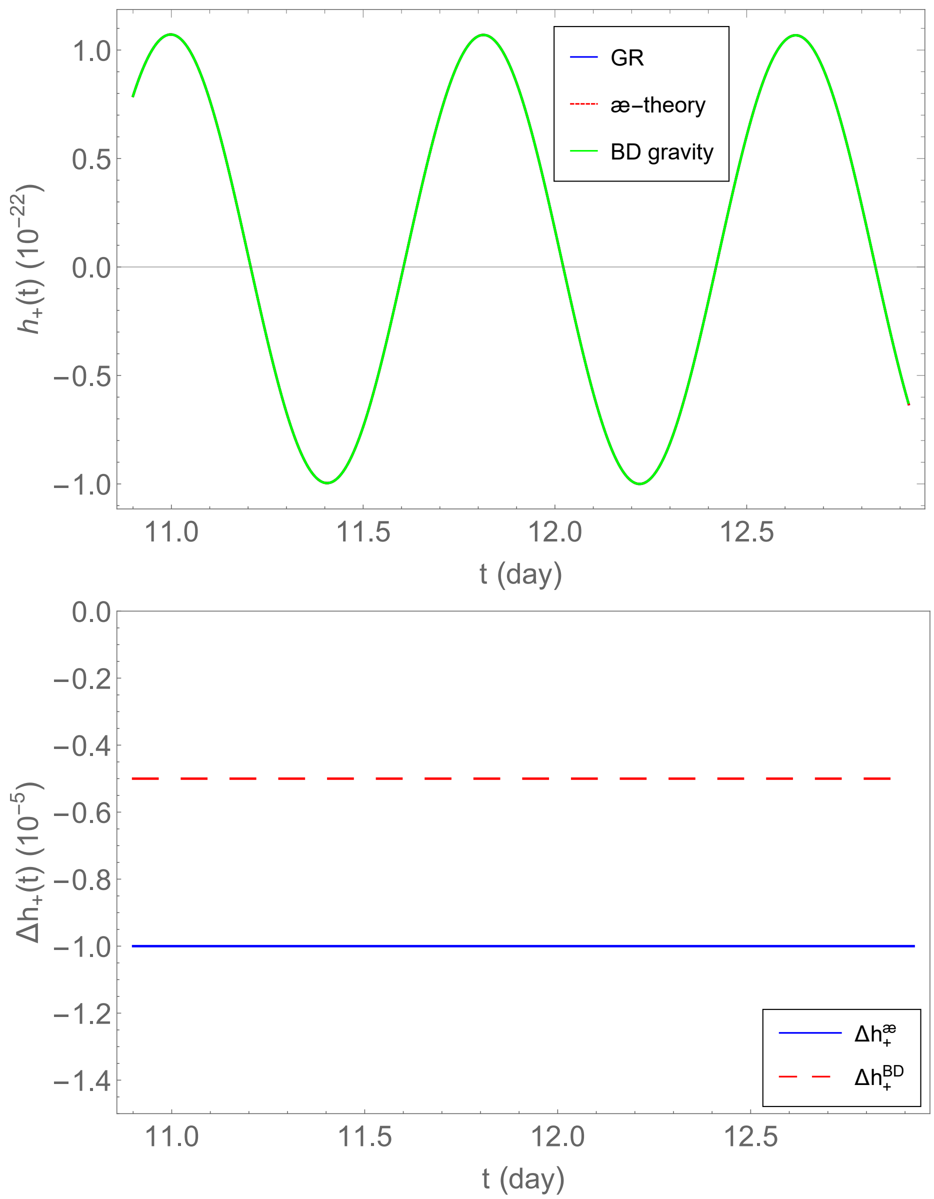

Figure 3.28: In the upper panel, the plus polarization h_+, respectively, in GR, æ-theory and BD gravity are plotted, while their relative differences with respect to GR, given by equations (3.10) and (3.21) are plotted out in the bottom panel.

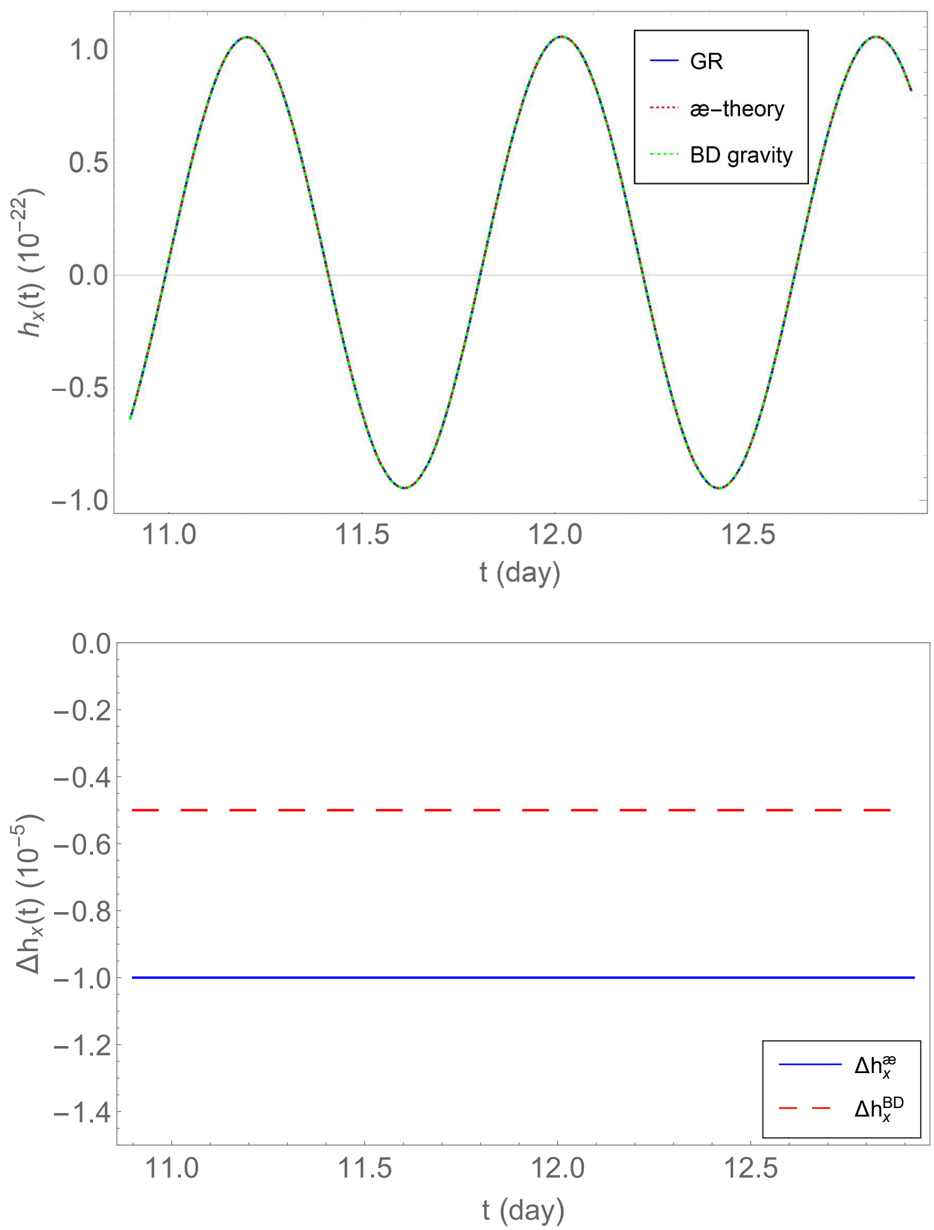

Figure 3.29: In the upper panel, the cross polarization $h_\times$, respectively, in GR, æ-theory and BD gravity are plotted, while their relative differences with respect to GR, given by equations (3.10) and (3.21) are plotted out in the bottom panel.

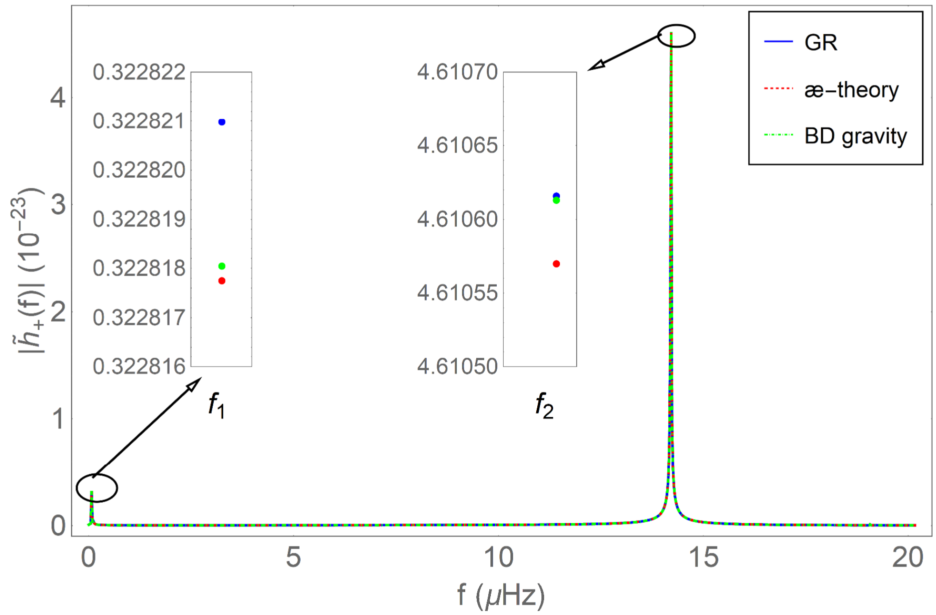

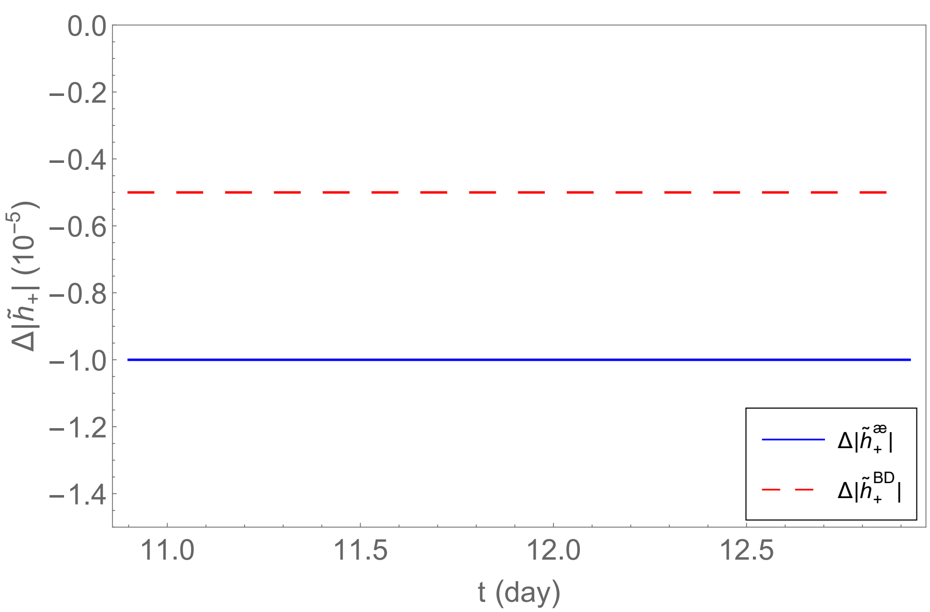

Figure 3.30: In the upper panel, DFTs of the plus polarization $\tilde{h}_+(f)$, respectively, in GR, æ-theory and BD gravity, are plotted out, in which the two peak frequencies have been marked. The inserts show the tiny differences at the two peak frequencies among the three different theories, where $f_1 = 0.068658$ μHz, $f_2 = 14.212$ μHz. In the bottom panel, their relative differences with respect to GR, given, respectively, by equations (3.11) and (3.22) are plotted out.

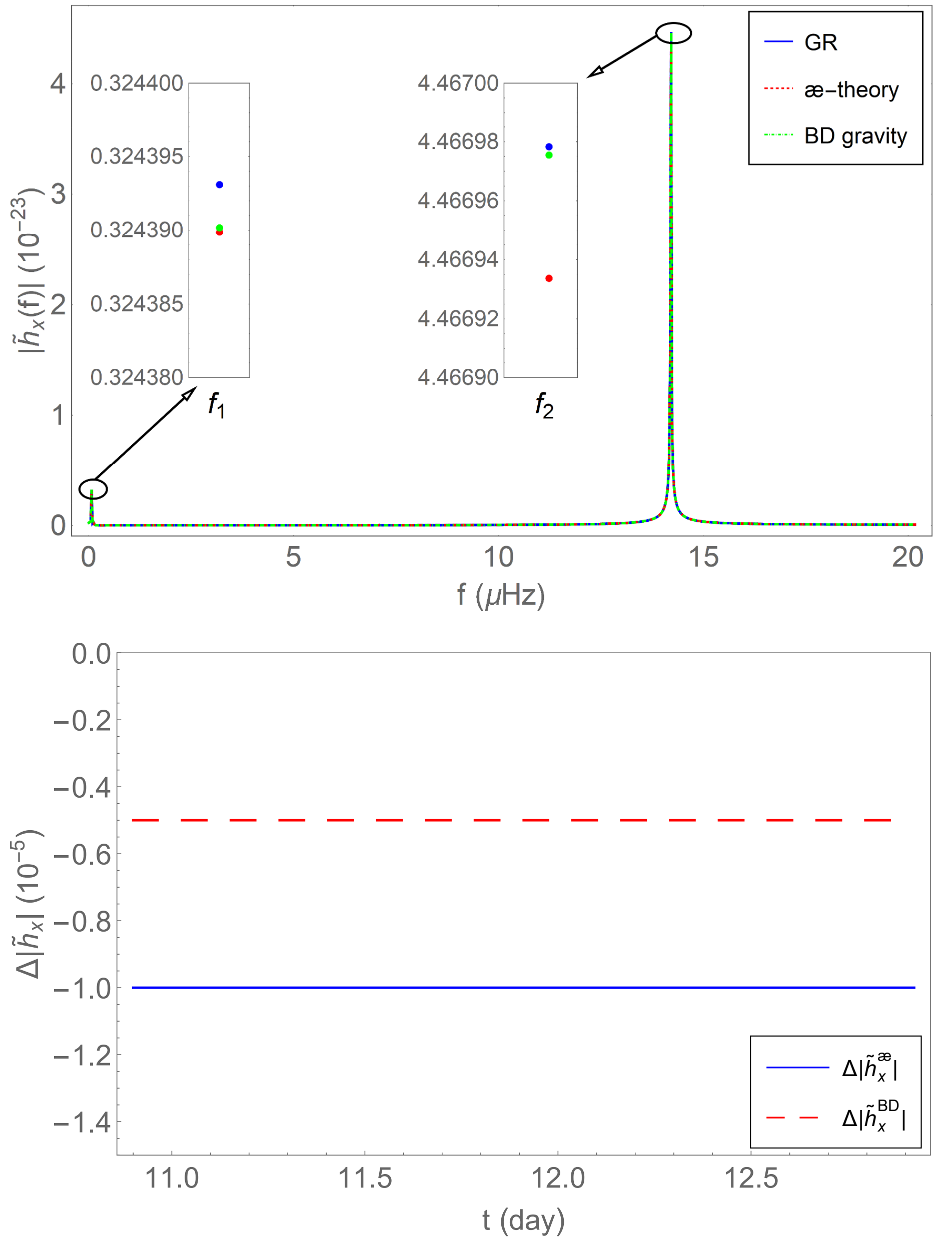

Figure 3.31: In the upper panel, DFTs of the cross polarization $\tilde{h}_\times(f)$, respectively, in GR, æ-theory and BD gravity are plotted out, in which the two peak frequencies have been marked. The inserts show the tiny differences at the two peak frequencies among the three different theories, where $f_1 = 0.068658$ μHz, $f_2 = 14.212$ μHz. In the bottom panel, their relative differences with respect to GR, given, respectively, by equations (3.11) and (3.22) are plotted out.

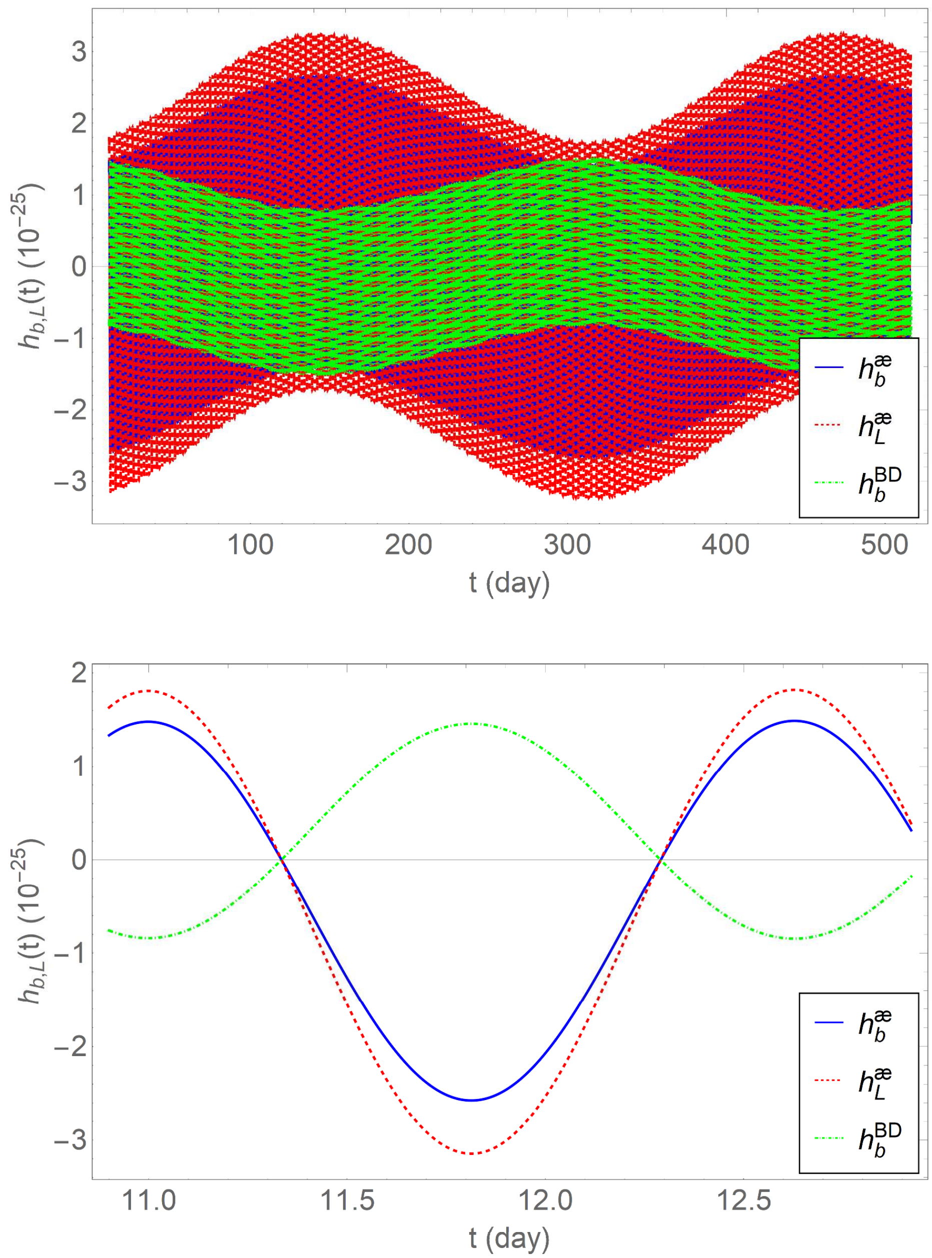

Figure 3.32: The breathing (h_b) and longitudinal (h_L) polarizations in æ-theory and the breathing polarization in BD gravity for about five hundreds days with another plot for about two days.

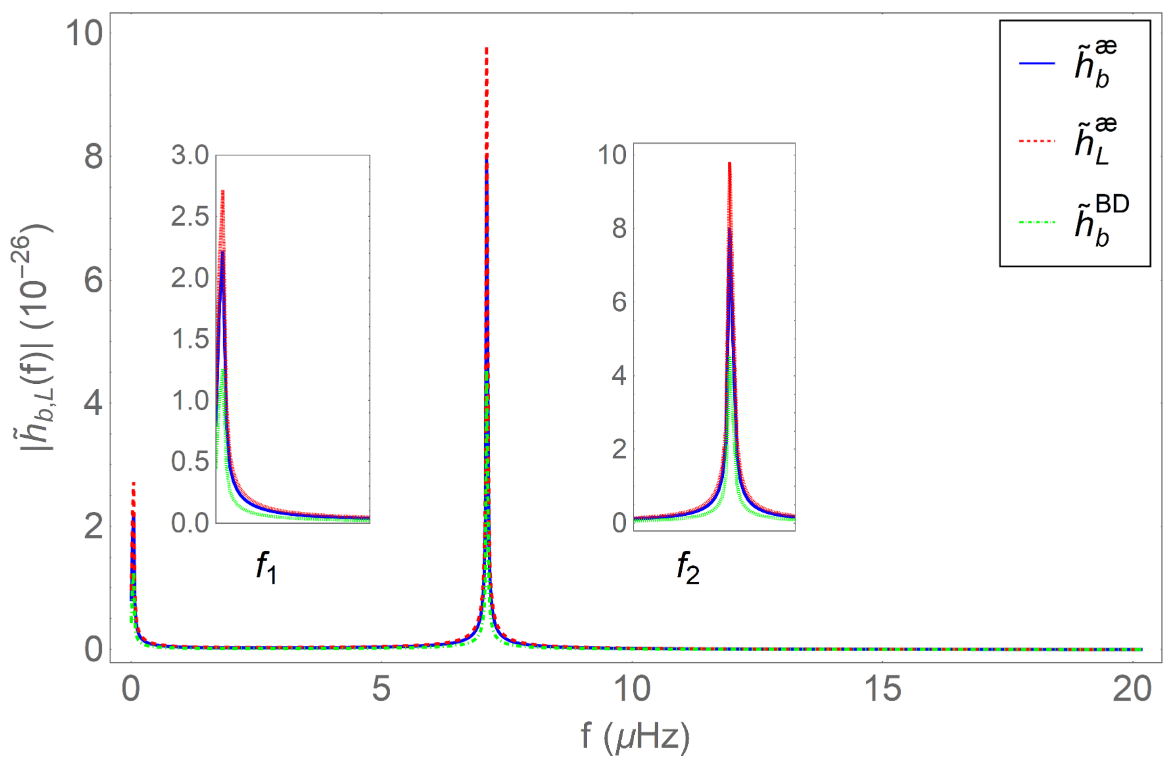

Figure 3.33: DFT of the breathing and longitudinal polarizations in æ-theory and the breathing polarization in BD gravity, where two peak frequencies have been marked. $f_1 = 0.045772\ \mu$Hz, $f_2 = 7.0947\ \mu$Hz.

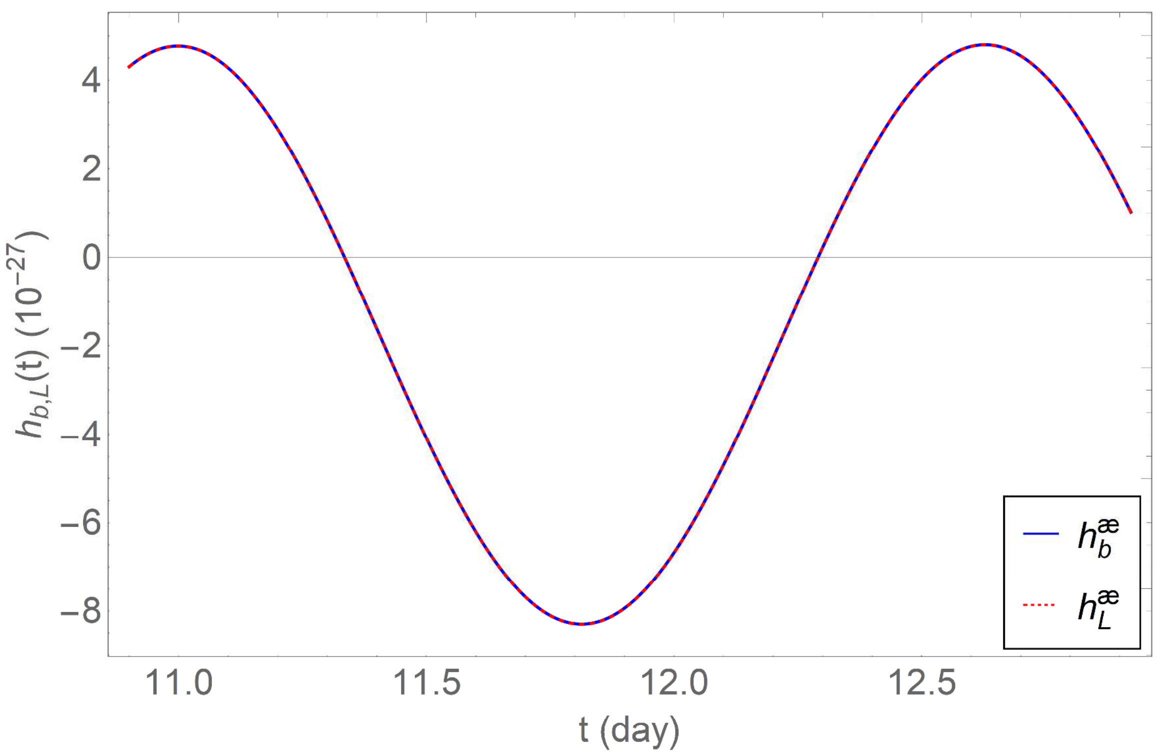

Figure 3.34: The breathing and longitudinal polarizations in æ-theory for different choice of parameters c_i's given by equation (3.14).

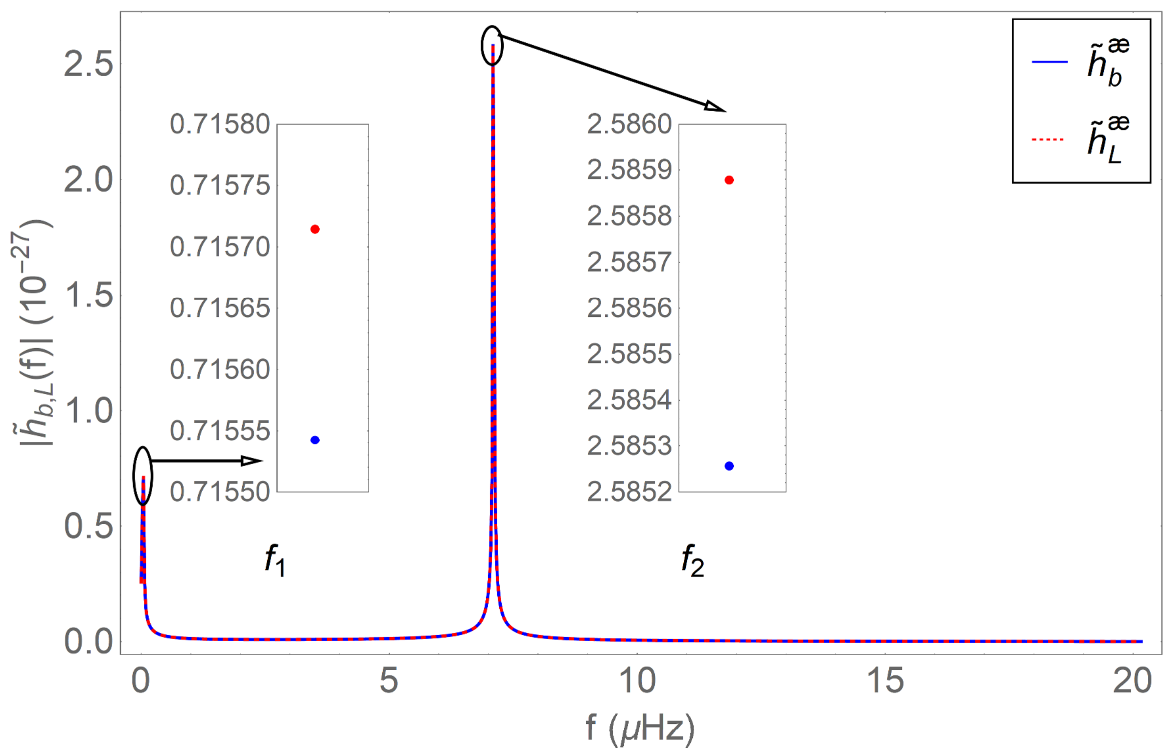

Figure 3.35: DFT of the breathing and longitudinal polarizations in æ-theory for different choice of parameters c_i's given by equation (3.14). $f_1 = 0.045772$ μHz, $f_2 = 7.0947$ μHz.

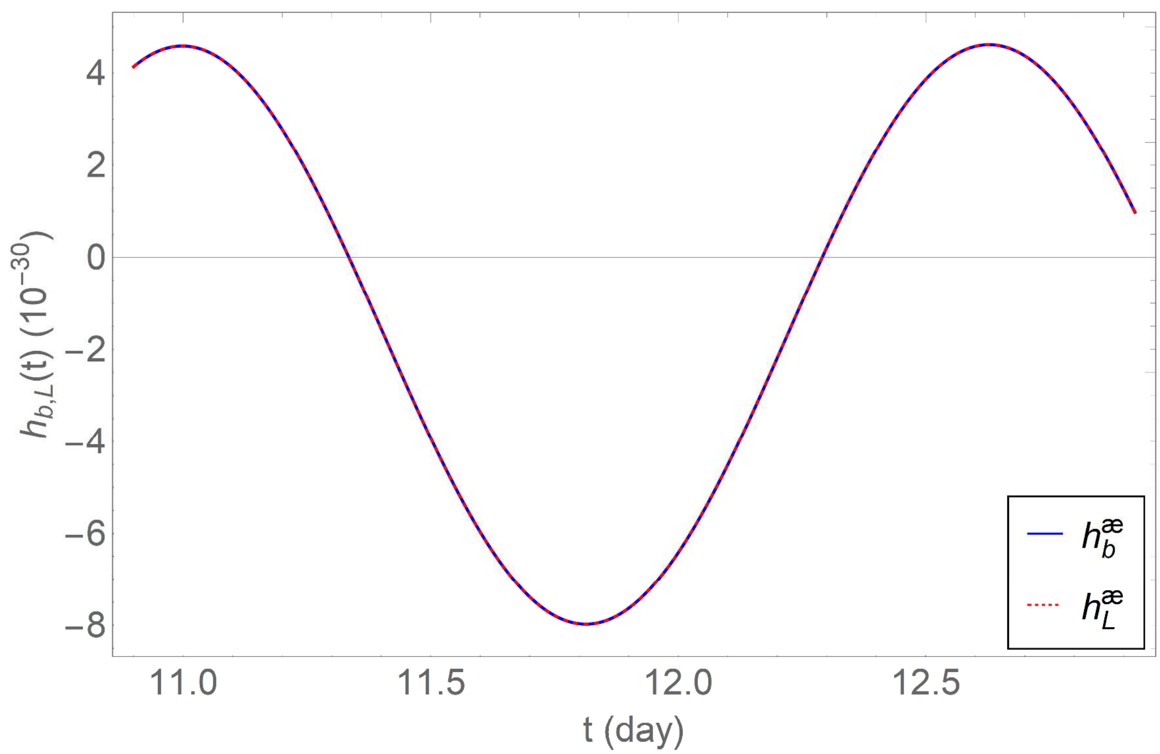

Figure 3.36: The breathing and longitudinal polarizations in æ-theory for different choice of parameters c_i's given by equation (3.15).

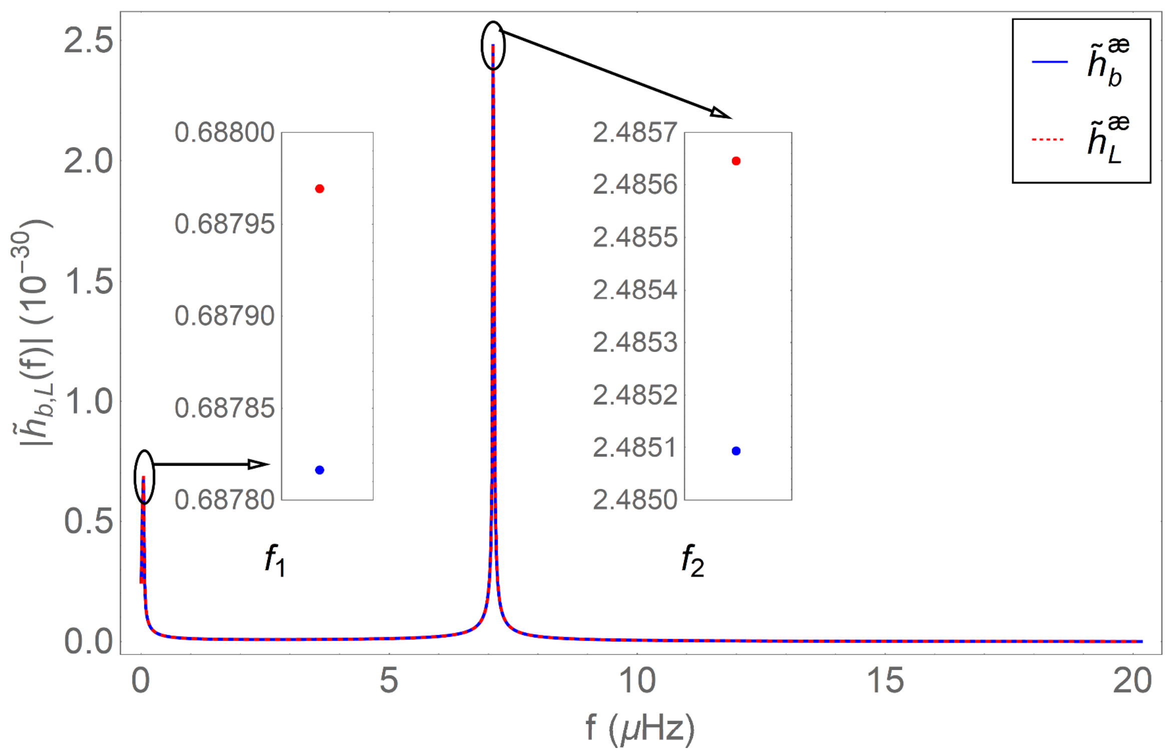

Figure 3.37: DFT of the breathing and longitudinal polarizations in æ-theory for different choice of parameters c_i's given by equation (3.15). $f_1 = 0.045772$ μHz, $f_2 = 7.0947$ μHz.

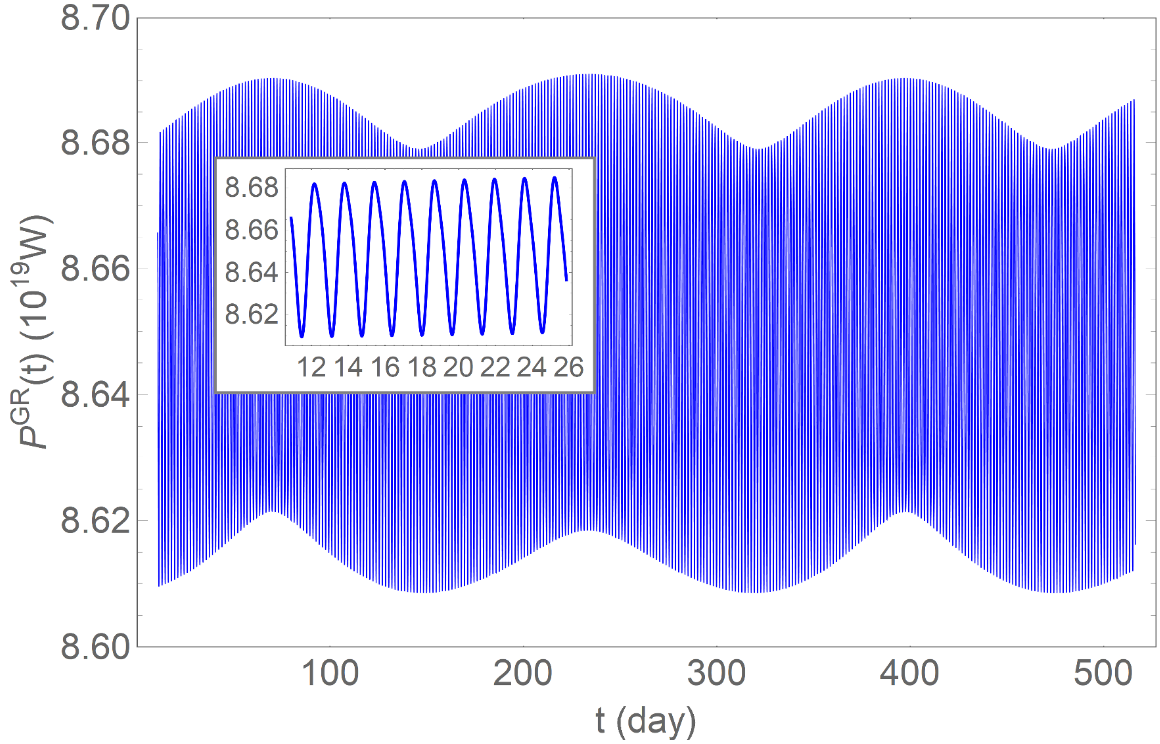

Figure 3.38: The instantaneous (time un-averaged) radiation power in GR for about 500 days with an insert for about 14 days.

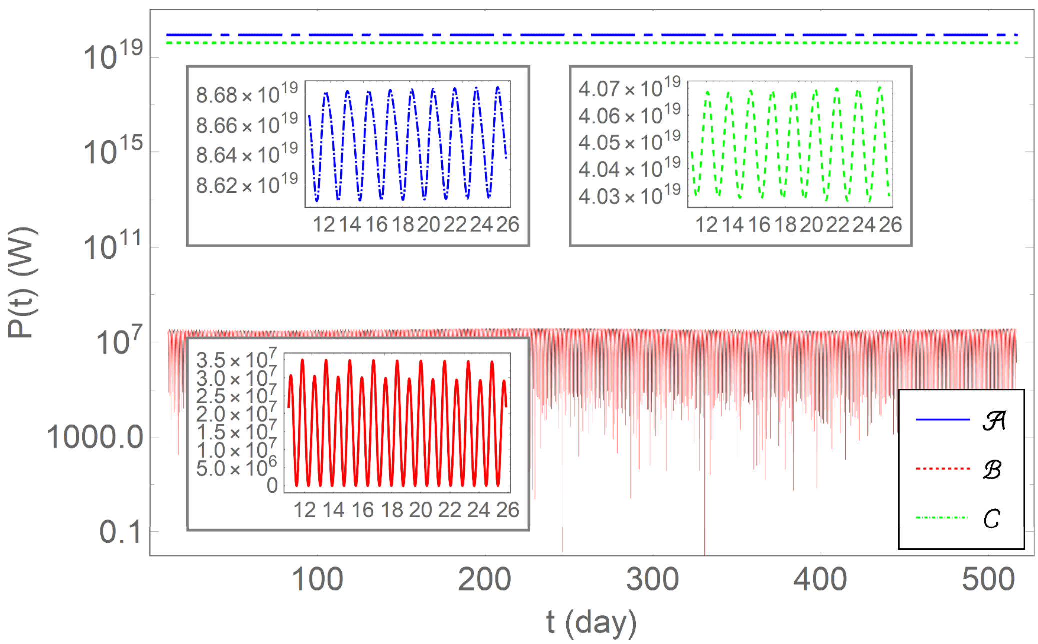

Figure 3.39: The instantaneous (time un-averaged) radiation power in æ-theory. Here the $\mathcal{A}$, $\mathcal{B}$ and $\mathcal{C}$ parts are plotted separately. The inserts show only 14 days.

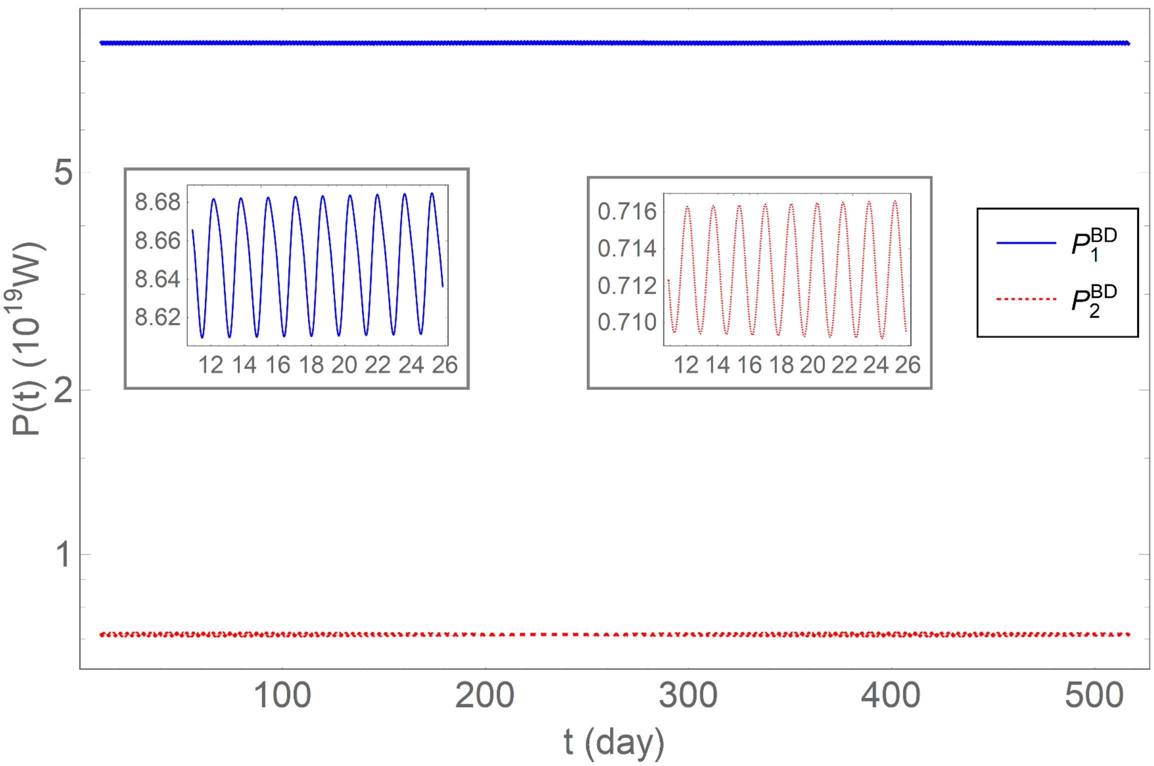

Figure 3.40: The instantaneous (time un-averaged) radiation power in BD gravity. Here the parts 1 and 2 are plotted separately. The inserts shows only 14 days.

CHAPTER FOUR

Black Hole Ringdown

Stellar mass binary black holes with a total mass between one and a few hundred solar masses are prime GW sources for the currently operating ground-based GW detectors Advanced LIGO [73] and Virgo [74]. Gravitational waves from binary black holes carry characteristic information about the astrophysical properties of the black holes, such as their masses and spins. These properties can be inferred by using highly accurate general relativistic waveform models, which describe the last stage of the binary black hole evolution: the ringdown of the remnant black hole.

The final state of binary black holes is a perturbed single black hole characterized by two parameters: the final remnant mass and spin angular momentum. The perturbed black hole radiates gravitational waves at a specific set of frequencies completely determined by the mass and spin. The segment of the gravitational wave signal associated with the single black hole's oscillations is known as the ringdown phase, as the perturbed black hole rings down analogous to a struck bell. The set of frequencies and damping times associated with a given black hole are known as quasinormal modes (QNMs), the damped oscillations connected to the underlying black hole geometry.

In the first section of this chapter, we study spherically symmetric static black holes (BHs) in Einstein-aether theory [36]. In the following section, we calculate the perturbation of the spherical BH background, that is, quasinormal modes.

4.1 Black Hole Solutions

4.1.1 Particle and Universal Horizons

It should be noted that the definition of BHs in æ-theory is different from that given in GR. In particular, in æ-theory there are three gravitational modes, the scalar, vector and tensor, which will be referred to as the spin-0, spin-1 and spin-2 gravitons, respectively. Each of these moves in principle with a different speed, given, respectively, by [87]

$$\begin{aligned} c_S^2 &= \frac{c_{123}(2-c_{14})}{c_{14}(1-c_+)(2+c_++3c_2)}, \\ c_V^2 &= \frac{2c_1-c_+(2c_1-c_+)}{2c_{14}(1-c_+)}, \\ c_T^2 &= \frac{1}{1-c_+}. \end{aligned} \tag{4.1}$$

The constants c_S, c_V and c_T represent the speeds of the spin-0, spin-1 and spin-2 gravitons, respectively.

Since the æ-theory possesses three different modes, and all of them are moving at different speeds, in general these different modes define different horizons [62]. These horizons are the null surfaces of the effective metrics,

$$g^{(A)}_{\alpha\beta} \equiv g_{\alpha\beta} - \left(c_A^2 - 1\right) u_\alpha u_\beta, \tag{4.2}$$

where $A = S, V, T$. The null surfaces for $A = S,\ V,\ T$ are called the spin-0 horizon (S0H), spin-1 horizon (S1H) and spin-2 horizon (S2H), respectively. These three different horizons will also be referred to as particle horizons for the corresponding gravitons, and are given by [36]

$$g^{(A)}_{\alpha\beta} N^\alpha N^\beta \Big|_{r=r_S} = 0, \tag{4.3}$$

where $N_\mu = \delta^r_\mu$, S stands for S0H, S1H, S2H, and r_S refers to the position of the corresponding horizon.

In contrast, the metric horizon (MH) is the null surface of metric $g_{\alpha\beta}$, or a particle horizon of $g^{(A)}_{\alpha\beta}$ with $c_A = 1$, given by

$$g_{\alpha\beta}N^\alpha N^\beta\Big|_{r=r_{\rm MH}} = 0, \tag{4.4}$$

where $r_{\rm MH}$ is the position of MH.

If a BH is defined to be a region that traps all possible causal influences, it must be bounded by a horizon corresponding to the fastest speed. In theories with the broken Lorentz invariance (LI), the dispersion relation of a massive particle contains generically high-order momentum terms [76],

$$E^2 = m^2 + p_k^2 k^2 \left(1 + \sum_{n=1}^{2(z-1)} q_n \left(\frac{k}{M_*}\right)^n\right), \tag{4.5}$$

from which we can see that both of the group and phase velocities become unbounded as $k \to \infty$, where E and k are the energy and momentum of the particle considered, and p_k and q_n's are coefficients depending on the species of the particle, while M_* is the suppression energy scale of the higher-dimensional operators. Therefore, in theories with the broken LI, a BH should be defined to be a region that traps all possible causal influences, including particles with arbitrarily large velocities ($c_A \to \infty$). Does such a region exists ?

To answer the above question, we first note that the causal structure of space-times in such theories is quite different from that given in GR, where the light cone at a given point p plays a fundamental role in determining the causal relationship of p to other events [77]. In a ultraviolet (UV) complete theory, the above dispersion

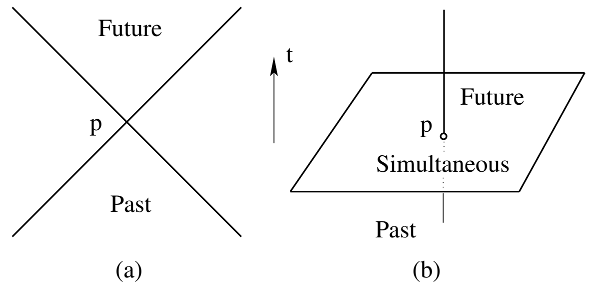

Figure 4.1: Illustration of causal structures of spacetimes in different theories of gravity [77]: (a) The light cone of the event p in special relativity. (b) The causal structure of the event p in Newtonian theory.

relationship is expected even in the gravitational sector [1]. In such theories, the causal structure is dramatically changed. For example, in the Newtonian theory, time is absolute and the speeds of signals are not limited. Then, the causal structure of a given point p is uniquely determined by the time difference $\Delta t \equiv t_p - t_q$ between the two events [cf. Fig. 4.1]. In particular, if $\Delta t > 0$, the event q is to the past of p; if $\Delta t < 0$, it is to the future; and if $\Delta t = 0$, the two events are simultaneous.

In theories with breaking LI, a similar situation occurs. Thus, to build the causal structure of spacetimes in such theories, a globally time-like coordinate should be first introduced [79, 80]. In particular, for a given spacetime, we first introduce a globally timelike scalar field ϕ [81]. In the spherically symmetric case, this globally timelike scalar field relates to the aether field u_μ via

$$u_\mu = \frac{\phi_{,\mu}}{\sqrt{-\phi_{,\alpha}\phi^{,\alpha}}}. \tag{4.6}$$

Then, similar to the Newtonian theory, this field defines globally an absolute time, and all particles are assumed to move along the increasing direction of the timelike scalar field, so the causality is well defined [cf. Fig. 4.2]. In such a spacetime,

[1] One such example is the healthy extension [84, 85] of Hořava gravity [76, 78], a possible UV extension of the khronometric theory.

there may exist a surface at which the aether field u_μ is orthogonal to the timelike Killing vector ζ ($\equiv \partial_v$), where v denotes the ingoing Eddington-Finkelstein (EF) coordinate, with which the element takes the form

$$ds^2 = -F(r)dv^2 + 2B(r)dvdr + r^2 d\Omega^2, \tag{4.7}$$

where $\Omega^2 \equiv d\theta^2 + \sin^2\theta d\varphi^2$ and $x^\mu = (v, r, \theta, \varphi)$. Given that all particles move along the increasing direction of the aether field, it is clear that a particle must cross this surface and move inward once it arrives at it, no matter how large its speed is [2]. This is a one-way membrane, and particles even with infinitely large speeds cannot escape from it once they are inside it. Thus it acts as an absolute horizon to all particles (with any speed), which is often called the universal horizon (UH) [76, 79, 80]. At the horizon, as can be seen from Fig. 4.2, we have [82],

$$\zeta \cdot u|_{r=r_{\rm UH}} = -\frac{1}{2A}(1+J)\Big|_{r=r_{\rm UH}} = 0, \tag{4.8}$$

where $J \equiv FA^2$, and $A(r)$ is one of the components of the aether field,

$$u^\alpha \partial_\alpha = A(r)\partial_v - \frac{1 - F(r)A^2(r)}{2B(r)A(r)}\partial_r. \tag{4.9}$$

4.1.2 An Analytical Solution

In this section, our main goal is to present one exact, asymptotically flat, static, spherically symmetric vaccum, single-parameter family of black hole solutions.

The vacuum field equations $E^{\mu\nu} \equiv G^{\mu\nu} - S^{\mu\nu} = 0$ and $Æ^\mu = 0$ can be divided into two groups [88, 89]: one represents the evolution equations, given by

$$E^{vv} = E^{\theta\theta} = Æ^v = 0, \tag{4.10}$$

[2] Particles even with infinitely large speeds will just move on these boundaries and cannot escape to infinity.

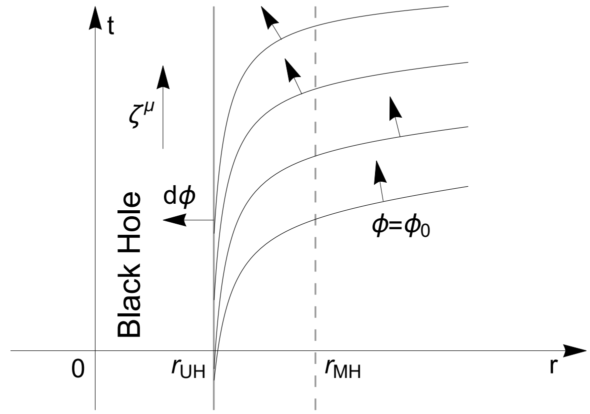

Figure 4.2: Illustration of the bending of the $\phi =$ constant surfaces, and the existence of the UH in a spherically symmetric static spacetime, where ϕ denotes the globally timelike scalar field, and t is the Painlevé-Gullstrand-like coordinates, which covers the whole spacetime [83]. Particles always move along the increasing direction of ϕ. The Killing vector $\zeta^{\mu} = \delta^{\mu}_{v}$ always points upward at each point of the plane. The vertical dashed line is the location of the metric (Killing) horizon, $r = r_{\mathrm{MH}}$. The UH, denoted by the vertical solid line, is located at $r = r_{\mathrm{UH}}$, which is always inside the MH.

and the other represents the constraint equation, given by

$$C^{v} = 0, \tag{4.11}$$

where $C^{\alpha} \equiv E^{r\alpha} + u^{r}Æ^{\alpha} = 0$, and $G^{\mu\nu}$ denotes the Einstein tensor. Note that in equation (35) of [89] two constraint equations $C^{v} = C^{r} = 0$ were considered. However, C^{r} and C^{v} are not independent. Instead, they are related to each other by the relation $C^{r} = (F/B)C^{v}$. Thus, $C^{v} = 0$ implies $C^{r} = 0$, so there is only one independent constraint.

On the other hand, the three evolution equations can be cast in the forms,

$$
\begin{aligned}
F'' &= \mathcal{F}\left(A, A', F, F', r, c_i\right) \\
&= \frac{1}{2r^2 A^4 \mathcal{D}}\Big(f_0 + f_1 F + f_2 F^2 + f_3 F^3 \\
&\qquad + f_4 F^4\Big),
\end{aligned}
\tag{4.12}
$$

$$
\begin{aligned}
A'' &= \mathcal{A}\left(A, A', F, F', r, c_i\right) \\
&= \frac{1}{2r^2 A^2 \mathcal{D}}\Big(a_0 + a_1 F + a_2 F^2 + a_3 F^3\Big),
\end{aligned}
\tag{4.13}
$$

$$
\begin{aligned}
\frac{B'}{B} &= \mathcal{B}\left(A, A', F, F', r, c_i\right) \\
&= \frac{1}{2r A^2 \mathcal{D}}\Big(b_0 + b_1 F + b_2 F^2\Big),
\end{aligned}
\tag{4.14}
$$

where a prime stands for the derivative with respect to r, and

$$
\mathcal{D} \equiv d_-\left(J^2 + 1\right) + 2d_+ J,
\tag{4.15}
$$

with $J \equiv FA^2$ and

$$
d_\pm \equiv (c_S^2 \pm 1)c_{14}(1 - c_{13})(2 + c_{13} + 3c_2).
\tag{4.16}
$$

The coefficients f_n, a_n and b_n are independent of $F(r)$ and $B(r)$ but depend on $F'(r)$, $A(r)$ and $A'(r)$, and are given explicitly by equations in Appendix A of [36]. The constraint equation (4.11) now can be cast in the form

$$
n_0 + n_1 F + n_2 F^2 = 0.
\tag{4.17}
$$

Thus, we have three dynamical equations and one constraint for the three unknown functions, F, A and B. As a result, the system seems over determined. However, a closer examination shows that not all of these equations are independent. For example, equation (4.14) can be obtained from equations (4.12), (4.13), and

(4.17). In fact, from equation (4.17), the function B can be written in the form

$$\begin{aligned}
B(r) \;\; = \;\; & \pm\frac{1}{2\sqrt{2}A^2}\Bigg\{2A^2\Big[4J(1+2c_2+c_{13}) \\
& \quad -(2c_2+c_{13})\big(J+1\big)^2\Big] \\
& +4rA\Big[2AJ'-4JA' \\
& \quad +c_2\big(J-1\big)\big(JA'-A'-AJ'\big)\Big] \\
& +r^2\Big[c_{14}\big(JA'+A'-AJ'\big)^2 \\
& \quad -(c_2+c_{13})\big(JA'-A'-AJ'\big)^2\Big]\Bigg\}^{1/2}. \qquad (4.18)
\end{aligned}$$

Recall that $J = FA^2$. Note that there are two branches of solutions for $B(r)$ with opposite signs, since equation (4.17) is a quadratic equation of B. However, only the "+" sign will give $B = 1$ at the spatial infinity, while the "-" sign will yield $B(r \to \infty) = -1$. Therefore, in the rest of the paper, we shall choose the '"+" sign in equation (4.18). By taking the derivative of equation (4.18) with respect to r, and then combining the obtained result with equations (4.12) and (4.13), one can obtain equation (4.14) [3].

To solve these equations, in this section we shall adopt the following strategy: choosing equations (4.12), (4.13) and (4.18) as the three independent equations for the three unknown functions, F, A, and B. The advantage of this choice is that equations (4.12) and (4.13) are independent of the function B. Therefore, we can first solve these two equations to find F and A, and then obtain the function B directly from equation (4.18).

[3] From this proof it can be seen that obtaining equation (4.14) from equation (4.18) the operation of taking the first-order derivatives was involved. Therefore, in principle these two equations are equivalent, modulated by an integration constant.

First we simplify the equations by setting $c_{14} = c_{13} = 0$, this choice satisfies observational constraints given by equations (1.6)-(1.11).

Equations (4.12)-(4.13) now reduce to

$$F'' = -\frac{2}{r}F' + \frac{c_2\hat{\mathcal{F}}(r)}{4r^2A^4}, \tag{4.19}$$

$$\begin{aligned} A'' &= \frac{2}{r^2(A+A^3F)}\Big[r^2(A')^2 - rAA' - A^2 \\ &\quad -rA^3A'(F+rF') + A^4F\Big] \\ &\quad -\frac{c_2\hat{\mathcal{F}}(r)}{4r^2(A+A^3F)}, \end{aligned} \tag{4.20}$$

where

$$\hat{\mathcal{F}}(r) \equiv \left[rA' - 2A + rA^2A'F + A^3\left(2F + rF'\right)\right]^2. \tag{4.21}$$

Combining equations (4.19) and (4.20), we find the following equation,

$$W'' + W'^2 + \frac{2}{r}W' - \frac{2}{r^2} = 0, \tag{4.22}$$

where

$$W \equiv \ln\left(\frac{1-FA^2}{A}\right). \tag{4.23}$$

Equation (4.22) has the general solution

$$W = \ln w_2 + \ln\left(\frac{1+w_1r^3}{r^2}\right), \tag{4.24}$$

where w_1 and w_2 are two integration constants. The combination of equations (4.23) and (4.24) yields,

$$F(r) = \frac{1}{A^2} - \frac{w_2}{A}\left(\frac{1}{r^2} + w_1r\right). \tag{4.25}$$

Substituting equation (4.25) into equation (4.19), we find

$$F'' = -\frac{2}{r}F' + F_0, \tag{4.26}$$

where $F_0 \equiv 9c_2 w_1^2 w_2^2/4$. Integrating equation (4.26), we find

$$F(r) \;=\; F_2\left(1-\frac{2m}{r}\right)+\frac{F_0}{6}r^2, \tag{4.27}$$

where m and F_2 are two other integration constants. On the other hand, from equation (4.25), we find that

$$\begin{aligned} A(r) \;=\; & -\frac{w_2}{2F}\left[\left(\frac{1}{r^2}+w_1 r\right)\right. \\ & \left. \pm\sqrt{\frac{4F}{w_2^2}+\left(\frac{1}{r^2}+w_1 r\right)^2}\,\right]. \end{aligned} \tag{4.28}$$

Substituting the above expressions for A and F into the constraint (4.18),

$$B \;=\; \sqrt{F_2}. \tag{4.29}$$

Note that the above solution is asymptotically flat only when $w_1 = 0$, for which we have

$$\begin{aligned} F(r) &= F_2\left(1-\frac{2m}{r}\right), \quad B(r) = \sqrt{F_2}, \\ A(r) &= -\frac{w_2}{2F}\left(\frac{1}{r^2}\pm\sqrt{\frac{4F}{w_2^2}+\frac{1}{r^4}}\right). \end{aligned} \tag{4.30}$$

Using the gauge residual $v' = C_0 v + C_1$ of the metric (4.7), without loss of the generality, we can always set $F_2 = 1$, so the corresponding metric takes the precise form of the Schwarzschild solution

$$ds^2 = -\left(1-\frac{2m}{r}\right)dv^2 + 2dvdr + r^2 d\Omega^2, \tag{4.31}$$

while the aether field is given by

$$A(r) \;=\; -\frac{w_2 \pm \sqrt{w_2^2+4r^3(r-2m)}}{2r(r-2m)}. \tag{4.32}$$

It should also be noted that equations (4.31) and (4.32) are a particular case of the solutions first found in [90] for the case $c_{14} = 0$ by further setting $c_{13} = 0$. The general solutions given by equations (4.27) - (4.29) are new.

4.2 Quasinormal Modes of Black Holes

Perturbations of black holes have been one of the main topics of relativistic astrophysics for the last few decades. They are of particular importance today because of their relevance to gravitational wave astronomy. In this section, the discussion includes perturbations of black hole solutions obtained in last section and the numerical solution of the master equation[4], that is, quasinormal modes (QNMs).

QNMs in GR have been studied extensively. Some relative studies have been done for scalar, vector and gravitational perturbations [93]. In addition, the calculation has been extended from Schwarzschild black holes (BHs) [94] to other more general cases, e.g., Kerr BHs [95, 96]. In this procedure, several different techniques of calculations were developed. For instance, the Wentzel-Kramers-Brillouin (WKB) approach [97–100], the continued fraction method [101], etc. [102–104]. Some of these methods also work in different modified theories of gravity [105, 106]. Additionally, some special scenarios, e.g., the eikonal limit, are studied [107].

QNMs in ae-theory are quite different from that in GR, because the boundary condition is now imposed at the universal horizon, and the master equation is singular at the metric horizon. We first take care of the singularity then calculate QNMs under the æ-theory by using the shooting method.

[4] The master equation is usually a single variable equation, which is the combination of equations of the perturbation fields.

4.2.1 *Master Equation*

First, let us consider the perturbations to the background solutions given by equation (4.31-4.32) with $w_2 = 3\sqrt{3}r_s^2/8$, which ensures the existence of the universal horizons

$$r_{UH} = \frac{3r_s}{4}, \tag{4.33}$$

where $r_s = 2m$.

To distinguish these from the perturbation fields, we denote background fields by $\bar{g}_{\mu\nu}$ and $\bar{u}^\mu$, respectively, so the total metric and aether are given by

$$g_{\mu\nu} = \bar{g}_{\mu\nu} + h_{\mu\nu}, \quad u^\mu = \bar{u}^\mu + w^\mu. \tag{4.34}$$

Working with only the the odd-parity parts, $h_{\mu\nu}$ and w^μ can be cast in the form,

$$h_{\mu\nu} = -\frac{1}{2}\sum_{l=0}^{\infty}\sum_{m=-l}^{l}\frac{r}{B}\times$$
$$\begin{pmatrix} 0 & 0 & -2C_{lm}\csc\theta\partial_\varphi Y_{lm} & 2C_{lm}\sin\theta\partial_\theta Y_{lm} \\ 0 & 0 & 2J_{lm}\csc\theta\partial_\varphi Y_{lm} & -2J_{lm}\sin\theta\partial_\theta Y_{lm} \\ sym & sym & -2rG_{lm}\csc\theta\big(\cot\theta\partial_\varphi - \partial_\theta\partial_\varphi\big)Y_{lm} & sym \\ sym & sym & rG_{lm}\big(\csc\theta\partial_\varphi^2 + \cos\theta\partial_\theta - \sin\theta\partial_\theta^2\big)Y_{lm} & 2rG_{lm}\big(\cos\theta\partial_\theta - \sin\theta\partial_\theta\partial_\varphi\big)Y_{lm} \end{pmatrix}, \tag{4.35}$$

$$w^\mu = \sum_{l=0}^{\infty}\sum_{m=-l}^{l}\frac{1}{r}\begin{pmatrix} 0 \\ 0 \\ -a_{lm}\csc\theta\partial_\varphi \\ a_{lm}\csc\theta\partial_\theta \end{pmatrix} Y_{lm}, \tag{4.36}$$

where $Y_{lm} = Y_{lm}(\theta,\varphi)$ stands for the spherical harmonics, and $C_{lm},\ G_{lm},\ J_{lm}$ and a_{lm} are functions of t and r only. Note that in calculating the field equations we will set $m = 0$ in the above expressions so that $\partial_\varphi Y_{lm}(\theta,\varphi) = 0$, giving the background spherical symmetry, and the corresponding linear perturbations do not depend on m [108].

When the spacetimes are vacuum, we have $T_{\mu\nu} = 0,\ T_{\mu} = 0$, and then the field equations reduce to

$$G_{\mu\nu} - S_{\mu\nu} = 0, \quad \AE^{\mu} = 0. \tag{4.37}$$

We substitutes equations (4.35) and (4.36) into (4.37), we obtain the following master equation

$$\left(\frac{4F}{r}\frac{\partial}{\partial v} + 2F\frac{\partial^2}{\partial v \partial r} + \eta_1 \frac{\partial^2}{\partial r^2} + \eta_2 \frac{\partial}{\partial r} + \eta_3\right) \mathcal{Y}_{lm} = 0, \tag{4.38}$$

where

$$\begin{aligned}
F &= 1 - \frac{2m}{r}, \quad \eta_1(r) = \frac{(r-2m)^2}{r^2}, \quad \eta_2(r) = \frac{(r-2m)(4r-6m)}{r^3}, \\
\eta_3(r) &= -\frac{(r-2m)[(l+2)(l-1)r - 6m]}{r^4}.
\end{aligned} \tag{4.39}$$

Notice that to write out the above expression, we changed to the ingoing Eddington–Finkelstein coordinates by $v = t + r_*$ with $dr_*/dr = 1/F$, so that the coordinates can cover the whole region $r \in (0, \infty)$.

QNMs are solutions of the equation (4.38), satisfying specific boundary conditions at the universal horizon and far from the black hole. At the universal horizon the boundary condition is a requirement of the pure ingoing waves

$$\mathcal{Y}_{lm} \propto e^{-i\omega(t+r_*)}, \quad r \to r_{UH}, \tag{4.40}$$

Another boundary condition is pure outgoing waves at spatial infinity

$$\mathcal{Y}_{lm} \propto e^{-i\omega(t-r_*)}, \quad r \to \infty. \tag{4.41}$$

Separation of variable leads to

$$\mathcal{Y}_{lm}(v,r) = e^{-i\omega v}(r-1)^{2i\omega}\Psi_{lm}(r), \tag{4.42}$$

for which equation (4.38) becomes (using $r_s = 1$)

$$\left(\alpha_1 \frac{d^2}{dr^2} + \alpha_2 \frac{d}{dr} + \alpha_3\right)\Psi(r) = 0, \tag{4.43}$$

where

$$\begin{aligned}
\alpha_1 &\equiv \frac{(r-1)^2}{r^2},\\
\alpha_2 &\equiv \frac{(r-1)[4r - 2i(r-2)r\omega - 3]}{r^3},\\
\alpha_3 &\equiv \frac{(r-1)}{r^4}\{3 + r[2 - l(l+1) + 4r\omega(\omega - i) + 6i\omega]\}.
\end{aligned} \tag{4.44}$$

4.2.2 *Shooting Method*

Introducing a function $\psi(r)$ via the relation,

$$\psi(r) \equiv r^2 e^{-ir\omega}(r-1)^{i\omega}\Psi, \tag{4.45}$$

we find that equation (4.43) can be cast in the form

$$\left(\omega^2 + \frac{d^2}{dr_*^2} - V_g\right)\psi = 0, \tag{4.46}$$

where

$$V_g(r,l) \equiv \frac{(r-1)[l(l+1)r-3]}{r^4}. \tag{4.47}$$

Note that V_g is the same as that given in GR [102]. Clearly, as $r \to +\infty$ equation (4.46) has the general solutions,

$$\psi|_{r\to\infty} = \hat{\psi}_+ e^{i\omega r_*} + \hat{\psi}_- e^{-i\omega r_*}, \tag{4.48}$$

where $\hat{\psi}_{\pm}$ are two integration constants. But considering the boundary condition of equation (4.41), we must set $\hat{\psi}_{-} = 0$. Thus, when r is very large but finite, we expect $\psi(r)$ to take the form

$$\psi = e^{i\omega r_*} \sum_{n=0}^{\infty} \frac{a_n}{r^n}, \tag{4.49}$$

where a_n are constants. Inserting this together with equation (4.45) into equation (4.42), we find that

$$\mathcal{Y} = e^{-i\omega(t-r)} \left[\frac{(r-1)^{i\omega}}{r^2} \sum_{n=0}^{\infty} \frac{a_n}{r^n} \right], \tag{4.50}$$

which indeed represents a purely out-going wave, so that the condition (4.41) is satisfied. On the other hand, substituting this into equation (4.46), we find that a_n's satisfy the following recursion relation,

$$\begin{aligned} 0 &= -2in\omega a_n + \left[(n-1)(n+2i\omega) - l^2 - l\right] a_{n-1} \\ &\quad + \left(l^2 + l - 2n^2 + 5n + 1\right) a_{n-2} \\ &\quad + (n-4) n a_{n-3}, \end{aligned} \tag{4.51}$$

from which we can write all a_n's ($n \geq 1$) in terms of a_0. Without loss of generality, we can always set $a_0 = 1$, as shown below.

In principle, once the boundary conditions are given, we can solve equation (4.43) to find out the spectrum of ω for any given l. However, noticing that equation (4.43) is singular at the MH $r = r_s$, we have to solve equation (4.43) on $r \in [r_{UH}, r_s - \epsilon] \cup [r_s - \epsilon, \infty)$, with $\epsilon \ll 1$.

To fulfill this, let us first expand $\Psi(r)$ as

$$\Psi = \sum_{n=0}^{\infty} d_n \left(r-1\right)^n, \tag{4.52}$$

where d_n's are constants. Inserting the above expression into equation (4.43), we find that the coefficients d_n's satisfy the following recursion relation,

$$\begin{aligned} 0 &= n(n+2i\omega)d_n \\ &\quad + \left(4 - l^2 - l + 2n^2 + 2in\omega - n + 4\omega^2\right) d_{n-1} \\ &\quad + \left[2\omega(4\omega + i) - l^2 - l + n^2 + n(-1 - 2i\omega)\right] d_{n-2} \\ &\quad + 2\omega(i - in + 2\omega)d_{n-3}. \end{aligned} \tag{4.53}$$

Thus, similar to a_n's given by equation (4.51), all these coefficients can be written in terms of d_0. What's more, for a similar reason, we will set $d_0 = 1$. Therefore, for any given ω and l, we find the general solution of $\Psi(r)$ in the neighborhood of $r = 1$.

On the other hand, as $r \to 3/4$, equation (4.43) reads,

$$0 \simeq \left\{\frac{d^2}{dr^2} - 10i\omega\frac{d}{dr} \quad + \frac{16}{3}\left[l^2 + l - 3\left(\omega^2 + i\omega + 2\right)\right]\right\}\Psi, \tag{4.54}$$

which has the general solutions, $\Psi(r) \simeq \hat{\Psi}_+ e^{-ik_+ r} + \hat{\Psi}_- e^{-ik_- r}$, where $\hat{\Psi}_\pm$ are two integration constants, and

$$k_\pm \equiv -5\omega \mp i\sqrt{\omega(16i - 9\omega) - \frac{16}{3}(l+3)(l-2)}. \tag{4.55}$$

Therefore, in the neighborhood of $r = 3/4$ there are two branches of $\Psi(r)$. For simplicity, we define the ratio of these two branches as $\alpha \equiv \hat{\Psi}_-/\hat{\Psi}_+$. We can further set $\hat{\Psi}_+ = 1$. Thus, we obtain

$$\Psi = \left(\alpha e^{-ik_- r} + e^{-ik_+ r}\right)\sum_{n=0}^{\infty} b_n \left(r - \frac{3}{4}\right)^n. \tag{4.56}$$

Substituting into equation (4.43), we can solve the coefficients b_n's ($n \geq 2$) recursively, and find that they will be given in terms of b_0 and b_1. However, due to the intricacy of these solutions we are not able to find a recursion relation this time.

Similar to a_0, without loss of generality, we can always set $b_0 = 1$, while b_1 will be determined through equation (4.52), which means $\Psi(r = r_s) = d_0 = 1$. Applying this condition to equation (4.56) at $r = r_s$, we are able to determine the value of b_1 in terms of ω and l.

To to solve equation (4.43), following [94] we introduce the function $\Phi(r)$ by

$$\Psi(r) = \exp\left(i\int^r \Phi(r)dr\right), \tag{4.57}$$

or equivalently

$$\Phi(r) = -i\frac{d\ln\Psi}{dr}. \tag{4.58}$$

Then, equation (4.43) reduces to

$$i\Phi' - \Phi^2 + \beta_1\Phi + \beta_2 = 0, \tag{4.59}$$

where

$$\begin{aligned} \beta_1(r,\omega) &\equiv \frac{2r[(r-2)\omega + 2i] - 3i}{(r-1)r}, \\ \beta_2(r,\omega,l) &\equiv \frac{3 + r[2 - l(l+1) + 4r\omega(\omega - i) + 6i\omega]}{(r-1)r^2}. \end{aligned} \tag{4.60}$$

It is remarkable to note that $\Phi(r)$ does not depend on the amplitudes of $\Psi(r)$ at any of the points $r = (r_{\pm},\ r_{\rm UH},\ r_{\rm max})$, with $r_{\pm}$ in the neighborhood of r_s. As a result, we can assign a_0, b_0 and d_0 any values. As mentioned previously, without loss of generality, we shall set all of them to one, $a_0 = b_0 = d_0 = 1$.

For convenience, we further introduce a new variable x by $x \equiv 2r/(r+3/4)$ in equation (4.59). Note that $r \in [3/4, 1) \cup (1, \infty)$ corresponds to $x \in [1, 8/7) \cup (8/7, 2)$. Therefore, equation (4.59) becomes

$$\frac{2i}{3}(2-x)^2 \frac{d\Phi}{dx} - \Phi^2 + \gamma_1 \Phi + \gamma_2 = 0, \tag{4.61}$$

where

$$\begin{aligned}
\gamma_1(x,\omega) &\equiv \frac{2x(11x-16)\omega - 32i(x-2)(x-1)}{x(7x-8)}, \\
\gamma_2(x,\omega,l) &\equiv \frac{16(2-x)}{3x^2(7x-8)} \\
&\quad \times \Big\{ x^2 \left[l^2 + l + 3\omega(\omega - 3i) + 2 \right] \\
&\qquad - 2x \left(l^2 + l - 6i\omega + 6 \right) + 16 \Big\}.
\end{aligned} \tag{4.62}$$

In this way, we obtain a complex ordinary differential equation (ODE) of the first order, which will be much easier to solve than equation (4.43). To solve equation (4.61) we use the shooting method. Specifically, for any given l, we integrate equation (4.61) as follows:

(a) With a good guess, we first choose a (complex) value of ω, and then from equations (4.52) and (4.53) create the "initial values" $\Psi_{\pm}(\omega) \equiv \Psi(r = r_{\pm}, \omega)$, where $r_{\pm} = r_s \pm \epsilon$, and ϵ is a small quantity. Then, we calculate $\Phi_{\pm}(\omega) \equiv \Phi(x = x_{\pm}, \omega)$ using equation (4.58), with $x_{\pm} = 2r_{\pm}/(r_{\pm} + 3/4)$.

(b) With the initial value $\Phi_{-}(\omega)$, integrate equation (4.61) from x_{-} to $x_{UH} = r_{UH}/(r_{UH} + 3/4)$ to obtain $\Phi_{\mathrm{UH}} \equiv \Phi(x_{\mathrm{UH}})$.

(c) Compare this value of Φ_{UH} (call it $\Phi_{\min}$) with the one given by equations (4.56) and (4.58), and if $\delta\Phi_{\min} \leq \epsilon_{\min}$, where $\epsilon_{\min}$ is a given small value, we say that such chosen ω satisfies the in-going wave boundary condition, and $\delta\Phi_{\min} \equiv$

$|\Phi_{\rm UH} - \Phi_{\rm min}|$. Otherwise we need to choose a different value of ω and repeat steps (b) to (c), until the condition $\delta\Phi_{\rm min} \le \epsilon_{\rm min}$ is fulfilled.

(d) With such determined ω we find the "initial value" $\Phi_{+}(\omega)$ by equations (4.52), (4.53) and (4.58), with which we integrate equation (4.61) from x_{+} to $x = x_{\rm max}$ (for a properly chosen $x_{\rm max}$), and obtain a value $\Phi_{\infty} \equiv \Phi(x_{\rm max})$.

(e) Compare such obtained Φ_{∞} (call it $\Phi_{\rm max}$) with the one obtained from equations (4.49), (4.51) and (4.58) . If $\delta\Phi_{\rm max} \equiv |\Phi_{\infty} - \Phi_{\rm max}| \le \epsilon_{\rm max}$, where $\epsilon_{\rm max}$ is another small quantity, we say that such obtained ω satisfies both boundary conditions, and it is exactly this value of ω that we are looking for. In this paper, we shall choose $\epsilon_{\rm min} = \epsilon_{\rm max} = 10^{-21}$. Otherwise, we say that this value of ω does not satisfy the boundary conditions, and should be excluded from the spectrum of the corresponding QNMs. In table 4.1, we list QNMs frequencies in ae-theory for $l = 2$ case.

Table 4.1: Results of ω in æ-theory for the $l = 2$ case.

α	ω	α	ω
-40	$0.73210 - 0.60667i$	40	$0.23060 - 0.90273i$
-38	$0.73480 - 0.59948i$	38	$0.23791 - 0.89574i$
-36	$0.73770 - 0.59195i$	36	$0.24559 - 0.88850i$
-34	$0.74084 - 0.58404i$	34	$0.25370 - 0.88098i$
-32	$0.74427 - 0.57569i$	32	$0.26229 - 0.87318i$
-30	$0.74802 - 0.56686i$	30	$0.27143 - 0.86507i$
-28	$0.75215 - 0.55747i$	28	$0.28122 - 0.85665i$
-26	$0.75675 - 0.54743i$	26	$0.29175 - 0.84789i$
-24	$0.76190 - 0.53662i$	24	$0.30317 - 0.83880i$
-22	$0.76774 - 0.52490i$	22	$0.31564 - 0.82937i$
-20	$0.77441 - 0.51207i$	20	$0.32937 - 0.81964i$
-18	$0.78215 - 0.49785i$	18	$0.34462 - 0.80968i$
-16	$0.79125 - 0.48186i$	16	$0.36173 - 0.79961i$
-14	$0.80213 - 0.46355i$	14	$0.38111 - 0.78972i$
-12	$0.81540 - 0.44207i$	12	$0.40325 - 0.78047i$
-10	$0.65847 - 0.89756i$	10	$0.42859 - 0.77270i$
-8	$0.64858 - 0.87874i$	8	$0.45730 - 0.76775i$
-6	$0.63629 - 0.85913i$	6	$0.48878 - 0.76732i$
-4	$0.62103 - 0.83906i$	4	$0.52119 - 0.77284i$
-2	$0.60219 - 0.81914i$	2	$0.55199 - 0.78433i$
-0.05	$0.57986 - 0.80083i$	0.05	$0.57860 - 0.79995i$

CHAPTER FIVE

Conclusion

In chapter one, we have derived all fundamental equations in the framework of Einstein-aether theory [62], and provide the most recent observational constraints on this theory's coupling constants. The theory violates locally the Lorentz symmetry and yet passes all the theoretical and observational tests carried out so far [42].

In chapter two, we have studied the strong field effects of N-body systems with the lowest PN order in the framework of Einstein-aether theory. All strong field effects are encoded into sensitivities. Due to the presence of two additional modes, the scalar and vector, in Einstein-aether theory, two additional parts also appear in the energy loss rate of the system, given respectively by the $\mathcal{B}$ and $\mathcal{C}$ terms in equation (2.108), representing the monopole and dipole contributions. In comparison with the quadruple contribution of GR, which is the order of $\mathcal{O}\left(v^2\right)$, the monopole contribution is only the order of $\mathcal{O}\left(c_{14}\right)\mathcal{O}\left(v^2\right)$, that is, it is about $\mathcal{O}\left(c_{14}\right) \lesssim \mathcal{O}\left(10^{-5}\right)$ order lower than that of GR. Here v is the relative velocity of the two compact objects. However, the dipole contributions can be much larger than those of the monopole. In particular, for a binary system with large differences between their binding energies, the dipole part can be as large as $\mathcal{O}\left(c_{14}\right)\mathcal{O}\left(G_N m/d\right)$, where m denotes the mass of the body and d the size of the body. For a realistic neutron star, we have $\mathcal{O}\left(G_N m/d\right) \simeq 0.1 \sim 0.3$, so that $\mathcal{O}\left(c_{14}\right)\mathcal{O}\left(G_N m/d\right) \simeq 10^{-2}\mathcal{O}\left(v^2\right)$. It should be noted that the scalar mode has contributions to all the three parts, quadrupole, dipole and monopole, while the vector mode has contributions only to the quadrupole and dipole parts, as can be seen clearly from equations (102)-(104) of Ref. [37]. On the other hand, the strong-field contributions are only of the orders of [33]

$$\delta\mathcal{W}_{\mathcal{A}}^{\rm NS} \lesssim \mathcal{O}\left(10^{-11}\right), \quad \delta\mathcal{W}_{\mathcal{B}}^{\rm NS} \lesssim \mathcal{O}\left(10^{-11}\right),$$

$$\delta\mathcal{W}_{\mathcal{C}}^{\rm NS} \lesssim \mathcal{O}\left(10^{-12}\right), \quad \delta\mathcal{W}_{\mathcal{D}}^{\rm NS} \lesssim \mathcal{O}\left(10^{-11}\right),$$

for a binary neutron star system, where $\delta\mathcal{W}_{\mathcal{A}}^{\rm NS}$, $\delta\mathcal{W}_{\mathcal{B}}^{\rm NS}$ and $\delta\mathcal{W}_{\mathcal{C}}^{\rm NS}$ represent the contributions of the strong field effects to the quadrupole, monopole and dipole parts of equation (2.108), while $\delta\mathcal{W}_{\mathcal{D}}^{\rm NS}$ denotes a cross term due to the motion of the center-of-mass of the system [39]. Clearly, these effects are much smaller than the ones mentioned above, and are beyond the detectability of the current generation of detectors. Thus we take the weak field limit or small sensitivity limit to the results in chapter three.

From the expressions of the six polarization modes of equation (2.99) we can see that the scalar longitudinal mode h_L is proportional to the scalar breathing mode h_b. Therefore, out of these six components, only five of them are independent. In addition, the scalar breathing and the scalar longitudinal modes are all suppressed by a factor $\mathcal{O}\left(c_{14}\right) \lesssim \mathcal{O}\left(10^{-5}\right)$ with respect to the transverse-traceless modes h_+ and $h_\times$, while the vectorial modes h_X and h_Y are suppressed by a factor $\mathcal{O}\left(c_{13}\right) \lesssim \mathcal{O}\left(10^{-15}\right)$. These conclusions should be also valid for general cases, and consistent with the analysis of triple systems presented in chapter three.

In chapter three, we apply the general formulas developed in chapter two to triple systems. In particular, we have studied the GWs, the response functions and the energy loss rates for three triple systems with different periodic orbits: one is the Simo's figure-eight configuration shown by Fig. 3.2, and the other two are the Broucke R7 and A16 configurations illustrated by Figs. 3.18 and 3.23. For a triple system, the GWs, the response function and energy loss rate depend not only on the configuration of orbits, but also on the orientation with respect to the detector and binding energies of the three compact bodies.

Then we focus on one relativistic three-body system PSR J0337+1517. We calculate the gravitational waveforms, their polarizations and Fourier transforms, as well as the radiation powers of the relativistic triple systems PSR J0337+1517, observed in 2014 [59]. This system consists of an inner binary and a third companion. The inner binary consists of a pulsar with mass $m_1 = 1.44M_\odot$ and a white dwarf with mass $m_2 = 0.20M_\odot$ in a 1.6 day orbit. The outer binary consists of the inner binary and a second dwarf with mass $m_3 = 0.41M_\odot$ in a 327 day orbit. The two orbits are very circular with eccentricities $e_I \simeq 6.9 \times 10^{-4}$ for the inner binary and $e_O \simeq 3.5 \times 10^{-2}$ for the outer orbit. The two orbital planes are remarkably coplanar with an inclination $\lesssim 0.01^o$ [See Fig. 3.1].

Our studies were carried out in three different theories, GR, BD gravity, and ae-theory. In GR, only the tensor mode exists, so a GW has only two polarization modes, the so-called, plus (h_+) and cross ($h_\times$) modes. Their amplitudes and Fourier transforms are shown in Figs. 3.2 - 3.4, from which it can be seen that their amplitude is about 10^{-23}, while their frequencies are peaked at two locations, $f_1^{+,\times} = 0.068658$ μHz (for the outer orbit) and $f_2^{+,\times} = 14.212$ μHz (for the inner orbit), respectively. These are about twice the inner and outer orbital frequencies of the triple system, and agree well with the GR predictions [46].

In ae-theory, all six polarization modes are different from zero, but the breathing (h_b) and longitudinal (h_L) modes are not independent. In comparing with h_+ and

$h_\times$, however, they are suppressed by a factor c_{14} which is observationally restricted to $c_{14} \lesssim 10^{-5}$ [42].

The effects of the parameters c_i's on h_b^{ae} and h_L^{ae} were also studied in detail, and we found that their amplitudes are weekly dependent on the choices of these parameters, while the frequencies of their Fourier transforms remain the same.

The other two independent polarization modes in ae-theory are the vector modes, h_X and h_Y, which are all proportional to c_{13}. The current observations from GW170817 [40] and GRB 170817A [41] on the speed of the tensor mode requires $c_{13} \lesssim 10^{-15}$. Therefore, these two modes are highly restricted by the limit of the speed of the tensor mode.

We also studied the radiation power due to the tensor, vector and scalar modes in ae-theory, and three different parts were plotted in Fig. 3.35. The amplitude of the quadrupole part ($\mathcal{A}$) contributed from all three modes [38] is comparable with that of GR. The monopole ($\mathcal{B}$) part has contributions only from the scalar mode, while the dipole ($\mathcal{C}$) part has contributions from both the scalar and vector modes, but does not have any contributions from the tensor mode, as expected in [38]. The monopole part is suppressed by a factor $c_{14} \lesssim \mathcal{O}\left(10^{-5}\right)$, but the dipole part is almost the same order as the quadrupole part. With the arrival of multi-band gravitational wave astronomy [91], joint observations of GW150914-like by LIGO/Virgo/KAGRA and LISA will improve constraints on the dipole emission [92]. Thus, the multi-band gravitational wave astronomy will provide a very promising direction to constrain ae-theory.

In chapter four, we calculated the QNMs of ae-theory. It is found that the frequencies are different from those in GR, with differences of about $\mathcal{O}(0.1)$, which means space-based GW detectors have the potential to rule out ae-theory in the near future.

APPENDICES

APPENDIX A

Gauge Transformation

In general, under a coordinates transformation

$$x^\alpha \rightarrow x'^\alpha(x), \tag{A.1}$$

we have

$$g_{\alpha\beta}(x) \rightarrow g'_{\alpha\beta}(x') = \frac{\partial x^\mu}{\partial x'^\alpha}\frac{\partial x^\nu}{\partial x'^\beta} g_{\mu\nu}(x), \tag{A.2}$$

$$u^\alpha(x) \rightarrow u'^\alpha(x') = \frac{\partial x'^\alpha}{\partial x^\beta} u^\beta(x). \tag{A.3}$$

Specificlly,

$$x^\alpha \rightarrow x'^\alpha(x) = x^\alpha + \xi^\alpha(x), \tag{A.4}$$

where $\xi^a \sim \epsilon$ and ϵ is a small quantity. The following results are valid to the first order in ϵ,

$$x^\alpha(x) = x'^\alpha - \xi^\alpha(x'). \tag{A.5}$$

where we have used Taylor expansion. Then equation (A.2) and (A.3) give

$$g'_{\alpha\beta}(x') = g_{\alpha\beta}(x) - \frac{\partial \xi^\mu(x')}{\partial x'^\beta} g_{\mu\alpha}(x) - \frac{\partial \xi^\mu(x')}{\partial x'^\alpha} g_{\mu\beta}(x), \tag{A.6}$$

$$u'^\alpha(x') = u^\alpha(x) + \frac{\partial \xi^\alpha(x)}{\partial x^\beta} u^\beta(x). \tag{A.7}$$

Suppose that we can expand $g_{\alpha\beta}$ and u^α in both reference frames as

$$g_{\alpha\beta}(x) = \eta_{\alpha\beta} + h_{\alpha\beta}(x), \tag{A.8}$$

$$u^\alpha(x) = \delta^\alpha_0 + \omega^\alpha(x), \tag{A.9}$$

where $h_{\alpha\beta} \sim \omega^\alpha \sim \epsilon$,

$$g'_{\alpha\beta}(x') = \eta_{\alpha\beta} + h'_{\alpha\beta}(x'), \tag{A.10}$$

$$u'^\alpha(x') = \delta^\alpha_0 + \omega'^\alpha(x'), \tag{A.11}$$

where $h'_{\alpha\beta} \sim \omega'^\alpha \sim \epsilon$. Then we have

$$h'_{\alpha\beta}(x') = h_{\alpha\beta}(x) - [\xi_{\alpha,\beta}(x') + \xi_{\beta,\alpha}(x')] \tag{A.12}$$

where $\xi_\alpha \equiv \xi^\mu \eta_{\mu\alpha}$,

$$\omega'^\alpha(x') = \omega^\alpha(x) + \dot{\xi}^\alpha(x) \tag{A.13}$$

If we further decompose ξ^α as follows

$$x'^0 = x^0 + \xi^0 \quad x'^i = x^i + \xi^i + \xi_{,i} \quad \xi^i_{\ ,i} = 0 \tag{A.14}$$

with $h_{\alpha\beta}$ $h'_{\alpha\beta}$ ω^α ω'^α as equation (2.2) and (2.3), we can reach equation (2.34).

APPENDIX B

Derivation of Equation (2.53)

$[\delta_{ij} \times \textit{equation } (2.44) - \delta_{ij} \times \textit{equation } (2.48) + 4 \times \textit{equation } (2.45)]$ gives

$$(1 + c_+ + 2c_2)\ddot{f}_{,ij} + (2 + 2c_2)\ddot{\phi}_{,ij} + 2h_{00,ij} - \Delta f_{,ij} = -16\pi G(\delta_{ij}\tau_{kk} - \delta_{ij}\tau^L_{kk} - 2\tau^T_{ij}). \tag{B.1}$$

In addition, we can solve equation (2.49) and equation (2.50) via Green's function, because they are just simply Poisson's equation,

$$F - c_{14}h_{00} = 4G\int d^3x' \frac{\tau_{00}(t, \vec{x}')}{|\vec{x} - \vec{x}'|} \equiv \Theta(t, \vec{x}), \tag{B.2}$$

$$(1 + c_2)\dot{f}_{,i} + c_{123}\dot{\phi}_{,i} = 4G\int d^3x' \frac{\tau^L_{i0}(t, \vec{x}')}{|\vec{x} - \vec{x}'|} \equiv \Theta_i(t, \vec{x}). \tag{B.3}$$

Therefore, we have

$$h_{00} = \frac{F - \Theta}{c_{14}}, \quad \dot{\phi}_{,i} = \frac{\Theta_i - (1 + c_2)\dot{f}_{,i}}{c_{123}}. \tag{B.4}$$

Inserting equation (B.4) into equation (B.1), we get

$$\begin{aligned} -\frac{[(2 + 2c_2)(1 + c_2) - (1 + c_+ + 2c_2)c_{123}]c_{14}}{(2 - c_{14})c_{123}}\ddot{f}_{,ij} + \Delta f_{,ij} = \\ \frac{c_{14}}{2 - c_{14}}\left[-\frac{2 + 2c_2}{c_{123}}\dot{\Theta}_{i,j} + \frac{2}{c_{14}}\Theta_{,ij} - 16\pi G(\delta_{ij}\tau_{kk} - \delta_{ij}\tau^L_{kk} - 2\tau^T_{ij})\right]. \end{aligned} \tag{B.5}$$

It can be written as

$$-\frac{1}{c_S^2}\ddot{f}_{,ij} + \Delta f_{,ij} = \tau'_{ij}. \tag{B.6}$$

APPENDIX C

Derivation of Equation (2.59)

Because

$$\frac{\partial}{\partial x^j}\left(\frac{1}{x}\right) = -\frac{\hat{x}^j}{x^2}, \quad \frac{\partial}{\partial x^j}\left(\hat{x}^i\right) = \frac{1}{x}(\delta_{ij} - \hat{x}^i\hat{x}^j), \tag{C.1}$$

and

$$\frac{\partial\tau(t-x/s,\vec{x}')}{\partial t} = \frac{\partial\tau}{\partial(t-x/s)}\frac{\partial(t-x/s)}{\partial t} = \frac{\partial\tau}{\partial(t-x/s)}, \tag{C.2}$$

$$\frac{\partial\tau(t-x/s,\vec{x}')}{\partial x^j} = \frac{\partial\tau}{\partial(t-x/s)}\frac{\partial(t-x/s)}{x^j} = \frac{\partial\tau}{\partial(t-x/s)}\frac{-1}{s}\frac{\partial x}{\partial x^j} = \frac{\partial\tau}{\partial t}\frac{-1}{s}\hat{x}^j, \tag{C.3}$$

$$\begin{aligned}
\frac{\partial}{\partial x^j}\psi(t,\vec{x}) &= \frac{4}{x}\sum_{m=0}^{\infty}\frac{1}{m!s^m}\frac{\partial^m}{\partial t^m}\int d^3x'\frac{\partial\tau(t-x/s,\vec{x}')}{\partial x^j}(x'^i\hat{x}^i)^m + O\left(\frac{1}{x^2}\right) \\
&= \frac{-1}{s}\hat{x}^j\frac{\partial}{\partial t}\frac{4}{x}\sum_{m=0}^{\infty}\frac{1}{m!s^m}\frac{\partial^m}{\partial t^m}\int d^3x'\tau(t-x/s,\vec{x}')(x'^i\hat{x}^i)^m + O\left(\frac{1}{x^2}\right) \quad \text{(C.4)} \\
&= \frac{-1}{s}\hat{x}^j\frac{\partial}{\partial t}\psi(t,\vec{x}) + O\left(\frac{1}{x^2}\right).
\end{aligned}$$

APPENDIX D

Derivation of Equation (2.70)

The source is described by $\tau_{ab} = \tau_{ab}(t, \vec{x})$, it satisfies

$$\tau_{ij,ij} = \tau_{ji,ij} = \tau_{j0,0j} = \tau_{0j,0j} - T_{j,0j} = \tau_{00,00} - T_{j,0j}, \tag{D.1}$$

where we first use the equation (2.21) then equation (2.40) then equation (2.21) again. Integrate the above over whole space as

$$\int d^3x\ x^i x^j \tau_{kl,kl} = \int d^3x\ x^i x^j (\tau_{00,00} - T_{k,0k}), \tag{D.2}$$

After integration by parts, the surface terms go away due to localized source ($x > d, \tau_{ab} = 0$),

$$\int d^3x\ \tau_{ij} = \frac{1}{2} \int d^3x\ x^i x^j \ddot{\tau}_{00} + \int d^3x\ \dot{T}_{(i} x_{j)}. \tag{D.3}$$

Since x is a dummy variable we can do $x \to x'$, $\tau_{ij}(t, \vec{x}) \to \tau_{ij}(t, \vec{x}')$,

$$\int d^3x'\ \tau_{ij} = \frac{1}{2} \int d^3x'\ x'^i x'^j \ddot{\tau}_{00} + \int d^3x'\ \dot{T}_{(i} x'_{j)}. \tag{D.4}$$

If we drop the higher order terms, $\tau_{00}(t, \vec{x}') = \sum_A m_A \delta^3(\vec{x}' - \vec{x}_A(t))$, $T_i(t, \vec{x}') = 0$,

$$\begin{aligned} \int d^3x'\ \tau_{ij}(t, \vec{x}') &= \frac{1}{2}\ \partial_t^2 \int d^3x'\ x'^i x'^j \sum_A m_A \delta^3(\vec{x}' - \vec{x}_A(t)) \\ &= \frac{1}{2}\ \partial_t^2 \sum_A m_A x_A^i(t) x_A^j(t). \end{aligned} \tag{D.5}$$

If we define

$$I_{ij}(t) \equiv \sum_A m_A x_A^i(t) x_A^j(t), \tag{D.6}$$

then

$$\int d^3x'\ \tau_{ij}(t, \vec{x}') = \frac{1}{2}\ \ddot{I}_{ij}(t). \tag{D.7}$$

or

$$\int d^3x' \; \tau_{ij}(t - x/c, \vec{x}') = \frac{1}{2} \; \ddot{I}_{ij}(t - x/c), \tag{D.8}$$

where c is the speed of light in vaccum.

APPENDIX E

Derivation of Equation (2.73)

$$
\begin{aligned}
\nu_i + \gamma_i = & \frac{4G}{x} \frac{c_+}{2c_1 - c_+ c_-} \left(\sum_m \frac{1}{m! c_V^m} \frac{\partial^m}{\partial t^m} \int d^3x' \tau_{i0}(t - x/c_V, \vec{x}')(x'^k \hat{x}^k)^m \right)^T \\
& + \frac{4G}{x} \frac{(c_+ - 1)}{2c_1 - c_+ c_-} \left(\sum_m \frac{1}{m! c_V^m} \frac{\partial^m}{\partial t^m} \int d^3x' T_i(t - x/c_V, \vec{x}')(x'^k \hat{x}^k)^m \right)^T \\
& \equiv \frac{4G}{x} \frac{c_+}{2c_1 - c_+ c_-} (1) + \frac{4G}{x} \frac{(c_+ - 1)}{2c_1 - c_+ c_-} (2).
\end{aligned}
\tag{E.1}
$$

(1) of equation (E.1) equals (only need $m = 0$ and $m = 1$ terms)

$$
\begin{aligned}
(1) &= \left(\int d^3x' \tau_{i0}(t - x/c_V, \vec{x}') + \frac{1}{c_V} \frac{\partial}{\partial t} \int d^3x' \tau_{i0}(t - x/c_V, \vec{x}')(x'^k \hat{x}^k) \right)^T \\
&= \left(\theta_i + \frac{1}{c_V} \int d^3x' \tau_{i0,0}(x'^k \hat{x}^k) \right)^T \\
&= \left(\theta_i + \frac{1}{c_V} \int d^3x' \left(\frac{\partial}{\partial x'^j} \tau_{ij} \right) (x'^k \hat{x}^k) \right)^T \\
&= \left(\theta_i - \frac{\hat{x}^k}{c_V} \int d^3x' \tau_{ik} \right)^T \\
&= \left(\theta_i - \frac{\hat{x}^k}{2c_V} \ddot{I}_{ik} \right)^T,
\end{aligned}
\tag{E.2}
$$

where we use equation (2.63), integration by parts, and equation (D.7).

(2) of equation (E.1) equals (only need $m = 0$ and $m = 1$ terms)

$$
(2) = \left(\int d^3x' T_i(t - x/c_V, \vec{x}') + \frac{1}{c_V} \frac{\partial}{\partial t} \int d^3x' T_i(t - x/c_V, \vec{x}')(x'^k \hat{x}^k) \right)^T. \tag{E.3}
$$

From equation (1.39)

$$
T_i(t - x/c_V, \vec{x}') = -\sum_A \tilde{m}_A \, \delta^3 (\vec{x}' - \vec{x}_A) (-\sigma_A) v_A^i, \tag{E.4}
$$

where the time dependence is through $\vec{x}_A = \vec{x}_A(t - x/c_V)$ and $v_A^i = v_A^i(t - x/c_V)$.

Therefore,

$$
\begin{aligned}
② &= -\left(-\sum_A \tilde{m}_A\sigma_A v_A^i - \frac{1}{c_V}\frac{\partial}{\partial t}\left(\sum_A \tilde{m}_A\sigma_A v_A^i x_A^k \hat{x}^k\right)\right)^T \\
&= -\left(-\sum_A \tilde{m}_A\sigma_A v_A^i - \frac{1}{c_V}\sum_A \tilde{m}_A\sigma_A \hat{x}^k \frac{\partial}{\partial t}(v_A^i x_A^k)\right)^T .
\end{aligned}
\tag{E.5}
$$

With this property

$$
\begin{aligned}
\frac{\partial}{\partial t}(v_A^i x_A^k) = (\dot{v}_A^i x_A^k + v_A^i \dot{x}_A^k) &= \frac{1}{2}(2\dot{v}_A^i x_A^k + 2v_A^i \dot{x}_A^k) \\
&= \frac{1}{2}(\dot{v}_A^i x_A^k + \dot{v}_A^i x_A^k + 2v_A^i v_A^k + x_A^i \dot{v}_A^k - x_A^i \dot{v}_A^k) \\
&= \frac{1}{2}\partial_t^2(x_A^i x_A^k) + \dot{v}_A^{[i} x_A^{k]},
\end{aligned}
\tag{E.6}
$$

$$
\begin{aligned}
② &= -\left(-\sum_A \tilde{m}_A\sigma_A v_A^i - \frac{1}{c_V}\sum_A \tilde{m}_A\sigma_A \hat{x}^k \left(\frac{1}{2}\partial_t^2(x_A^i x_A^k) + \dot{v}_A^{[i} x_A^{k]}\right)\right)^T \\
&= -\left(-\sum_A \tilde{m}_A\sigma_A v_A^i - \frac{\hat{x}^k}{2c_V}\left(\partial_t^2 \sum_A \tilde{m}_A\sigma_A (x_A^i x_A^k) + 2\sum_A \tilde{m}_A\sigma_A \dot{v}_A^{[i} x_A^{k]}\right)\right)^T \\
&= -\left(\Sigma^i - \frac{\hat{x}^k}{2c_V}\left(\ddot{\mathcal{I}}_{ik} + \mathcal{V}_{ik}\right)\right)^T ,
\end{aligned}
\tag{E.7}
$$

where we define

$$
\Sigma^i \equiv -\sum_A \tilde{m}_A\sigma_A v_A^i, \quad \mathcal{I}_{ik} \equiv \sum_A \tilde{m}_A\sigma_A (x_A^i x_A^k), \quad \mathcal{V}_{ik} \equiv 2\sum_A \tilde{m}_A\sigma_A \dot{v}_A^{[i} x_A^{k]}. \tag{E.8}
$$

equation (E.3) and (E.7) gives a useful property,

$$
\int d^3x' T_k = -\Sigma_k. \tag{E.9}
$$

equation (E.1), (E.2), and (E.7) give

$$
\begin{aligned}
\nu_i + \gamma_i = &\frac{4G}{x}\frac{c_+}{2c_1 - c_+c_-}\left(\theta_i - \frac{\hat{x}^k}{2c_V}\ddot{I}_{ik}\right)^T \\
&- \frac{4G}{x}\frac{c_+ - 1}{2c_1 - c_+c_-}\left(\Sigma^i - \frac{\hat{x}^k}{2c_V}\left(\ddot{\mathcal{I}}_{ik} + \mathcal{V}_{ik}\right)\right)^T .
\end{aligned}
\tag{E.10}
$$

Combining with equation (2.64), I get

$$
\begin{aligned}
\nu_i = &-\frac{2G}{x}\frac{1}{2c_1 - c_+c_-}\left(\frac{\hat{x}^k}{c_V}\left(\frac{c_+}{1-c_+}\ddot{I}_{ik} + \ddot{\mathcal{I}}_{ik} + \mathcal{V}_{ik}\right) - 2\Sigma^i\right)^T \\
&+ \frac{4G}{x}\frac{c_+ - 2c_1 + c_+c_-}{(1-c_+)(2c_1 - c_+c_-)}\theta_i^T .
\end{aligned}
\tag{E.11}
$$

For any symmetric tensor ψ_{ij} and its traceless partner $\Psi_{ij} = \psi_{ij} - \frac{1}{3}\delta_{ij}\psi_{kk}$, there is a useful property,

$$(\hat{x}_j \Psi_{ij})^T = (\hat{x}_j \psi_{ij})^T, \tag{E.12}$$

because,

$$(\hat{x}_j \delta_{ij})^T = \tilde{P}_{ik}(\hat{x}_j \delta_{kj}) = (\delta_{ik} - \hat{x}^i \hat{x}^k)(\hat{x}_j \delta_{kj}) = \hat{x}_i - \hat{x}^i = 0. \tag{E.13}$$

Using equation (E.12), ν_i can be written as

$$\begin{aligned}\nu_i = &-\frac{2G}{x}\frac{1}{2c_1 - c_+ c_-}\left(\frac{\hat{x}^k}{c_V}\left(\frac{c_+}{1-c_+}\ddot{Q}_{ik} + \ddot{\mathcal{Q}}_{ik} + \mathcal{V}_{ik}\right) - 2\Sigma^i\right)^T \\ &+ \frac{4G}{x}\frac{c_+ - 2c_1 + c_+ c_-}{(1-c_+)(2c_1 - c_+ c_-)}\theta_i^T,\end{aligned} \tag{E.14}$$

where Q_{ik} and $\mathcal{Q}_{ik}$ are traceless partner of I_{ik} and $\mathcal{I}_{ik}$.

APPENDIX F

Derivation of Equation (2.75)

$$
\begin{aligned}
F &= \frac{4}{x}\frac{Gc_{14}}{2-c_{14}}\sum_{m=0}^{\infty}\frac{1}{m!c_S^m}\frac{\partial^m}{\partial t^m}\int d^3x'\tau_{ii}(t-x/c_S,\vec{x}')(x'^k\hat{x}^k)^m \\
&- \frac{4}{x}\frac{Gc_{14}}{2-c_{14}}\frac{2+3c_2+c_+}{c_{123}}\sum_{m=0}^{\infty}\frac{1}{m!c_S^m}\frac{\partial^m}{\partial t^m}\int d^3x'\tau^L_{ii}(t-x/c_S,\vec{x}')(x'^k\hat{x}^k)^m \\
&+ \frac{4}{x}\frac{Gc_{14}}{2-c_{14}}\frac{2}{c_{14}}\sum_{m=0}^{\infty}\frac{1}{m!c_S^m}\frac{\partial^m}{\partial t^m}\int d^3x'\tau_{00}(t-x/c_S,\vec{x}')(x'^k\hat{x}^k)^m \\
&\equiv \frac{4}{x}\frac{Gc_{14}}{2-c_{14}} ① - \frac{4}{x}\frac{Gc_{14}}{2-c_{14}}\frac{2+3c_2+c_+}{c_{123}} ② + \frac{4}{x}\frac{Gc_{14}}{2-c_{14}}\frac{2}{c_{14}} ③.
\end{aligned}
\tag{F.1}
$$

① of equation (F.1) equals (only need m=0 term)

$$
① = \int d^3x'\tau_{ii}(t-x/c_S,\vec{x}') = \frac{1}{2}\ddot{I}_{ii}, \tag{F.2}
$$

where we use equation (D.7).

② of equation (F.1) equals (only need m=0 term)

$$
\begin{aligned}
② &= \int d^3x'\tau^L_{ii} = \int d^3x' tr\left(\tau^L_{ij}\right) = tr\left(\int d^3x'\tau^L_{ij}\right) = tr\left(\left(\int d^3x'\tau_{ij}\right)^L\right) \\
&= tr\left(\frac{1}{2}\ddot{I}^L_{ij}\right) = \frac{1}{2}\hat{x}_i\hat{x}_k\ddot{I}_{ik},
\end{aligned}
\tag{F.3}
$$

because

$$
I^L_{ij} = I_{ij} - I^T_{ij} = I_{ij} - \tilde{P}_{ik}I_{kj} = I_{ij} - (\delta_{ik} - \hat{x}_i\hat{x}_k)I_{kj} = \hat{x}_i\hat{x}_k I_{kj}. \tag{F.4}
$$

Instead of I_{ij}, we prefer Q_{ij},

$$
② = \frac{1}{2}\hat{x}_i\hat{x}_j\ddot{Q}_{ij} + \frac{1}{6}\ddot{I}_{ii}. \tag{F.5}
$$

③ of equation (F.1) equals (only need m=0, m=1, and m=2 terms)

$$
\begin{aligned}
③ &= \int d^3x'\tau_{00} + \frac{1}{c_S}\frac{\partial}{\partial t}\int d^3x'\tau_{00}x'^k\hat{x}^k + \frac{1}{2c_S^2}\frac{\partial^2}{\partial t^2}\int d^3x'\tau_{00}x'^k\hat{x}^k x'^l\hat{x}^l \\
&= \theta + \frac{1}{c_S}\int d^3x'\tau_{00,0}x'^k\hat{x}^k + \frac{1}{2c_S^2}\frac{\partial^2}{\partial t^2}\int d^3x'\sum_A \tilde{m}_A\delta^3(\vec{x}' - \vec{x}_A)x'^k\hat{x}^k x'^l\hat{x}^l
\end{aligned}
\tag{F.6}
$$

where we use equation (2.68), and $\tau_{00} = \sum_A \tilde{m}_A\delta^3(\vec{x} - \vec{x}_A)$ to the leading order.

The second integral in equation (F.6) is

$$
\begin{aligned}
\frac{\hat{x}^k}{c_S}\int d^3x'\tau_{0i,i}x'^k &= \frac{-\hat{x}^k}{c_S}\int d^3x'\tau_{0i}\frac{\partial x'^k}{\partial x'^i} = \frac{-\hat{x}^k}{c_S}\int d^3x'\tau_{0k} \\
&= \frac{-\hat{x}^k}{c_S}\int d^3x'(\tau_{k0} + T_k) = \frac{-\hat{x}^k}{c_S}\theta_k + \frac{-\hat{x}^k}{c_S}\int d^3x'T_k \\
&= \frac{-\hat{x}^k}{c_S}\theta_k - \frac{-\hat{x}^k}{c_S}\Sigma_k,
\end{aligned}
\tag{F.7}
$$

where we use conservation law equation (2.63), integration by parts, equation (2.40), and equation (E.9).

The third integral in equation (F.6) is

$$
\begin{aligned}
&\frac{1}{2c_S^2}\frac{\partial^2}{\partial t^2}\sum_A \tilde{m}_A x_A^k\hat{x}^k x_A^l\hat{x}^l \\
&= \frac{1}{2c_S^2}\frac{\partial^2}{\partial t^2}\sum_A m_A x_A^k\hat{x}^k x_A^l\hat{x}^l - \frac{1}{2c_S^2}\frac{\partial^2}{\partial t^2}\sum_A s_A m_A x_A^k\hat{x}^k x_A^l\hat{x}^l \\
&= \frac{1}{2c_S^2}\frac{\partial^2}{\partial t^2}I_{kl}\hat{x}^k\hat{x}^l - \frac{1}{2c_S^2}\frac{\partial^2}{\partial t^2}\mathcal{I}_{kl}\hat{x}^k\hat{x}^l \\
&= \frac{1}{2c_S^2}\frac{\partial^2}{\partial t^2}(Q_{kl}\hat{x}^k\hat{x}^l + \frac{1}{3}I_{ii}) - \frac{1}{2c_S^2}\frac{\partial^2}{\partial t^2}(\mathcal{Q}_{kl}\hat{x}^k\hat{x}^l + \frac{1}{3}\mathcal{I}_{ii}),
\end{aligned}
\tag{F.8}
$$

where $\tilde{m}_A = (1 - s_A)m_A$, and $\sigma_A\tilde{m}_A = s_A m_A$, please refer to equation (37) and (38) in [38], the definition of I_{ij} and $\mathcal{I}_{ij}$ are given by equation (D.6) and (E.8).

Therefore, ③ of equation (F.1) equals (only need m=0, m=1, and m=2 terms)

$$
\begin{aligned}
③ = \theta &+ \frac{-\hat{x}^k}{c_S}\theta_k + \frac{-\hat{x}^k}{c_S}\Sigma_k + \frac{1}{2c_S^2}\frac{\partial^2}{\partial t^2}(Q_{kl}\hat{x}^k\hat{x}^l + \frac{1}{3}I_{ii}) \\
&- \frac{1}{2c_S^2}\frac{\partial^2}{\partial t^2}(\mathcal{Q}_{kl}\hat{x}^k\hat{x}^l + \frac{1}{3}\mathcal{I}_{ii})
\end{aligned}
\tag{F.9}
$$

In conclusion, F is

$$
\begin{aligned}
F &= \frac{4}{x}\frac{Gc_{14}}{2-c_{14}}\frac{1}{2}\ddot{I}_{ii} - \frac{4}{x}\frac{Gc_{14}}{2-c_{14}}\frac{2+3c_2+c_+}{c_{123}}\left(\frac{1}{2}\hat{x}_i\hat{x}_j\ddot{Q}_{ij}+\frac{1}{6}\ddot{I}_{ii}\right)\\
&+\frac{4}{x}\frac{Gc_{14}}{2-c_{14}}\frac{2}{c_{14}}\left(\theta+\frac{-\hat{x}^k}{c_S}\theta_k-\frac{-\hat{x}^k}{c_S}\Sigma_k+\frac{1}{2c_S^2}(\ddot{Q}_{kl}\hat{x}^k\hat{x}^l+\frac{1}{3}\ddot{I}_{ii})-\frac{1}{2c_S^2}(\ddot{\mathcal{Q}}_{kl}\hat{x}^k\hat{x}^l+\frac{1}{3}\ddot{\mathcal{I}}_{ii})\right)\\
&=\frac{4}{x}\frac{Gc_{14}}{2-c_{14}}\left[\left(\frac{1}{c_{14}c_S^2}-\frac{2+3c_2+c_+}{2c_{123}}\right)\hat{x}_i\hat{x}_j\ddot{Q}_{ij}+\left(\frac{1}{2}-\frac{2+3c_2+c_+}{6c_{123}}+\frac{1}{3c_S^2c_{14}}\right)\ddot{I}_{ii}\right.\\
&\left.-\frac{\hat{x}^k\hat{x}^l}{c_{14}c_S^2}\left(\ddot{\mathcal{Q}}_{kl}+\frac{1}{3}\delta_{kl}\ddot{\mathcal{I}}_{ii}\right)+\frac{2}{c_{14}c_S}\hat{x}^k\Sigma_k+\frac{2}{c_{14}}\left(\theta-\frac{\hat{x}^k}{c_S}\theta_k\right)\right]\\
&=\frac{4}{x}\frac{Gc_{14}}{2-c_{14}}\left[\frac{3}{2}(Z-1)\,\hat{x}_i\hat{x}_j\ddot{Q}_{ij}+\frac{1}{2}Z\ddot{I}_{ii}-\frac{\hat{x}^k\hat{x}^l}{c_{14}c_S^2}\left(\ddot{\mathcal{Q}}_{kl}+\frac{1}{3}\delta_{kl}\ddot{\mathcal{I}}_{ii}\right)+\frac{2}{c_{14}c_S}\hat{x}^k\Sigma_k\right]\\
&+\frac{4}{x}\frac{Gc_{14}}{2-c_{14}}\frac{2}{c_{14}}\left(\theta-\frac{\hat{x}^k}{c_S}\theta_k\right),
\end{aligned}
\tag{F.10}
$$

where the definition of Z is given by equation (2.76).

BIBLIOGRAPHY

[1] S. Carlip, Quantum Gravity in 2+1 Dimensions, Cambridge Monographs on Mathematical Physics (Cambridge University Press, Cambridge, 2003).

[2] L. Pilo, PoS EPS-HEP2011, 076 (2011).

[3] M.F. Paulos, A.J. Tolley, JHEP 09, 002 (2012).

[4] A. Wang, Int. J. Mod. Phys. D26 (2017) 1730014.

[5] T. Jacobson, D. Mattingly, Phys.Rev. D64, 024028 (2001).

[6] T. Jacobson, PoS QG-PH, 020 (2007).

[7] D. Mattingly, Living Rev.Rel.8:5,2005.

[8] M. Pospelov and Y. Shang, Phys. Rev. D 85, 105001 (2012).

[9] T. Jacobson, Phys. Rev. D81, 101502 (2010).

[10] O. Sarbach, E. Barausse, J. A. Preciado-López, Class. Quantum Grav. 36 165007 (2019).

[11] R. M. Wald, General Relativity, (University of Chicago Press, Chicago, 1984).

[12] M. Fierz, Helv. Phys. Acta 29, 128-134 (1956).

[13] P. Jordan, Z. Phys. 157, 112-121 (1959).

[14] C. Brans and R. H. Dicke, Phys. Rev. 124, 925 (1961).

[15] C.M. Will, Living Rev. Rel. 17, 4 (2014).

[16] I.H. Stairs, Living Rev. Rel. 6, 5 (2003).

[17] B.P. Abbott, et al., Phys. Rev. Lett. 116(6), 061102 (2016).

[18] B.P. Abbott, et al., Phys. Rev. Lett. 116(24), 241103 (2016).

[19] B.P. Abbott, et al., Phys. Rev. Lett. 118(22), 221101 (2017).

[20] B.P. Abbott, et al., Phys. Rev. Lett. 119(14), 141101 (2017).

[21] B.P. Abbott, et al., Phys. Rev. Lett. 119, 161101 (2017).

[22] B. P. Abbott, et al., 2017 ApJL 851 L35.

[23] H. Audley, et al., arXiv:1702.00786 [astro-ph.IM].

[24] E.Barausse, N. Yunes, and K. Chamberlain, Phys. Rev. Lett. 116, 241104 (2016).

[25] S. Naoz, Annu. Rev. Astron. Astrophys. 54 (2016) 441.

[26] K. Fuhrmann, et al, Astrophys. J. 836 (2017) 139.

[27] A. Tokovinin, et al, A&A 450 (2006) 681.

[28] A. Archibald, et al, Nature 559 (2018) 73.

[29] T. Liu, X. Zhang, W. Zhao, K. Lin, C. Zhang, S. Zhang, X. Zhao, T. Zhu, A. Wang, Phys. Rev. D 98, 083023 (2018).

[30] X. Zhang, W. Zhao, T. Liu, K. Lin, C. Zhang, X. Zhao, S. Zhang, T. Zhu, A. Wang, JCAP01(2019)019.

[31] X. Zhang, W. Zhao, T. Liu, K. Lin, C. Zhang, X. Zhao, S. Zhang, T. Zhu, A. Wang, Astrophysical. J. 874 (2019) 121

[32] K. Lin, S. Zhang, C. Zhang, X. Zhao, B. Wang, A. Wang, Phys. Rev. D 102, 024034 (2020)

[33] K. Lin, X. Zhao, C. Zhang, T. Liu, B. Wang, S. Zhang, X. Zhang, W. Zhao, T. Zhu, and A. Wang, Phys. Rev. D 99, 023010 (2019).

[34] X. Zhao, C. Zhang, K. Lin, T. Liu, R. Niu, B. Wang, S. Zhang, X. Zhang, W. Zhao, T. Zhu, A. Wang, Phys. Rev. D 100, 083012 (2019).

[35] C. Zhang, X. Zhao, Phys. Rev. D 101, 044002 (2020).

[36] C. Zhang, X. Zhao, K. Lin, S. Zhang, W. Zhao, and A. Wang, Phys. Rev. D 102, 064043 (2020).

[37] B. Z. Foster, Phys. Rev. D 73, 104012 (2006).

[38] B. Z. Foster, Phys. Rev. D 76, 084033 (2007).

[39] K. Yagi, D. Blas, E. Barausse, and Nicolas Yunes, Phy. Rev. D 89, 084067 (2014).

[40] B.P. Abbott, et al., Phys. Rev. Lett. 119, 161101 (2017).

[41] B.P. Abbott, et. al., Astrophys. J. 848, L13 (2017).

[42] J. Oost, S. Mukohyama and A. Wang, Phys. Rev. D 97, 124023 (2018).

[43] Burgess, C., Hayman, P., Williams, M. et al., J. High Energ. Phys. 2017, 106 (2017).

[44] R. Arnowitt, S. Deser, and C. W. Misner, ”Gravitation: an introduction to current research”, Louis Witten ed. (Wiley 1962), chapter 7, pp 227–265, arXiv:gr-qc/0405109.

[45] C. M. Will, Theory and Experiment in Gravitational Physics, (Cambridge University Press, Cambridge, 1993).

[46] M. Maggiore, Gravitational Waves Volume 1: Theory and Experiments, (Oxford University Press, New York, 2016).

[47] K. Lin, X. Zhao, C. Zhang, T. Liu, B. Wang, S. Zhang, X. Zhang, W. Zhao, T. Zhu, and A. Wang, Phys. Rev. D 99, 023010 (2019).

[48] Poisson, E. and Will, C., Gravity: Newtonian, Post-Newtonian, Relativistic, (Cambridge University Press, Cambridge, 2014).

[49] Alexander Saffer, et al., 2018 Class. Quantum Grav. 35 055011.

[50] X. Li and S. Liao, Sci. China Phys. Mech. Astron. 60, 129511 (2017).

[51] Y. Torigoe, K. Hattori, and H. Asada, Phys. Rev. Lett. 102, 251101 (2009).

[52] C. Moore, Phys. Rev. Lett. 70, 3675 (1993).

[53] V. Dmitrasinovic, M. Suvakov, and A. Hudomal, Phys. Rev. Lett. 113, 101102 (2014).

[54] M. Suvakov and V. Dmitrasinovic, Phys. Rev. Lett. 110, 114301 (2013).

[55] M. Suvakov, Celest. Mech. Dyn. Astron. 119, 369 (2014).

[56] http://three-body.ipb.ac.rs

[57] K. Fuhrmann, et al., Astrophys. J. 836 139 (2017) .

[58] A. Tokovinin, et al., A&A 450 681-693 (2006) .

[59] S. M. Ransom, et al., Nature 505, 520 (2014) .

[60] L. Shao, Phys. Rev. D 93, 084023 (2016).

[61] C. Simò, in Celestial Mechanics, edited by A. Chenciner, R. Cushman, C. Robinson, and Z. J. Xia (Am. Math. Soc., Providence, RI, 2002).

[62] T. Jacobson, PoS QG-PH, 020 (2007).

[63] C. Brans and R. H. Dicke, Phys. Rev. 124, 925 (1961).

[64] C. Will, Class. Quantum Grav. 35, 085001 (2018).

[65] L. Shao, Phys. Rev. D 93, 084023 (2016).

[66] C. J. Moore, R. H. Cole and C. P. L. Berry, Class. Quantum Grav. 32, 015014 (2015).

[67] C.M. Will, Astrophys. J. 214, 826 (1997).

[68] X. Zhang, et al., Phys. Rev. D 95, 124008 (2017).

[69] A.M. Archibald, et al., Nature 559, 73 (2018).

[70] V. Dmitrasinovic, M. Suvakov, and A. Hudomal, Phys. Rev. Lett. 113, 101102 (2014).

[71] A. Sesana, Phys. Rev. Lett. 116, 231102 (2016).

[72] E. Berti, K. Yagi, and N. Yunes, Gen. Relativ. Grav. 50, 46 (2018).

[73] The LIGO Scientific Collaboration, et al., 2015 Class. Quantum Grav. 32 074001.

[74] F Acernese, et al., 2015 Class. Quantum Grav. 32 024001.

[75] Akutsu, T., Ando, M., Arai, K., Arai, Y., Araki, S., Araya, A., et al. (2019). KAGRA: 2.5 generation interferometric gravitational wave detector. Nat. Astron. 3, 35–40. doi: 10.1038/s41550-018-0658-y

[76] A. Wang, Inter. J. Mod. Phys. D26, 1730014 (2017).

[77] J. Greenwald, J. Lenells, J. Lu, V.H. Satheeshkumar, A. Wang, Phys. Rev. D 84, 084040 (2011).

[78] P. Hořava, JHEP 0903 (2009) 020; Phys. Rev. D 79, 084008 (2009).

[79] D. Blas and S. Sibiryakov, Phys. Rev. D 84, 124043 (2011).

[80] E. Barausse, T. Jacobson and T.P. Sotiriou, Phys. Rev. D 83, 124043 (2011).

[81] K. Lin, E. Abdalla, R.-G. Cai and A. Wang, Int. J. Mod. Phys. D 23, 1443004 (2014).

[82] K. Lin, O. Goldoni, M.F. da Silva, and A. Wang, Phys. Rev. D 91, 024047 (2015).

[83] K. Lin, V.H. Satheeshkumar, and A. Wang, Phys. Rev. D 93, 124025 (2016).

[84] D. Blas, O. Pujolas, and S. Sibiryakov, Phys. Rev. Lett. 104, 181302 (2010).

[85] D. Blas, O. Pujolas, and S. Sibiryakov, JHEP 04 (2011) 018.

[86] T. Jacobson and D. Mattingly, Phys. Rev. D 64, 024028 (2001).

[87] T. Jacobson and D. Mattingly, Phys. Rev. D 70, 024003 (2004).

[88] C. Eling and T. Jacobson, Class. Quantum. Grav. 23, 5643 (2006).

[89] E. Barausse, T. Jacobson and T.P. Sotiriou, Phys. Rev. D 83, 124043 (2011).

[90] P. Berglund, J. Bhattacharyya and D. Mattingly, Phys. Rev. D 85, 124019 (2012).

[91] A. Sesana, Phys. Rev. Lett. 116, 231102 (2016).

[92] E. Berti, K. Yagi, and N. Yunes, Gen. Relativ. Grav. 50, 46 (2018).

[93] S. Iyer, Phys. Rev. D 35, 12 (1987).

[94] S. Chandrasekhar, F. R. S., and S. Detweiler, Proc. R. Soc. Lond. A. 344, 411-452 (1975).

[95] S. Detweiler, Astrophys. J. 239, 292-295 (1980).

[96] E. Seidel and S. Iyer, Phys. Rev. D 41, 2 (1990).

[97] B. F. Schutz and C. M. Will, Astrophys. J. 291, L33-L36 (1985).

[98] S. Iyer and C. M. Will, Phys. Rev. D 35, 12 (1987).

[99] R. A. Konoplya, Phys. Rev. D 68, 024018 (2003).

[100] J. Matyjasek and M. Opala, Phys. Rev. D 96, 024011 (2017).

[101] E. W. Leaver, Proc. R. Soc. Lond. A. 402, 285-298 (1985).

[102] R. A. Konoplya and A. Zhidenko, Rev. Mod. Phys. 83, 793 (2011).

[103] C. Gundlach, R. H. Price and J. Pullin, Phys. Rev. D 49, 883 (1994).

[104] B. Wang, C.-Y. Lin and C. Molina, Phys. Rev. D 70, 064025 (2004).

[105] X. Li and S. Zhao, Phys. Rev. D 101, 124012 (2020).

[106] O. J. Tattersall and P. G. Ferreira, Phys. Rev. D 99, 104082 (2019).

[107] H. Yang, D. A. Nichols, F. Zhang, et al., Phys. Rev. D 86, 104006 (2012).

[108] T. Regge and J. A. Wheeler, Phys. Rev. 108, 4 (1957).